The role of mTOR-dependent translation in aged microglia phenotype

Doctoral thesis

to obtain a doctorate (PhD)

from the Faculty of Medicine

of the University of Bonn

Ignazio Antignano

from Mugnano di Napoli, Italy

2024

Written with authorization of

the Faculty of Medicine of the University of Bonn

First reviewer: Prof. Dr. Martin Fuhrmann

Second reviewer: Prof. Dr. Eicke Latz

Day of oral examination: 24.06.2024

From Deutsches Zentrum für Neurodegenerative Erkrankungen (DZNE) in Bonn

Department of Immune regulation

Director: Dr. Melania Capasso

Sic itur ad astra

Virgilio (Eneide, IX, 641)

Table of Contents

List of abbreviations

4EBP1	Eukaryotic initiation factor 4E-binding protein 1
AKT	alternatively named as Protein kinase B (PKB)
AMPK	AMP-activated protein kinase
Aβ	Amyloid beta
BBB	Blood-brain barrier
BMDMs	Bone Marrow-derived Macrophages
CNS	Central Nervous System
Csf	Colony-stimulating factor
Csf-1r	Colony-stimulating factor (CSF)-1 receptor
DCs	Dendritic cells
eIF4E	Eukaryotic initiation factor 4E
EP2	Prostaglandin E_2 receptor 2
HIF-1α	Hypoxia-inducible factor 1α
IL-10	Interleukin-10
IL-12p40	Interleukin-12 subunit p40
IL-23	Interleukin-23
IL4R-α	Interleukin-4 receptor subunit alpha
IL-6	Interleukin-6
LPS	Lipopolysaccharide

MHC	Major histocompatibility complex
MHCII	Major histocompatibility complex II
mRNA	Messenger ribonucleic acid
mTOR	mammalian Target Of Rapamycin
mTORC1	mammalian Target Of Rapamycin Complex 1
mTORC2	ammalian Target Of Rapamycin Complex 2
NF-κB	Nuclear factor kappa-light-chain-enhancer of activated B cells
PBMC	Peripheral blood mononuclear cells
PGE2	Prostaglandin E2
PI3K	Phosphoinositide 3-kinase
ROS	Reactive oxygen species
rRNA	Ribosomal ribonucleic acid
S6K1	p70 S6 Kinase 1
SAC	Staphylococcus aureus cells
Sirt1	Sirtuin 1
TLRs	Toll-like receptors
TNF-α	Tumor necrosis factor alpha
TREM2	Triggering Receptor Expressed on Myeloid Cells-2
tRNA	Transfer ribonucleic acid

TSC1	Tuberous sclerosis complex 1
TSC2	Tuberous sclerosis complex 2

1. Introduction

1.1. Aging: a silent global crisis

Aging is a complex biological process leading to a gradual decline in physiological integrity and functions throughout the adulthood (López-Otín et al., 2013) . As such, it represents the major risk factor for a large number of chronic illnesses, such as cancer, diabetes, cardiovascular diseases as well as neurodegenerative pathologies (Franceschi et al., 2018). In the last centuries, the amelioration of socio-economical conditions and a greater accessibility to treatments for life-threatening diseases have strongly contributed to augmenting life expectancy worldwide (Y. C. Yang et al., 2016). Consequently, as lifespan increases, so does the aging population. According to the World Health Organization (WHO), the number of people over 65 years old is projected to more than double over the next three decades, reaching over 1.5 billion people in 2050 (Figure 1A-B) (*World Report on Ageing And HeAltH*, 2015). This will potentially lead to the exposure of a larger number of people to age-related diseases, representing a considerable burden for healthcare and welfare systems (Franceschi et al., 2018). That said, studying the fundamental biology underlying aging process represents a fundamental step in order to provide solutions that can mitigate the burden of age-related illnesses.

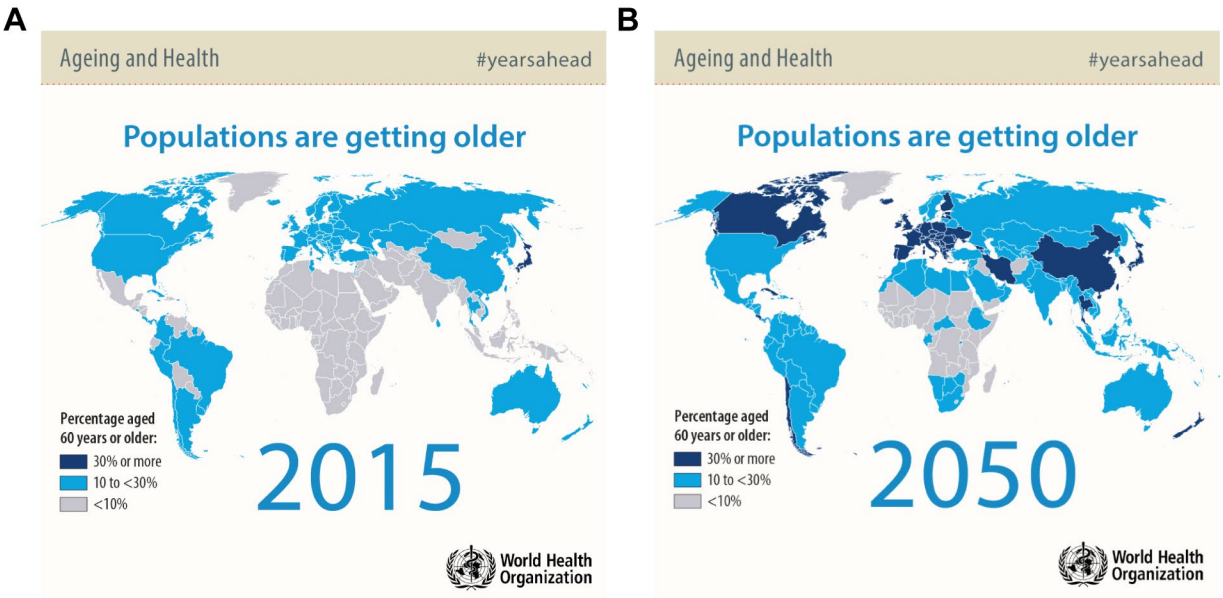

Figure 1 Population are getting older
(**A**) Proportion of population aged 60 years or older, by country, in 2015.

(**B**) Proportion of population aged 60 years or older, by country, 2050 projections.
Images extracted from (*World Report on Ageing And HeAltH*, 2015)

The emergence of novel technologies and the progressive findings of research studies on aging are strongly contributing to understanding its biology. Over the last decade, a better understanding of the processes responsible for aging has emerged, as illustrated in the review by López-Otín et al., 2023. A summary of the hallmark of aging is represented in Figure 2.

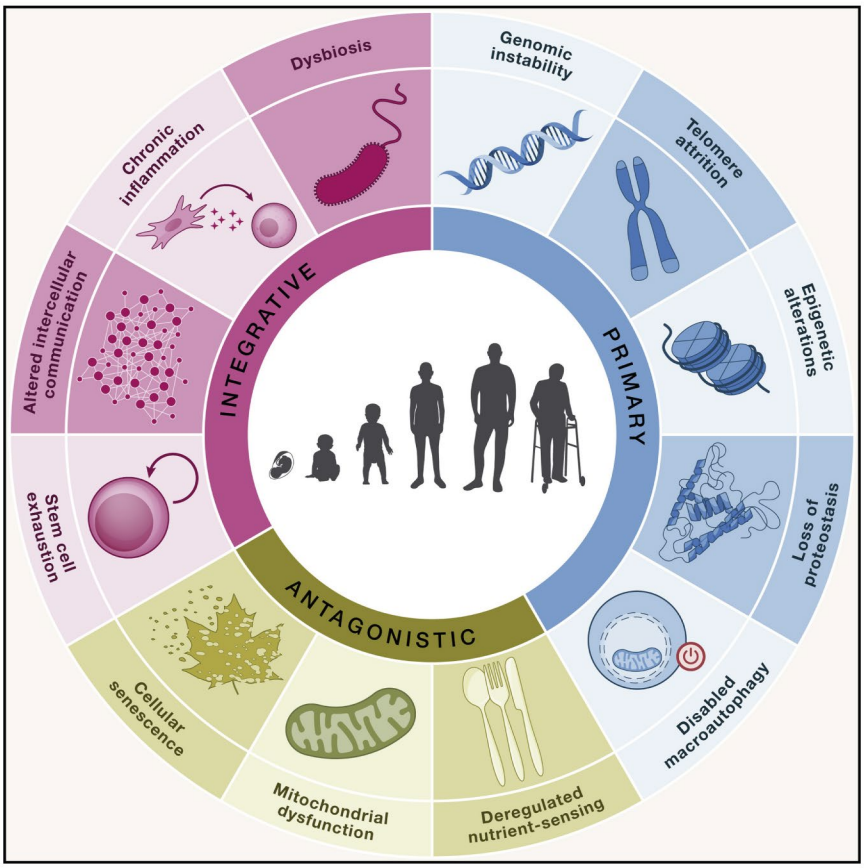

Figure 2 Hallmark of Aging
Schematic representation of the “hallmarks of aging” based on the new classification. Cartoon extracted from López-Otín et al., 2023

According to the criteria highlighted in the review, aging is now defined by twelve hallmarks (Figure 1.2), described as: 1) genomic instability, caused by a gradual increase in DNA damage, occurring in the nucleus and/or in mitochondria; 2) telomere attrition, such as the progressive shortening of telomeres after cell division; 3) epigenetic alterations, such as

changes in DNA methylation, post-translational modifications of histones and chromatin remodeling; 4) loss of proteostasis, due to a defective autophagy flux, thereby causing a progressive accumulation of erroneously translated, incomplete or misfolded proteins; 5) disabled macroautophagy, which impairs organelle turnover; 6) deregulated nutrient-sensing network, caused by the deregulation of pathways sensing the availably of nutrients, such as the IGF1 signaling, the PI3K/AKT/mTOR signaling cascade, AMPK or sirtuin-regulated pathways; 7) mitochondrial dysfunction, due to altered metabolic flux, enhanced production of ROS, accumulation of mitochondrial DNA mutations 8) cellular senescence, a state where a variety of signals induces a permanent cell-cycle arrest leading to cellular phenotype changes; 9) stem cell exhaustion, a condition leading to a decline in tissue renewal at steady-state and tissue repair upon injury, including defects in hematopoiesis that ultimately leads to immunosenescence; 10) altered intercellular communication, due to deficiencies in neural, neuroendocrine and hormonal signaling pathways; 11) chronic inflammation, a slow long-term process with pathological local phenotypes due to a decline of immune functions; and 12) dysbiosis, characterized by the disruption of the bidirectional communication between the host and the intestinal microbiome, which contributes to a multitude of physiological processes responsible for the overall maintenance of host health.

1.2. Microglia: the sentinels of the Central Nervous System

1.2.1. Microglia origin and functions

Microglia are the macrophage-like innate immune cells of the Central Nervous System (CNS) involved in the immune defense and maintenance of CNS homeostasis (R. C. Paolicelli et al., 2022). Fate-mapping studies in mice have finally elucidated that microglia have a mesodermal origin (Yona et al., 2013). More precisely, microglia derive from c-kit^{+}/CD45^{-} erythromyeloid progenitors that arise in the yolk-sac as result of a primitive hematopoiesis occurring from E8.5 post-conception. Then, from E9.0/9.5, they colonize the neuroepithelium, giving rise to embryonic microglia (Yona et al., 2013). These events are tightly regulated by a transcriptional program governed by the expression of IRF-8 and its downstream transcription factor PU.1, whereas other myeloid-derived transcriptional factors, such as MYB, ID2, BATF3 and KLF4, are redundant (Ginhoux et al., 2013; Kierdorf et al., 2013). The formation of the blood-brain barrier (BBB) at E13.5 further

isolates the developing brain; hence, no contribution derives from the bone marrow hematopoiesis, as it occurs at later stage. Within the first two weeks after birth, microglia population differentiate, rapidly expand and colonize the whole CNS. Due to their innate capability of self-renew, this population is maintained throughout the lifespan, with no or little contribution from bone marrow-derived monocytes at steady state, as previously hypothesized (Ginhoux & Prinz, 2015). Nonetheless, a greater contribution in aging has been recently proposed (Silvin et al., 2022).

Microglia play multifaceted roles within the CNS. As part of the innate immune system, they constantly scavenge the brain parenchyma, sensing and surveying the microenvironment (Helmut et al., 2011). The detection of external signals, such as invading pathogens, or insults generated locally by damaged or dying cells in the CNS, triggers a coordinated immune response aimed to resolve injuries, prevent detrimental effects of inflammation and support tissue repair and remodeling (Borst et al., 2021). During brain development, microglia contribute to neurogenesis and neuronal differentiation through the phagocytosis of neuronal progenitors cells or by the secretion of proliferative-stimulating factors, such as protease inhibitor TIMP-1, the chemokines CXCL1 and RANTES, and the cytokine IL-6 (Choi et al., 2008; Sierra et al., 2010). In the post-natal brain, microglia are involved in the refinement of synaptic connections, a process also known as synaptic pruning (Scott-Hewitt et al., 2020). This process is crucial for the normal formation and remodeling of neural circuits, thus shaping the final connectivity of synapses in the brain (Faust et al., 2021; Sierra et al., 2010). Indeed, deficiency or dysregulation in microglial pruning activity has been implicated in numerous neurological diseases like autism and schizophrenia. Conversely, over-activation of microglia leading to excessive synaptic pruning has also been linked to various neurodegenerative conditions (Cangalaya et al., 2023; Ding et al., 2021; Morrison & Baxter, 2012).

Despite a different developmental pathway, microglia similarly express a multitude of macrophage markers, such as the integrin CD11b, the surface glycoprotein F4/80, the colony-stimulating factor (CSF)-1 receptor (CSF-1R, also known as CD115), the inhibitory immune receptor CD200R, the fractalkine receptor CX3CR1, and the calcium binding protein IBA1. Additionally, microglia express the pan-hematopoietic marker CD45, which

is often used to discriminate microglia from other brain-infiltrated immune cells due its lower expression in microglia compared to circulating monocytes (Jurga et al., 2020).

Collectively, these features point to microglia as being a key cell type in CNS.

1.2.2. Microglia phenotype in aging

The phenotype of aged microglia has primarily been characterized in rodent models. Early studies reported that they had an altered morphology with shortened and less complex branching, particularly in the white matter (Perry et al., 1993). Further evidences, such as higher levels of activation markers (CD4, MHCII, CD45) and larger inclusions indicative of an enhanced phagocytic activity, led to the hypothesis that aged microglia had an activated, primed phenotype, with the propensity to respond more strongly to insults (Perry et al., 1993; Peters et al., 1991; Vaughan & Peters, 1974). Phenotypically, primed microglia are characterized by a reduced expression of homeostatic and inhibitory genes (CD200, CX3CL1, CD47, Sialic acid) and upregulation of immune stimulatory mediators (MHC, CD86, CD68, CR3, CR4, CD14, pattern recognition receptors such as TLRs and Clec7a)(Niraula et al., 2017; Norden et al., 2015) . These alterations have been observed across various aged brain regions, with more marked changes in white matter and caudal areas of the CNS, thereby indicating that these regions may be more susceptible to age-related insults(Hart et al., 2012) . Upon an inflammatory challenge (i.e. following peripheral administration of LPS), aged microglia boost the production of pro-inflammatory cytokines (TNF-α, IL-1β, IL-6) to a greater extent than younger counterparts (Godbout et al., 2005; Henry et al., 2009; Keane et al., 2021). Although they still express anti-inflammatory mediators, such as IL10 and IL4R-α, these cytokines cannot counteract the excess of inflammation due to a lower cellular responsiveness (Fenn et al., 2012). Consequently, microglia fail to return to homeostasis and this prolonged inflammatory state further exacerbates cognitive impairment, sickness and depressive-like behaviors, which are commonly observed in neuroinflammation settings (Godbout et al., 2005, 2008; Henry et al., 2009; Y. Huang et al., 2008). Besides an altered responsiveness and morphology, aged microglia are also characterized by a reduced phagocytosis of neuronal debris, apoptotic bodies and misfolded proteins, which typically accumulate in the aging brain (Gabandé-Rodríguez et al., 2020; Mosher & Wyss-Coray, 2014). One of the responsible factor is CD22, a negative regulator of microglia phagocytosis, whose expression

increases over age (Grabert et al., 2016; Hickman et al., 2013). Indeed, genetic or pharmacological inhibition of CD22 significantly enhanced the clearance of myelin debris, restoring the age-related microglial phenotype, and ameliorated cognitive functions (Pluvinage et al., 2019). Furthermore, these changes were accompanied by an improvement of microglia surveillance and motility, as well as by a rescue of microglia homeostatic morphology as observed via two-photon imaging (Aires et al., 2021). Interestingly, CD22 is not expressed by human microglia but it is rather released as soluble form by oligodendrocytes. Its biding to the insulin-like growth factor 2 receptor (IGF2R), expressed on microglia, impairs lysosome protein trafficking (Pluvinage et al., 2021). These data further highlight how human and rodents evolutionarily diverge and suggests how the validation of our findings from mouse models in human samples is fundamental.

A well-tuned metabolism is also important for immune cells in order to maintain homeostasis and to mount an immune response efficiently (Ganeshan & Chawla, 2014). Aging severely impairs cellular bioenergetics by altering nutrients-sensing networks as well as mitochondrial integrity and functions (López-Otín et al., 2023). In the context of microglia, several studies reported that aged microglia present severe metabolic defects. These changes have been associated with an increased pro-inflammatory PGE2 signaling in aged microglia (Minhas et al., 2021). Indeed, the activation of PGE2 through EP2 receptor promoted the sequestration of glucose into glycogen via the AKT–GSK3β–GYS1 pathway leading to a reduction of glucose flux, lower mitochondria respiration and ATP production. This energy-depleted state ultimately promotes the accumulation of the TCA metabolite succinate, which, in turn, stabilizes the activity of HIF-1α, an activator of pro-inflammatory cytokine expression (Minhas et al., 2021). Interestingly, genetic deletion or pharmacological inhibition of PGE2 reverted this phenotype towards a more anti-inflammatory profile in aged microglia and peripheral myeloid cells. These changes were also accompanied by a marked reduction of circulating pro-inflammatory cytokines in the blood and aged hippocampi, causing an amelioration of hippocampal plasticity and memory function to levels found in young mice. Notably, a similar result was obtained by using a brain-impermeable EP2 antagonist, further corroborating previous evidences that age-associated neuroinflammation and cognitive decline can be reverted by acting on peripheral cells (Minhas et al., 2021). Relative to lipid metabolism, aged microglia are also

characterized by the presence of insoluble, lipofuscin-like lysosomal inclusions containing poorly-digested myelin fragments derived from myelin degeneration, which naturally occurs in the white matter with age (Safaiyan et al., 2016). Furthermore, hippocampal microglia have been showed to accumulate lipid droplets with age (Marschallinger et al., 2020). RNA-sequencing of this microglia subset, defined as Lipid droplets-associated microglia (LDAM), showed defects in phagocytosis, an increased generation of ROS and inflammatory cytokines production associated with a signature similar to microglia derived from LPS-treated mice. Interestingly, genes regulating lipid-droplet formation in LDAM are similarly expressed in models of neurodegeneration, indicating that aged microglia may partially share a common signature or acquire a phenotype that might accelerate neurodegeneration (Marschallinger et al., 2020).

1.2.3. Microglia heterogeneity in aging

The recent advent of new high-throughput technologies has significantly contributed to shed the light on microglia heterogeneity, which appears to be largely influenced by microenvironmental cues. The first study reporting a regional heterogeneity of aged microglia derived from a transcriptome analysis from different brain regions over the mouse lifespan (Grabert et al., 2016). All regions showed a slight increase of immune regulatory genes expression over age, however, the greatest differences were observed in the cerebellum and hippocampus. Aged cerebellar microglia seemed to undergo a shift towards a more immune-alert state, with a strong upregulation of genes involved in interferon pathway, such as regulatory factors (*Irf7, Stat2, Oals2*) and effectors of antiviral response (*Sp100, Csprs, Isg20, Ifitm* family*, Bst2 and Zbp1*), as well as immune receptors (*Cd300ld, Trem1, Sirp1a, Cd200r4, Cd200lb*). On the other hand, aged hippocampal microglia downregulated genes involved in cell adhesion and migration (*CD36, CD93, Pf4*), endocytosis and phagocytosis (*Arhgef3*, *Dab2*, *Itsn1*, and *Vav3*) along with the MHCII-related genes *H2-Aa* and *H2-Ab1* (Grabert et al., 2016). This suggested a defective sampling of hippocampal microglia, which might explain why this region is particularly vulnerable to deposition of age- and diseases-related misfolded proteins (Grabert et al., 2016).

With the emergence of RNA sequencing at single cell resolution (hereafter abbreviated sc-RNAseq), multiple studies have revealed a much more heterogeneous scenario of

microglia phenotypes in both ageing and neurodegenerative conditions. The first comprehensive sc-RNAseq study was published by Hammond and coworkers (Hammond et al., 2019a). Here, the majority of microglia displayed a slight altered phenotype, nevertheless, two clusters, named OA2 and OA3, progressively expanded with age along with a monocyte and macrophage cluster (Mono/Mac), both indicative of a shift toward a more reactive immune state. While OA2 cluster showed an upregulation of inflammatory molecules, such as the chemokine *Ccl3* and *Ccl4*, Galrctin3 (*Lgals3*), Cystatin F (*Cst7*), and the inflammatory cytokine *Il1b*, OA3 subset upregulated genes involved in interferon response type I signaling, such as *Ifitm2*, *Rtp4* and *Oasl2***,** which may play a role in modulating inflammation (Hammond et al., 2019a). In a later report, Sala Frigerio and colleagues drew similar conclusion (Sala Frigerio et al., 2019). Although microglia were isolated from brain cortex and hippocampus, two age-dependent clusters were found, both showing signatures that similarly overlapped with those previously described in Hammond et al.. The activated response microglia (defined as ARM) upregulated genes involved in inflammatory processes (*Cst7, Clec7a, Itgax*), tissue regeneration (*Spp1, Gpnmb, Dkk2*) as well as in antigen presentation (*Cd74, H2-Ab1, H2-Aa, Ctsb, and Ctsd*). By similarity, the second cluster, named as interferon response microglia (IRM), was represented by a higher expression of genes involved in the interferon response (Sala Frigerio et al., 2019). Nevertheless, few considerations have to be pointed out. First, in both studies these states seem to be the result of a progressive expansion of clusters that were poorly represented, but still detectable, at younger age. Secondly, despite the increase, these subsets only represented a small percentage of the whole microglia population in the aged brain, with the inflammatory responsive microglia (OA2 and ARMs) representing the highest percentage of cells accumulating in aging (Antignano et al., 2023). Therefore, as the majority of microglia still showed a slightly altered homeostatic profile in both studies, it is likely that these clusters might be part of a physiological evolutionary state that expand in response to alterations occurring in the microenvironment of healthy aging brain and may potentially drive the onset of age-associated diseases (Antignano et al., 2023). In this regard, Safaiyan and colleagues further investigated by sc-RNAseq differences of gray versus white matter-resident microglia (Safaiyan et al., 2021). The latter was previously reported to be enriched in lipofuscin-like inclusions containing myelin debris, as described above (Safaiyan et al., 2016). Beside two large and commonly shared homeostatic

signatures, two main microglia subsets were found to accumulate with age, specifically in the white matter. The so-called white-matter associated microglia (WAM) were associated with myelin degeneration and upregulated lipid metabolism and phagosome-related genes (*ApoE, Cst7, Bm2, Lyz2, Cd63 and Clec7a*), as well as cathepsins (*Cstb, Ctss, Ctsz*) and MHCII-related genes (Safaiyan et al., 2021). Moreover, WAM typically clustered in nodules consisting of 3-5 cells with larger cell bodies and thick processes engaged in clearing myelin debris. On the other hand, the second cluster defined as “activated microglia” was characterized by a more pronounced upregulation of genes involved in protein synthesis regulation, such as ribosomal proteins and translational factors, as well as mitochondrial genes (Safaiyan et al., 2021), many of which were part of microglia response to aging (Ximerakis et al., 2019). Both WAM and “activated microglia” subsets were also found in two previous databases described above (Hammond et al., 2019b; Sala Frigerio et al., 2019), indicating a certain robustness of the different methods utilized by different research groups (Safaiyan et al., 2021). A summary of the overlapping genes signatures derived from microglia clusters that have been found in aged animals is represented by Figure 3.

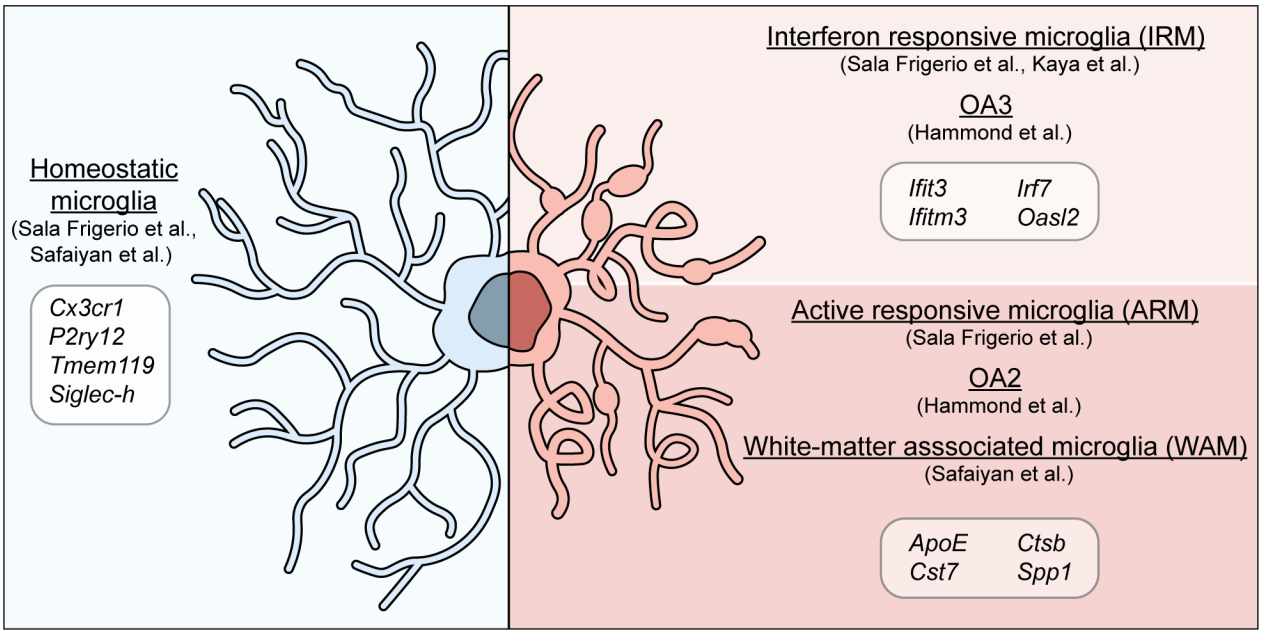

Figure 3 Gene signatures of aged microglia subsets from scRNA-seq studies. Several sc-RNA sequencing studies have investigated microglia pheotype in the context of aging. The majority of cells exhibit a homeostatic gene signature, generally characterized by highly branched morphology with extended processes. On the other hand, aged mice demonstrate an enrichment of two distinct subpopulations of microglia

(depicted in light pink and red). While there is some variation in the signatures across different studies, they share common features such as upregulation of IFN-regulated genes (IRM, OAR) or genes associated with inflammation, phagocytosis, and lipid metabolism (ARM,OA2,WAM). Aged microglia exhibit shortened and thickened processes containing either phagocytic debris or lipid accumulations; however it's still unclear whether these subtypes possess similar or distinctive morphological characteristics. Picture extracted from Antignano et al., 2023

Overall, although we currently have a broad understanding of microglia heterogeneity, the effective functions of these clusters remain to be clarified (Antignano et al., 2023). The characterization of these microglial states has primarily relied on bulk and single-cell transcriptome studies, nonetheless, gene expression profiles may not always correlate to protein abundance, as we reported in our study and I describe in this PhD thesis (Keane et al., 2021). To address these points, the integration of multidimensional data analysis through multi-omics approaches offers a promising avenue to explore the diversity of microglia subsets (R. Paolicelli et al., 2022). Emerging techniques such as spatial transcriptomics (Chen et al., 2020; Kiss et al., 2022), translatomics and proteomics, (Flowers et al., 2017; Iwasaki & Ingolia, 2017; Sanz et al., 2019), which are currently available even at single-cell resolution (Gebreyesus et al., 2022; Taylor et al., 2021; VanInsberghe et al., 2021a), can significantly advance our knowledge. By leveraging these innovative methodologies, we can gain a deeper insight into microglia states and contributions to brain physiology and age-related disorders, paving the way to novel therapeutic interventions.

1.2.4. Microglia senescence in the aged brain

Many research groups attempted to determine whether aged microglia phenotypes are associated to senescence. Cellular senescence is defined by an irreversible cell-cycle arrest mediated by cyclin-dependent kinase inhibitors (Cdkn2a/p16^{INK4}, Cdkn1a/p21$^{WAF1/Cip1}$)(Gorgoulis et al., 2019). Additionally, senescent cells are characterized by severe macromolecular and organelle damage, as well as by a senescence-associated secretory phenotype (SASP), which includes chemokines, pro-inflammatory cytokines and remodeling factors that affect surrounding cells (Gorgoulis et al., 2019). In the context of microglia, different phenotypes have been observed based on

sex and brain areas investigated. In the hippocampus of female mice, the highest frequency of p16-positive cells that accumulate over age was represented by Tmem119-positive microglia and Ly6c2-positive monocyte subpopulations. At transcriptional level, these two clusters were defined by an increased expression of senescence-associated genes (*Cdkn2a, Cdkn1a, Blc2*), chemoattractant SAPS factors (*Ccl2-5, Spp1*), MHC genes and lysosomal stress markers (*Lgals3, Lgals3bp*) (X. Zhang et al., 2022). Importantly, these microglia subsets also showed an overlapping DAM-like signature (*Apoe, B2m,Cst7,Fth1, Iftm3, Itgax, Lpl*), accompanied by a downregulation of homeostatic genes (*Cx3cr1, Hexb, Marcks, P2ry12, Selplg, Tmem110*) (X. Zhang et al., 2022). The contribution of $p16^{INK4}$-positive cells to age-related phenotypes has been determined by the systemic clearance of highly-expressing p16 cells, induced by the administration of the drug AP20187 (AP) in the *INK-ATTAC* mouse model. (Baker et al., 2011a; W. Wang et al., 2001) Interestingly, the treatment exclusively reduced p16-positive microglia subset in aged females, without affecting additional microglia subsets (X. Zhang et al., 2022), as also confirmed by others (Baker et al., 2011; Ogrodnik et al., 2021;). Of note, targeting p16-positive senescent cells strongly reduced brain infiltrating immune cells (monocytes, neutrophils, dendritic cells, B cells and T cells) (Baker et al., 2011; Ogrodnik et al., 2021; X. Zhang et al., 2022), which generally tend to accumulate in the aging brain (Dulken et al., 2019; Mrdjen et al., 2018). The age-dependent increase in *Cdkn2a* expression in microglia was further corroborated in an additional study in which the frequency of p16-positive cells was measured by sc-RNAseq based on the expression of a reporter under the control of the p16 promoter in p16-3MR transgenic mice (Talma et al., 2021). However, despite p16-positive microglia clustered in two distinctive subsets, senescence-associated genes were found to be enriched more in the DAM cluster, suggesting a non-linear correlation between p16 and senescence (Talma et al., 2021).

Overall, the previously described evidences showed that the clearance of high expressing p16 cells in *INK-ATTAC* AP-treated mice was not restricted to a specific cell type (i.e. microglia) but affects the whole body, meaning that the effects observed after the depletion of $p16^{INK4}$-positive cells are a result of a global, systemic contribution (Antignano et al., 2023). Furthermore, although high expression of p16 is recognized as a marker of senescence, not all senescent cells express p16 and its induction alone is not sufficient to indicate a senescent state as previously reported. For instance, alginate-encapsulated

senescent cells injected intraperitoneally in young mice were mostly surrounded by F4/80^{+} macrophages subpopulation with an increased expression of p16^{INK4} and senescence-associated beta-galactosidase (SaβG) (Antignano et al., 2023). The upregulation of these two well-known senescence markers was due to a physiological response to stimuli rather than being an age-related effect, and it occurs in a p53-independent manner, which is instead required in modulating cellular senescence and organismal aging (Antignano et al., 2023).

Based on these points, a senescence state in microglia cannot be uniquely defined by an individual factor, such as p16, and additional senescent markers should be considered. To this date, it remains to be further elucidated the extent of senescence among aged microglia and what role it plays (Antignano et al., 2023).

1.3. The mechanistic Target of Rapamycin (mTOR) signaling pathway

1.3.1. Structure and biology of mTOR

mTOR is a serine/threonine kinase belonging to the phosphoinositide 3-kinase (PI3K) family and it is a key regulator of cellular growth, proliferation and bioenergetics. Its dysregulation leads to the onset of several human diseases, including cancer, neurodegeneration and metabolic disorders .

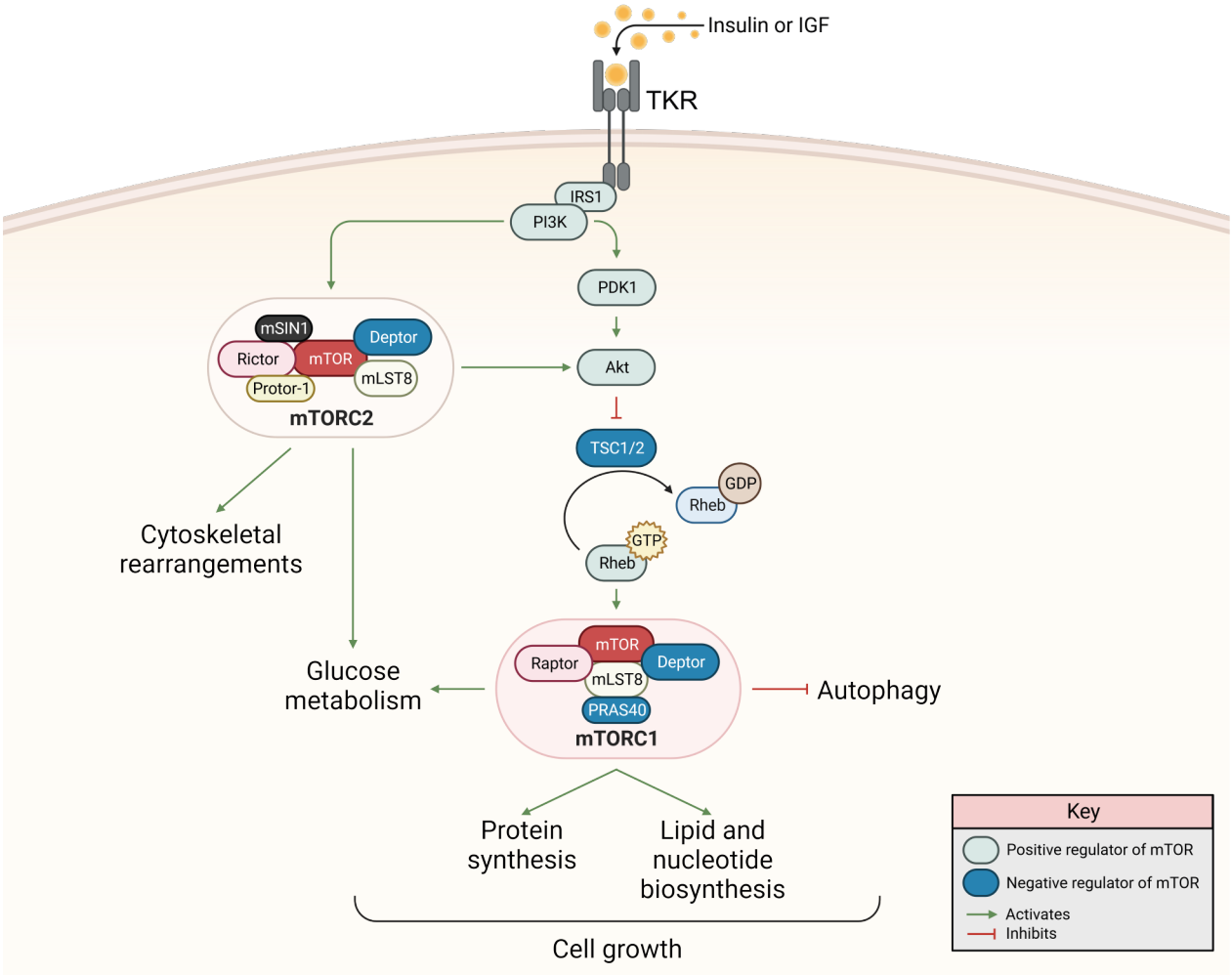

Figure 4 the mTOR signaling pathway at glance.
Schematic representation of the mTOR signaling pathway described in paragraph 1.3.1
Picture created with Biorender.com

mTOR functions as the catalytic subunit of two distinct complexes, namely mTORC1 and mTORC2, which differ in their composition, activation, substrates, and functions (Saxton & Sabatini, 2017). mTORC1 consists of three core components: Raptor, mLST8, and mTOR itself. Additionally, it includes two negative regulatory components called Deptor and PRAS40. While the exact roles of Raptor and mLST8 still remains to be clarified, it is believed that Raptor acts as a scaffolding protein necessary for the assembly of mTORC1 and the recruitment of its downstream effectors. On the other hand, mTORC2 comprises six components: Rictor, mSIN1, Protor-1, mLST8, Deptor, and mSIN1. Deptor serves as a negative regulatory subunit for both mTORC1 and mTORC2, while mSIN1 and Rictor are essential for mTORC2 assembly (Laplante & Sabatini, 2009).

mTOR functions as a rheostat, capable of sensing changes in both extracellular and intracellular cues and modulating the cellular response accordingly. Activation of tyrosine kinase receptor signaling by PI3K leads to the phosphorylation of AKT, a downstream target, by PDK1. AKT activation is required to inhibit the activity of the tuberous sclerosis complex (TSC), which exerts a negative control over mTORC1 by acting as a GTPase-activating protein (GAP) for Rheb1, a small GTPase. When the TSC complex is active, it promotes the hydrolysis of guanosine triphosphate (GTP) by Rheb, converting it to guanosine diphosphate (GDP). In its inactive state, Rheb1 fails to interact with and activate mTORC1. Activated AKT, in turn, phosphorylates TSC2 at specific sites, resulting in complete inhibition of the TSC complex. This inhibition allows Rheb1 to remain in its active GTP-bound state, fully activating mTORC1 (Laplante & Sabatini, 2009).

The intricate regulatory mechanisms involving mTOR, its complexes and interacting proteins play a pivotal role in cellular homeostasis and have implications for various physiological and pathological processes. Understanding these intricate pathways provides valuable insights into the molecular basis of diseases and may pave the way for the development of targeted therapeutic strategies (Saxton & Sabatini, 2017).

1.3.2. mTORC1 activation

mTORC1 activity is stimulated by a broad spectrum of intracellular and extracellular cues, including growth factors, amino acids and energy levels, aimed to maintain the correct balance between cellular behavior and the environment (Laplante & Sabatini, 2009).

Growth factors, such as insulin, insulin-like growth factor 1 (IGF1) or other mitogens, stimulate mTORC1 activity mainly via PI3K/AKT/TSC signaling cascade described above. Furthermore, growth factors can also modulate mTORC1 activity independently of TSC and Rheb1 through PRAS40, an endogenous inhibitor of mTORC1. Generally, PRAS40 associates with Raptor, thereby inhibiting Rheb-driven mTORC1 activation. However, upon insulin stimulation, Akt phosphorylates PRAS40, leading to its sequestration by the 14-3-3 protein and restoring mTORC1 activity. The duration and the extent of mTORC1 activation are also tightly regulated, in order to restore TSC activity after stimulation. As part of a negative feedback loop, mTORC1 substrate S6K1 directly phosphorylates and inhibits insulin receptor substrate 1 (IRS-1), blocking further the insulin-mediated activation of PI3K/AKT pathway (Saxton & Sabatini, 2017).

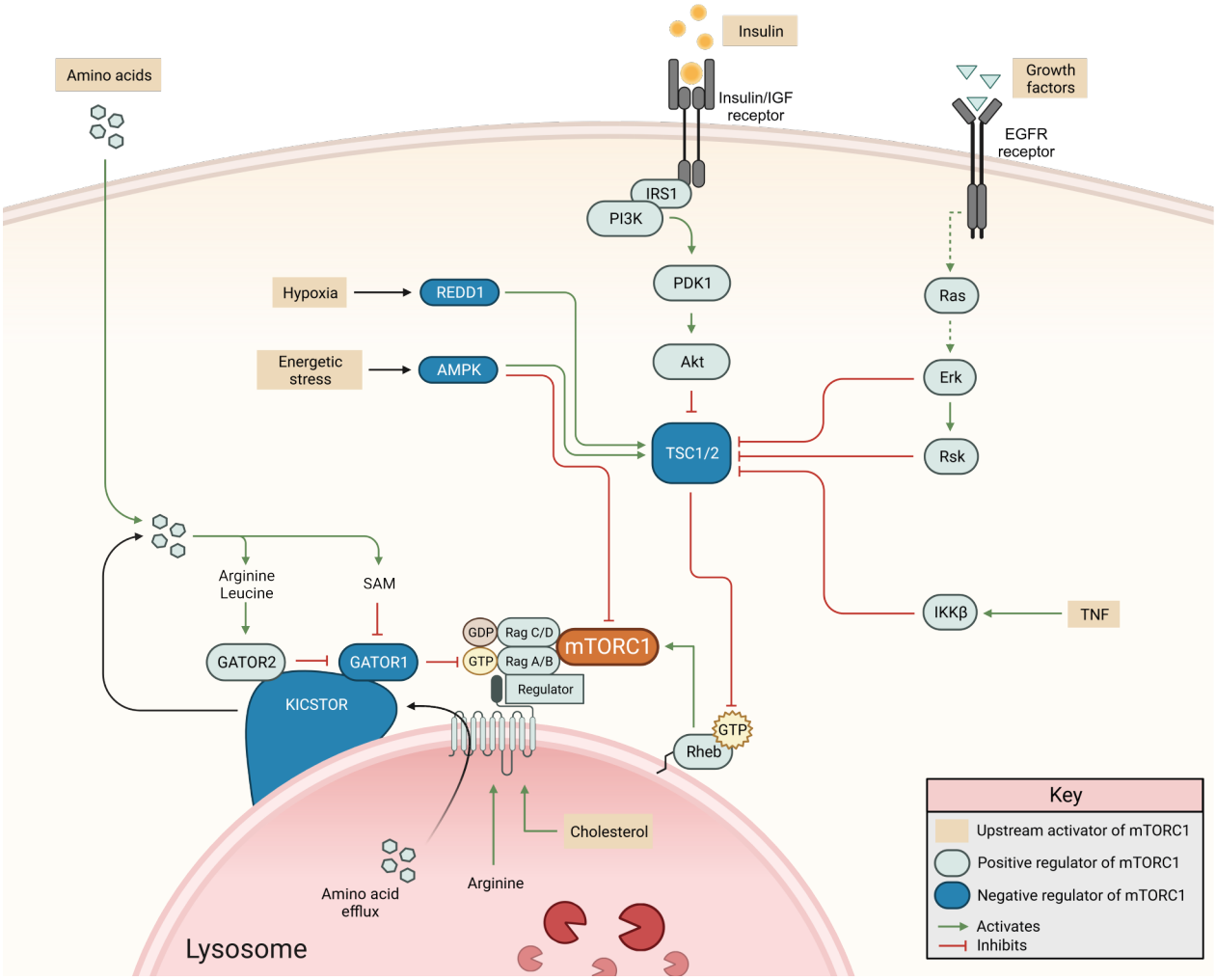

Figure 5 Upstream regulators of the mTORC1 signaling pathway

Positive upstream regulator of mTORC1 pathway described in paragraph 1.3.2.
Picture created with Biorender.com

mTORC1 activation by amino acids involves the Rag GTPases, heterodimeric proteins anchored to the lysosome by the pentameric Ragulator complex. Under nutrient-rich conditions, Rag GTPases interact with Raptor, leading to the recruitment of mTORC1 from the cytosol to the lysosomal surface. This allows mTORC1 to interact with lysosomal Rheb1, which, in turn, fully activate the mTORC1 kinase activity (G. Y. Liu & Sabatini, 2020; Saxton & Sabatini, 2017). However, new results indicate that Rheb1 is also anchored to ER/Golgi membranes. This would suggest that Rheb1 could funtion as a bridge, allowing mTORC1 to interact with ER/Golgi compartments. However, the recruitment of mTORC1 to the lysosomal surface is still an indispensable step for its complete activation (Hao et al., 2018).

Rag GTPases activity is controlled by GATOR protein complexes and Ragulator itself in response to a pool of amino acid. The GATOR1 complex functions as a GTPase-activating protein for RagA/B, thereby promoting the inactive GDP-bound state and inhibiting mTORC1 when cytosolic amino acid level fall. On the other hand, Ragulator promotes Rag activation by acting as a guanine nucleotide exchange factor. Furthermore, the activity of GATOR1 is regulated by several upstream factors: KICSTOR, a large protein complex that anchors GATOR1 onto the lysosome and is critical for cellular responses to amino acid deprivation; SAMTOR, which activates GATOR1 while being blocked by high level of S-adenosylmethionine; and GATOR2, which inhibits GATOR1 in the presence of high concentration of Leucine and Arginine. Although these core components significantly contribute, more players and steps in the nutrient-sensing mechanism are being discovered, highlighting the complexity of the mTORC1 regulatory network (G. Y. Liu & Sabatini, 2020; Saxton & Sabatini, 2017). Thus, mTORC1 integrates amino acid and nutrient signals through a complex mechanism, which allows appropriate tuning of cell growth and metabolic processes in response to environmental conditions.

The correct sensing of cellular energetics is fundamental to maintain the correct balance between anabolic and catabolic processes, both largely governed by mTORC1. An important metabolic checkpoint is represented by the AMP-activated protein kinase

(AMPK), a master regulator of cellular energy state. Glucose withdrawal or periods of intense metabolic exertion can deplete cellular ATP stores, leading to the consecutive increase in the AMP:ATP ratio. This triggers the activation of AMPK, which inhibits mTORC1 activity, both directly and indirectly. It directly phosphorylates Raptor, leading to mTORC1 deactivation and, simultaneously, it activates TSC2, a negative regulator of mTORC1. Conversely, adequate or surplus energy conditions strongly reduce the activity of AMPK, thereby restoring mTORC1 activity and allowing it to promote anabolic processes and cell growth (G. Y. Liu & Sabatini, 2020; Saxton & Sabatini, 2017).

1.3.3. mTORC1 regulation of protein synthesis

The major function of mTORC1 is to promote protein synthesis, the most energy-demanding anabolic process in growing cells, through which the genetic information stored in messenger RNAs is encoded into proteins (Buttgereit & Brand, 1995; Hershey et al., 2019a). mTORC1 regulate mRNA translation mainly through the phosphorylation of two main downstream effectors: the cap-dependent eukaryotic initiation factor 4E (eIF4E)-binding proteins (4EBPs), and the protein p70 S6 Kinase 1 (p70S6K1, abbreviated as S6K1).

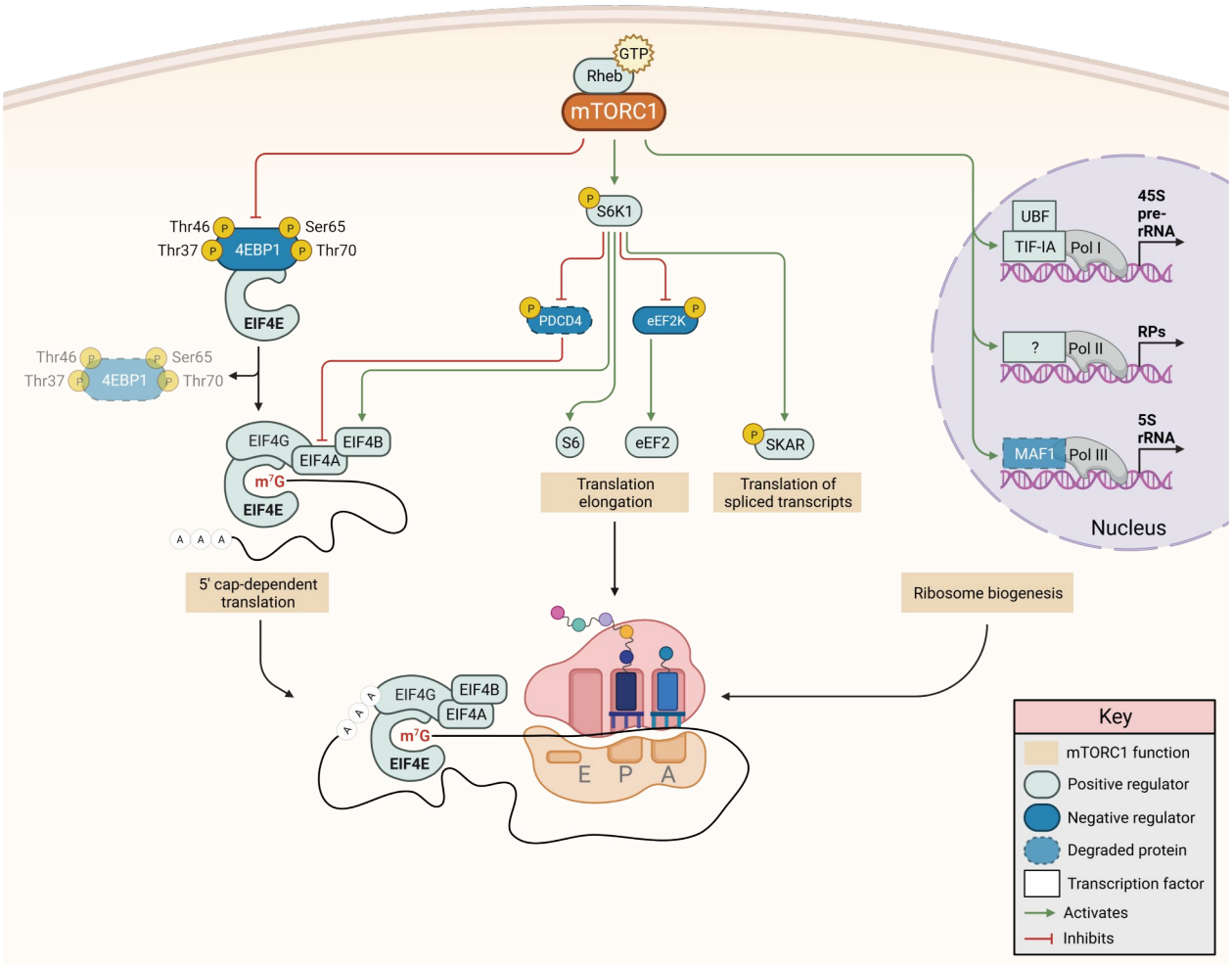

Figure 6 mTORC1 regulation of protein synthesis
Different downstream effectors of mTORC1 regulating translation initiation and elongation, and ribosome biogenesis described in paragraph 1.3.3.
Picture created with Biorender.com

Among three isoforms that have been discovered over the last decades (4EBP1, 2 and 3), 4EBP1 is the best characterized protein (Poulin et al., 1998). Seven phosphorylation sites have been described in the human 4EBP1, such as Thr-37, Thr-46, Ser-65, Thr-70, Ser-83, Ser-101, and Ser-112. Of note, the first five phosphorylation sites are phylogenetically conserved among all species (Qin et al., 2016). Phosphorylation of Thr-37 and Thr-46 is considered as a priming event and causes a conformational change in 4EBP1 allowing the phosphorylation of Thr-70 and Ser-65 (Gingras et al., 1999a, 2001a). Although Thr-37 and Thr-46 have been proved to be phosphorylated by mTOR *in vitro*, they are not inhibited by Rapamycin ; Thr-70 phosphorylation, on the other hand, has been shown to be mTOR-independent (Thoreen et al., 2009) and likely targeted by another kinase, such as Erk2 (Herbert et al., 2002). In quiescent cells, 4E-BPs largely remain unphosphorylated and suppress cap-dependent translation by sequestering the cap-binding protein eIF4E, a key translation factor that binds to mRNA molecules containing a m^7G cap structure at the 5' end (Matsuo et al., 1997). Therefore, the function of 4EBPs is exclusively to regulate cap-dependent, but not cap-independent, translation at the initiation stage (Pause et al., 1994). In a nutrient-enriched cellular environment, mTORC1 signaling activation leads to hyperphosphorylation of 4EBPs and release of eIF4E, enabling it to associate with eIF4G1/eIF4G3, two scaffold proteins that bind to and activate the DEAD-box RNA helicase eIF4A. Collectively, all these factors form the heterotrimeric initiation factor complex eIF4F (Sonenberg & Hinnebusch, 2009), a fundamental step that allows initiation of translation. The subsequent binding of the eIF4F complex with the poly-A binding proteins (PABPs) promotes mRNA activation and circularization, allowing the ribosomal 43S pre-initiation complex to bind within the 5' end of the mRNA to search for the start codon AUG. Finally, the recognition triggers the release of several translation factors involved in the earlier stages and facilitates the joining of the ribosomal 60S subunit, resulting in the formation of the 80S complex. The ribosome is now ready to move along the mRNA transcript, adding amino acids to the growing polypeptide chain by base pairing of corresponding aminoacyl-tRNA until it encounters a stop codon, thereby causing the termination of protein synthesis and the initiation of ribosome recycling (Jackson et al., 2010).

mTORC1 also phosphorylates S6K1 on its hydrophobic motif (T389), leading to its kinase activation (Magnuson et al., 2012). The best characterized function of the kinase is to phosphorylate its namesake target, the ribosomal protein S6 (RPS6), an evolutionary conserved protein localized on the ribosomal 40S subunit (Meyuhas, 2015). Although mice with mutations in RPS6 phosphorylation have been associated to impaired glucose homeostasis and reduced muscle strength, its functional role at the molecular level has not been fully elucidated. One hypothesis is that its location on the small ribosomal subunit may influence ribosome activity during translation initiation or elongation. S6K1 also supports translation initiation by phosphorylating the initiation factor eIF4B, a positive regulator of cap-dependent translation, and the eIF4A inhibitor programmed cell death 4 (PDCD4), an inhibitor of the mRNA helicase eIF4A. PDCD4 phosphorylation promotes its own degradation by the proteasome, enabling eIF4A to unwind secondary structures located within the 5'-untranslated region (5'-UTR) of the mRNA (Dorrello et al., 2006). Additionally, in concert with mTORC1, S6K1 seems to be involved in the regulation of ribosome biogenesis by upregulating the transcription of ribosomal RNA (rRNA), the dominant component of newly assembled ribosomes (Chauvin et al., 2013). This is achieved by enhancing the activity of RNA polymerase I and III, through the phosphorylation of the regulatory factors upstreaming binding factor (UBF), the transcription factor 1A (TIF-1A) and MAF1 (Hannan et al., 2003; Mayer et al., 2004; Michels et al., 2010; Shor et al., 2010).

Taken together, both 4EBPs and S6Ks regulatory features lead to multifaceted effects that regulate protein synthesis.

1.3.3.1. mTOR-dependent translation regulation of gene expression

In response to environmental changes, cells must rapidly reprogram themselves via a spatiotemporal coordination of multiple gene expression layers. Relative to protein synthesis, gene expression regulation can be mediated by *trans*-activing regulatory proteins, such as RNA-binding proteins (RBPs), which specifically recognize *cis*-elements in mRNAs, such as nucleotide sequences, secondary structures or combinations thereof. These features are generally placed in the untranslated regions (UTRs) of mRNA, although some have also been reported to localize in coding regions. One of the best

examples of selective translation is mediated by mTORC1 itself. Specifically, mTORC1 promotes the translation of mRNAs with 5' oligopyrimidine tracts, defined as "TOPs/TOP-like" motifs, which interact with components of the translational machinery, including ribosomal proteins (Hershey et al., 2019). This occurs via a 4EPB1- and S6K-independent mechanism and it involves three mTORC1 effectors, the RBPs TIA-1, TIAR and LARP1 (G. Y. Liu & Sabatini, 2020; Saxton & Sabatini, 2017).

Translation control is also mediated by the cap-mRNA binding protein eIF4E through various mechanisms. Generally, increased eIF4E activity has only a marginal effect on global translation, but it strongly boosts the translation of certain mRNAs subsets characterized by long and highly structured 5' UTRs (Hershey et al., 2019). Some of these are particularly relevant in the context of immunology, such as the transcription factors IRF7 and GATA-3, and the cytokine IL-4. In addition, a second set of eIF4E-sentitive mRNAs is translationally regulated via the mitogen-activated protein kinase (MAPK)-MNK1 and MNK2 signaling cascade, which phosphorylate eIF4E on a single serine residue (Ser209) (Piccirillo et al., 2014). Interestingly, the set of mRNAs sensitive to phospho-eIF4E are equally involved in the regulation of immune functions, such as the transcription factor IRF8 (H. Xu et al., 2012), the chemokine CCL5 (RANTES)(Nikolcheva et al., 2002), the transcription factor NF-κB inhibitor IκBα (Herdy et al., 2012).

In conclusion, mTORC1 signaling and its own downstream effector eIF4E act as a translation control hub that can specifically regulate the upregulation of certain genes, including immune genes.

1.3.4. mTORC1 regulation of energetic homeostasis

mTORC1 regulates energetic homeostasis in response to various upstream environmental cues such as nutrient levels, energy availability as well as stress signals. The integration of such a complex cellular network is crucial for supporting cell growth, proliferation and survival (G. Y. Liu & Sabatini, 2020; Saxton & Sabatini, 2017).

mTORC1 positively promotes lipid biosynthesis by activating the transcription factors Sterol Regulatory Element Binding Protein 1/2 (SREBP1/2) and peroxisome proliferator-activated receptor γ (PPARγ). Through an S6K-dependent mechanism, SREPBs activation induce the expression of genes involved in the biosynthesis of fatty acids and

cholesterol, which are needed for the formation of new membranes as cell size increases. Additionally, mTORC1 also catalyzes the phosphorylation of Lipin 1, a phosphatidic acid phosphatase localized in the nucleus. When phosphorylated, Lipin 1 is expelled from the nucleus and facilitates the nuclear accumulation of SREBPs (G. Y. Liu & Sabatini, 2020; Saxton & Sabatini, 2017).

To sustain cellular proliferation, mTORC1 promotes the biosynthesis of de-novo purine and pyrimidine nucleotides, which are essential for DNA replication and rRNA synthesis. This is achieved through two major mTORC1 downstream effectors. For the purine synthesis, mTORC1 promotes the activation of the activating transcription factor 4 (ATF4) and its downstream target, the mitochondrial enzyme methylene tetrahydrofolate dehydrogenase 2 (MTHFD2). On the other hand, mTORC1/S6K1 axis promotes the activation of the rate-limiting enzyme responsible for pyrimidine biosynthesis, the carbamoyl phosphate synthetase 2, aspartate transcarbamylase, dihydroorotase (CAD) (G. Y. Liu & Sabatini, 2020; Saxton & Sabatini, 2017).

Activation of mTORC1 also dictates the metabolic fate of glucose through several mechanisms in order to support cell growth. First of all, mTORC1 enhances glycolysis by promoting the expression of glycolytic enzymes through the activation of the hypoxia-inducible factor 1-alpha (HIF1α). In the same context, SREBPs also contribute to boost the metabolic flux through the pentose phosphate pathway, which supplies NADPH and carbon-rich precursors for lipid and nucleotide biosynthesis. To sustain the vast energy demand needed for cell growth, mTORC1 also promotes mitochondria biogenesis through the formation of yin-yang 1 (YY1)-PPARγ coactivator 1α (PGC1α), and the 4EBP1-dependent translation of nuclear-encoded mitochondrial transcripts (G. Y. Liu & Sabatini, 2020; Saxton & Sabatini, 2017).

In summary, mTORC1 plays a central role in controlling key metabolic processes that underpin cellular growth and survival, responding to various environmental and intracellular signals.

1.3.5. mTORC1 regulation of autophagy and catabolism

mTORC1 plays a critical role in the regulation of autophagy, a catabolic cellular process involved in the degradation of damaged organelles, misfolded or aggregated proteins and biomolecules which takes place in the lysosome (G. Y. Liu & Sabatini, 2020; Saxton & Sabatini, 2017). The intracellular degradation ensures a correct balance between the synthesis, degradation and recycling of cellular components in response to nutrients level and intracellular and extracellular cues, representing an alternative avenue of energy source (G. Y. Liu & Sabatini, 2020; Saxton & Sabatini, 2017). mTORC1 negatively regulates autophagy, acting on both early and late stages of this process. Under nutrient-replete conditions, during which mTORC1 activity is upregulated, it phosphorylates two key autophagy-initiating proteins, such as Unc-51-like kinase 1 (ULK1) and autophagy-related gene 13 (ATG13). This prevents the initiation of autophagy by blocking the formation of autophagosomes, vesicles responsible for engulfing cellular components for degradation (Hosokawa et al., 2009; J. Kim et al., 2011). On the other hand, active mTORC1 also phosphorylates ultraviolet irradiation resistance–associated gene (UVRAG) as well as Rab7, causing respectively the suppression of the autophagosome-lysosome fusion and late endosome maturation into lysosomes (Y. M. Kim et al., 2015). By regulating autophagy in response to nutrient availability, mTOR acts as a crucial switch that fine-tunes cellular processes, ensuring the efficient utilization of resources and maintenance of cellular integrity.

1.4. The role of mTOR signaling in the regulation of immune responses

The first evidence that mTORC1 signaling plays a role in regulating myeloid immune responses was reported by Weichhart *et al.* in 2008 (Weichhart et al., 2008). Upon LPS or *Staphylococcus aureus* cells (SAC) exposure, mTOR inhibition by Rapamycin boosts the production of pro-inflammatory cytokines, such as IL-12p40, IL-6, TNF-α and IL-23, and decreases the expression of the anti-inflammatory cytokine IL-10 in human PBMC, primary human monocytes and myeloid DCs. These findings have been further corroborated in $Tsc2^{-/-}$ murine embryonic fibroblast (MEF) transfected with an IL-12p40 luciferase reporter plasmid. TSC2 is a negative regulator of mTOR, therefore $Tsc2^{-/-}$ cells have a constitutive activation of the mTOR kinase. In LPS-stimulated $Tsc2^{-/-}$ MEFs, mTOR

hyperactivation causes a marked decrease of IL-12p40 and a partial decrease of IL-6, accompanied by an increase of IL-10 compared to $Tsc2^{+/+}$ MEFs. Similarly, TSC2-silenced THP-1 cells yield the same outcome (Weichhart et al., 2008). At a molecular level, the immunostimulatory effect of mTOR inhibition can be explained by several independent mechanisms. Upon LPS stimulation, mTORC1 negatively regulates the activity of the transcription factor NF-κB (Weichhart et al., 2008), a master regulator of the immune response controlling the expression of pro-inflammatory cytokines (T. Liu et al., 2017). Indeed, the inhibition of mTOR by Rapamycin leads to an increase of DNA-binding activity of NF-κB by activating the p65-transactivation domain (Weichhart et al., 2008), which is a requisite for recruiting co-factors enhancing the transcription of NF-κB-dependent genes (Perkins, 2007). These results are also confirmed in a more recent report, where genetic loss of mTOR and Raptor, a positive regulator of mTOR functions, enhanced the M1 macrophage phenotype in $mTOR^{fl/fl}$ and $Raptor^{fl/fl}:LysM^{Cre}$ BMDMs both *in-vitro* and *in-vivo* models of sepsis and influenza infection (Collins et al., 2021). This work expands our understating about the molecular features of mTOR inhibition. Indeed, the loss of mTOR and Raptor promotes histone acetylation of H3K27 at both IL-6 and TNF-α promoters, which is directly linked to a decreased glycolysis and oxidative phosphorylation observed in $mTOR^{fl/fl}$ and $Raptor^{fl/fl}:LysM^{Cre}$ BMDMs (Collins et al., 2021). The low metabolic flux leads to a lower production of NAD^+, an essential co-factor of class III histone deacetylase Sirt1, thereby impairing its activity. A reduced Sirt1 activity is also observed upon Rapamycin treatment, linking these results with the previous evidences by Weichhart and co-workers (Weichhart et al., 2015). Since Sirt1 also regulates the acylation status of the NF-κB subunit p65 (H. Yang et al., 2012), these epigenetic changes along with a metabolic reprogramming induced by mTOR inhibition are collectively responsible for a shift towards an enhanced pro-inflammatory profile. At the same time, pharmacological or genetic inhibition of mTORC1 inhibits IL-10 expression at the transcriptional level through at least three non-mutually exclusive mechanisms: 1) by reducing the phosphorylation of the transcription factor STAT3 and its activity (Weichhart et al., 2008); 2) by blocking the induction of the transcription factor MAF under the control of mTOR-S6K-PDCD4-TWIST2 axis (Weichhart et al., 2015); and 3) by enhancing the activity of GSK3-β, which in turn blocks the nuclear translocation and the activity of the transcription factor CREB (Weichhart et al., 2015).

1.5. mTOR regulation of microglia functions

Several reports have indicated so far that mTOR signaling is also essential for the regulation of microglia functions, with either beneficial or detrimental outcomes based on the context investigated. One of the first reports was based on experiments to clarify the role of microglia activation in cerebral ischemia, a condition leading to extensive neuronal death due to hypoxia (Lu et al., 2006). Exposure of primary rat microglia and BV2 cell line to lower oxygen availability led to induction of nitric oxide synthase (iNOS) with the consecutive production and release of nitric oxide (NO), a free radical which is neurotoxic at higher concentration. NOS is induced upon HIF-1α activation, a transcriptional factor involved in regulating cellular responses to hypoxic conditions, and it is under mTORC1 regulation. Indeed, inhibition of mTORC1 with rapamycin significantly decreased the expression of HIF-1α and iNOS in microglia under hypoxia conditions, demonstrating for the first time that PI3K/mTORC1/HIF-1α signaling is involved in the regulation of NO production in microglia (Lu et al., 2006). Daojing Li and coworkers further highlighted that mTORC1 is involved in the regulation of microglia immune responses following brain ischemia and stroke (Li et al., 2016). The inhibition of mTORC1 with Rapamycin or in $Raptor^{fl/fl}CX3CR1^{CreERT}$ mice significantly reduced brain lesions size and edema, attenuated behavioral deficits and improved post-stroke inflammation after middle cerebral artery occlusion (MCAO), a model employed to mimic ischemia in mice (Li et al., 2016). Additionally, mTORC1 inhibition resulted in reduced microgliosis to the site of injury and strongly downregulated the production of inflammatory mediators (Li et al., 2016). These reports indicated an anti-inflammatory role of mTOR inhibition, contrary to what had been reported by Weichhart et *al.* in other myeloid cells (Weichhart et al., 2008b, 2015).

mTORC1 activation in microglia has been also proved to be beneficial in mouse models of Alzheimer's diseases (AD) (Shi et al., 2022). Indeed, selective loss of *Tsc1*, a negative regulator of mTOR, increased Aβ clearance, improved lysosome function, reduced spine loss and ameliorated cognitive functions in 5XFAD mice (Shi et al., 2022). Interestingly, mTORC1 activation also led to the upregulation of TREM2 expression (Shi et al., 2022), a microglia receptor associated with an elevated risk of developing AD when its activity is compromised (Hou et al., 2022). On the other hand, mTOR inhibition by a short and long

treatment with Rapamycin reverted this phenotype, further corroborating a previous report that maintaining an active mTOR signaling is essential to restore cellular bioenergetics that are impaired in AD (Ulland et al., 2017).

Collectively, these results sustain the importance of mTOR signaling in the regulation of microglia immune response and phenotype in different conditions.

1.6. mTOR-dependent translation is upregulated in aged microglia

The microglia research field has greatly progressed in the last decade. High throughput methods have provided a more comprehensive understanding of their functions, nonetheless, molecular mechanisms that are responsible for the aged microglia phenotype have not been fully elucidated yet. To this end, our publication (Keane et al., 2021) was the first to implicate increased mTOR signaling in aged microglia. In the following paragraphs of this chapter, I will describe the results generated by Lily Keane and other lab members, in order to introduce my contribution.

1.6.1. The microglia aging phenotype already starts by middle age

In order to investigate what molecular features are responsible for the age-related microglia phenotype, FACS-sorted microglia were purified from young (6-months), middle-aged (15-months) and old (23 months) C57BL/6J animals and subjected to RNA-Seq analysis (Figure 7A, schematic). Principal component analysis (PCA) of microglia samples revealed a distinct clustering of samples based on age (Figure 7B). About 805 genes were found to be differently expressed between young and aged groups, of which 344 genes were commonly shared between young versus aged and middle-aged versus young comparisons (Figure 7C). Interestingly, a large number of genes was expressed in a monotonic fashion, with either upregulated or downregulated in middle-aged mice and further increased or decreased in older mice (Figure 7C). Relative to neuroinflammation, aged microglia upregulated a certain number of inflammatory genes, such as pro-inflammatory cytokines (*Csf1*, *Tnf*, *Il1a,* and *Il1b*), cytokine receptors such as *Il1r* and *Il2rb2* receptor subunit (Figure 7D – top left panel); and chemokines (Figure 7D – bottom left panel). Furthermore, genes involved in microglia priming such as *Anxa5*, *Cd52*, *Apoe*, *Axl*, *Lgals3bp*, *Tlr2*, *Clec7a* (*dectin-1*), *Cd11c*, *Cst7,* and *Spp1* were significantly

upregulated in microglia at 15 months of age, suggesting that microglia were already primed at middle-age, with the phenotype becoming more defined by 23 months (Figure D – top right panel).

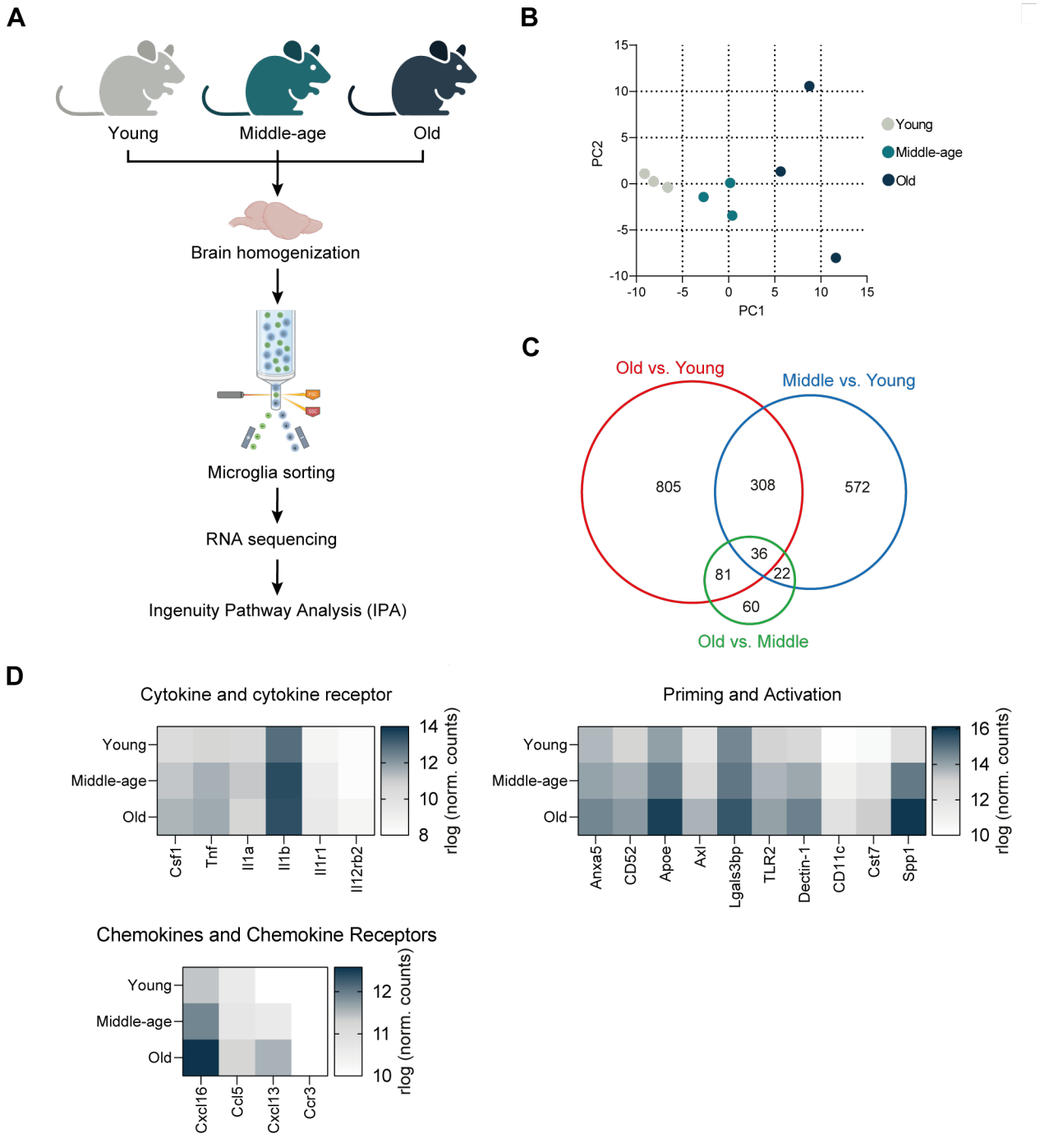

Figure 7 Microglia phenotype changes by middle age.
(**A**) Workflow of FACS-sorted microglia isolated from young (6 months), middle-age (15 months) and old (22 months) Wild-type animals, subjected to bulk RNA-sequencing and pathway data analysis. (**B**) Principal component analysis (PCA) of RNA-seq analysis from

microglia samples from young (grey), middle-age (dark cyan) and aged (dark blue). (**C**) Venn diagram showing differently expressed genes across comparisons, based on DESeq2 FDR-corrected *P* values. (**D**) Rlog-normalized counts of cytokines and cytokines receptor (top left panel), microglia priming genes (top right panel) and chemokines and chemokines receptor, based on the DESeq2 analysis. Data extracted from Keane et al., 2021.

1.6.2. mTOR-dependent translation increases with age

Ingenuity Pathway Analysis (IPA) of differently expressed genes between young and aged microglia showed that three top main pathways controlling mRNA translation are dysregulated in ageing: a) eIF2 signaling, b) mTOR signaling, and c) eIF4E and p70S6K signaling; the latter is downstream of the mTORC1 pathway (Figure 8A). Notably, many genes encoding for ribosomal proteins and subunits of the eIF3 initiation complex were commonly shared by the three pathways and found upregulated with age (Figure 8B). Despite a clear indication of an aging effect on protein synthesis regulation via mTORC1 signaling, IPA could not determine whether these pathways were upregulated or downregulated, due to low z-score. To elucidate this point, phosphorylation of the two key downstream effectors of mTORC1-dependent translation, namely 4EBP1 and the ribosomal protein S6, was examined in adult microglia over the mouse lifespan. Phospho-flow cytometry analysis revealed an age-dependent increase of phospho-4EBP1 at threonine 37/46 (Figure 8C). On the other hand, S6 phosphorylation at serine 240/244 showed very higher level already at young age, with a milder increase with age (Figure 8D). These findings suggested that 4EBP1 signaling was significantly more affected by age-related changes in microglia and this is why I subsequently focused my attention on 4EBP1.

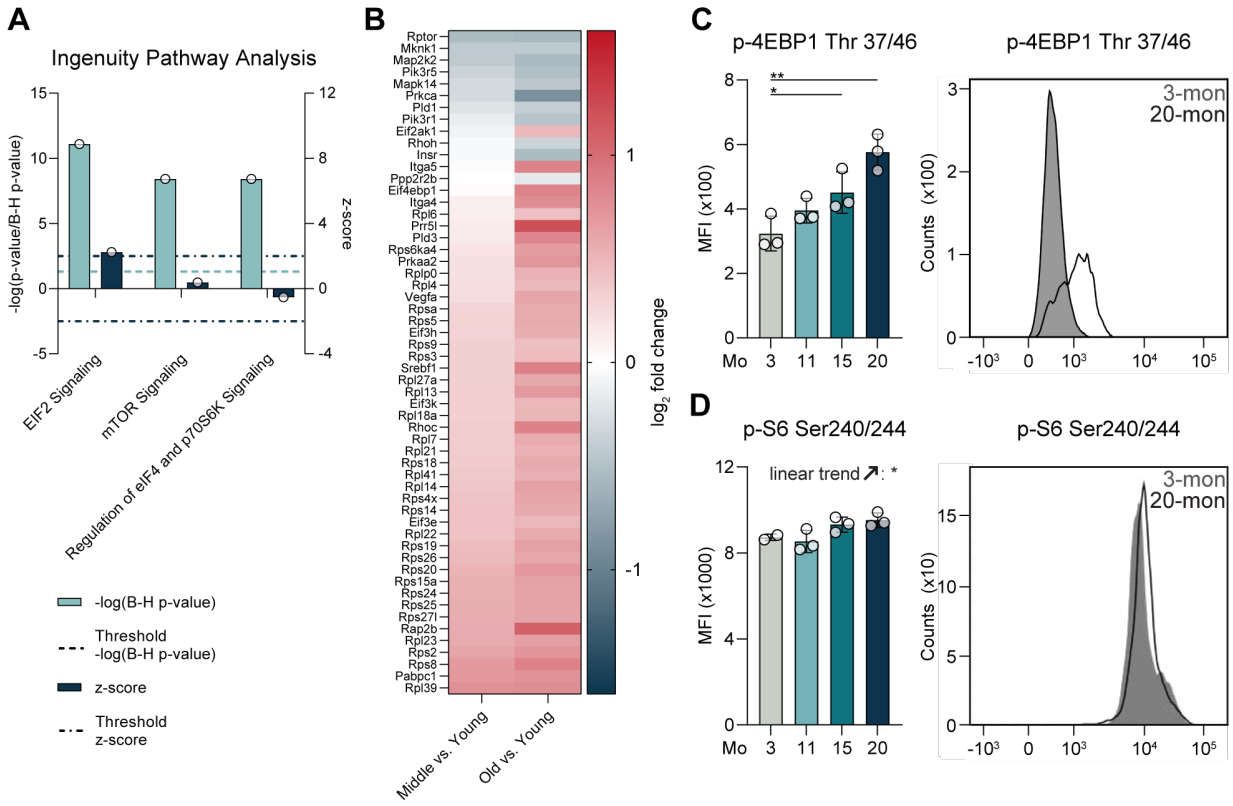

Figure 8 The mTOR pathway is dysregulated in microglia with age.
(**A**) Ingenuity Pathway Analysis (IPA) based on all differentially expressed genes between young and old microglia RNA-Seq data, showing the 3 most significantly dysregulated pathways. Data shown in light blue are –log(*P* value) with Benjamini and Hochberg correction for multiple comparisons. For each pathway, the *z* score is shown in dark blue. (**B**) Heatmap showing differentially expressed genes in at least 1 of the 3 most significant IPA pathway hits in middle-aged versus young and old versus young microglia, *n* = 3 for both groups. (**C** and **D**) Flow cytometry analysis of (**C**) p-4EBP1 Thr37/46 and (**D**) p-S6 Ser240/244 in adult microglia isolated from 3-, 11-, 15-, and 20-month-old female mice shown as Median Fluorescence Intensity (MFI). Panels on the right-hand side are representative histograms for p-4EBP1 and p-S6. *n* = 3 for all groups. (All data are represented as mean ± SD; **P* < 0.05, ***P* < 0.01; 1-way ANOVA). Data extracted from Keane et al., 2021.

1.6.3. Enhanced translation boosts aged microglia responses solely at protein level

To define whether the increase of phospho-4EBP1 and p-S6 in ageing microglia correlated with the aged microglia phenotype and increased microglia activation, young (3 months) and old (16 months) mice were challenged with a sublethal dose of LPS (5 mg/Kg) via an intraperitoneal (i.p) injection for 4 hours. Notably, aged microglia exhibited an increase in 4EBP1 and S6 phosphorylation upon LPS treatment (Figure 9A). Given the role of mTORC1 in protein synthesis regulation (see paragraph 1.3.3), transcription and protein content of pro-inflammatory mediators were assessed in isolated adult microglia. As expected, the systemic inflammation caused a strong induction of cytokine transcription, however, no differences were detected between young and aged groups (Figure 9B – left panels). On the other hand, there was a notable increase in the protein production of the investigated cytokine in aged microglia compared to controls (Figure 9B – right panels). Collectively, these findings indicated that mTORC1 pathway is upregulated in microglia with age and it might boost microglia inflammatory phenotype through increased mTOR-dependent translation of inflammatory genes.

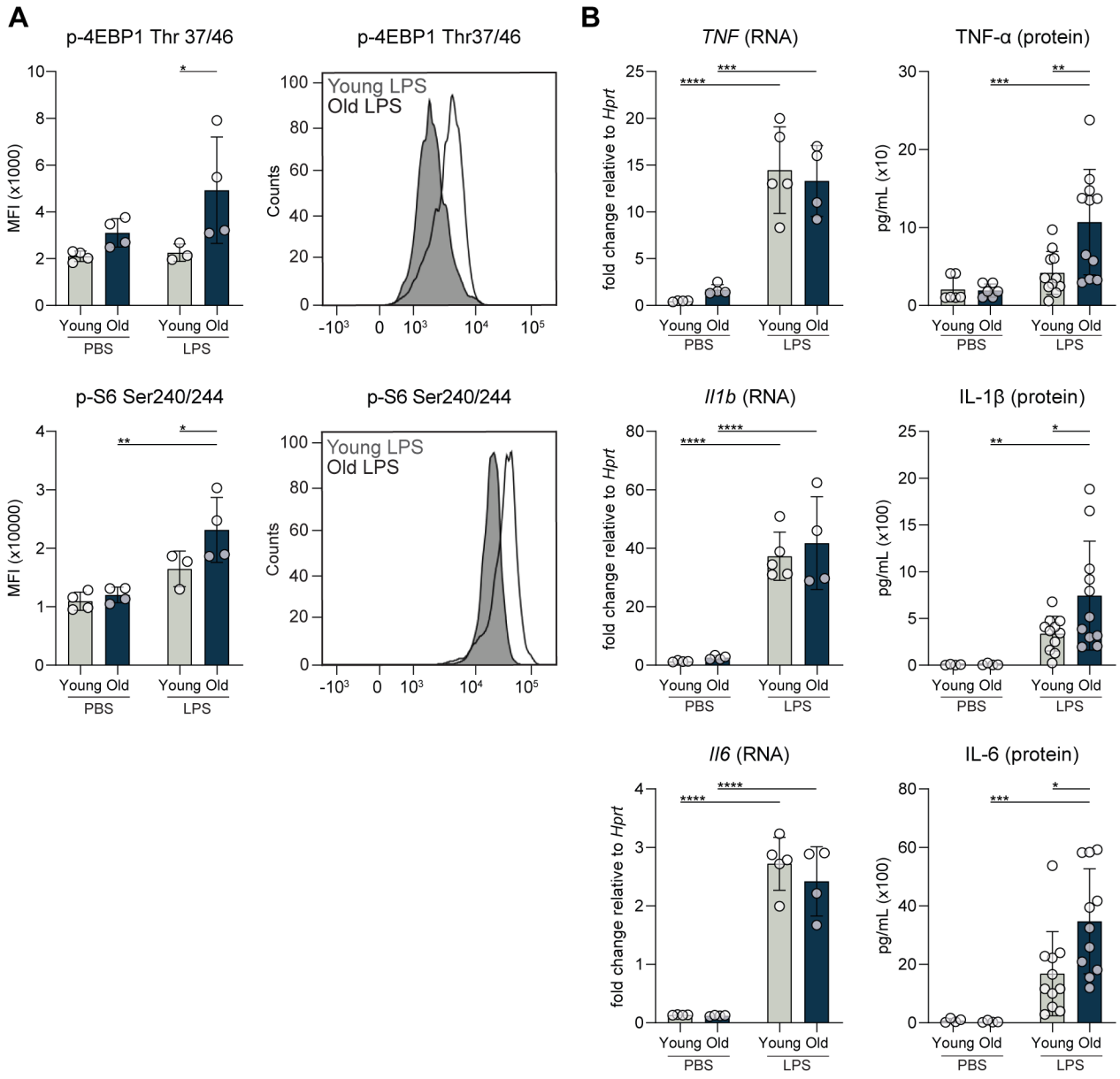

Figure 9 Microglia from LPS-challenged aged mice show increased 4EBP1 and S6 phosphorylation, together with increased cytokine production only at the protein level.

Female mice, 3 and 16 months old, were subjected to an intraperitoneal injection of PBS or 5 mg/kg of LPS and euthanized 4 hours later. (**A**) Flow cytometry of p-4EBP1 Thr37/46 (upper panels) and p-S6 Ser240/244 (lower panels) in microglia isolated from 3- and 16-month-old mice after LPS or PBS treatment (n = 3–4). (**B**) Gene expression and protein levels of inflammatory cytokines in microglia after in vivo LPS challenge. Left panels: Gene expression measured by RTqPCR, reported as fold change relative to *Hprt* expression. Right panels: protein levels assessed in microglia protein lysates, measured with the Legendplex assay system (n = 4–10). All data are represented as mean ± SD *P < 0.05, **P < 0.01, ***P < 0.001, ****P < 0.0001; 2-way ANOVA. Data extracted from Keane et al., 2021.

2. Material and Methods

2.1. Equipment

Table 2.1 Equipment

Equipment	Supplier
Balances	Precision Balance 2100g, Fisher Scientific Analytical Balance 210g, Fisher Scientific
Beakers	Schott
Bio Imaging System	Stella 3200, Raytest
Cell counter	CASY Cell Counter and Analyzer, OMNI Life Science
Centrifuges	Megafuge 40-R TX-1000, Thermo Scientific Centrifuge 5424 R, Eppendorf Centrifuge 5424, Eppendorf
Flow Cytometer	FACSymphony A5, BD Bioscience FACSCelesta, BD Bioscience
Fluorometer for nucleic acid quantification	Qubit 4 Fluorometer, Invitrogen
Forceps	F.S.T. (Fine Science Tools)
Freezer	Liebherr
Gel electrophoresis chambers	Mini Gel Tank, Invitrogen XCell SureLock Mini-Cell, Invitrogen Owl EasyCast B1 and B2 Mini, Thermo Scientific Biometra Compact L/XL, Analytic Jena
Gel electrophoresis power supplies	Power 300 XL, Fisher Scientific Power Supply Mini 300V Plus, Fisher Scientific
Glass bottles	Schott
Heating blocks	ThermoMixer F1.5, Eppendorf ThermoMixer C, Eppendorf

Ice machine	Manitowoc RF0266A
Incubator	Incu-Line, VWR ICO 240, Memmert
Laminar flow hood	Safe2020 Class II, Thermo Scientific
Measuring cylinders	Schott
Microplate reader	FLUOstar Omega, BMG Labtech
Microscope	ZOE™ Fluorencent Cell Imager, BioRad LSM700, Zeiss LSM900, Zeiss LSM980, Z
Microwave	MW 7875, Severin
Motorized pipette controller	FisherBrand
PCR cycler	C1000 Touch Thermal Cycler, BioRad
pH Meter	Accumet AE150, Fisher Scientific
Pipettes	Research plus Single-channel, Eppendorf Multipette E3, Eppendorf Pipetman L Multichannel, Gilson
Plate shaker	Titramax 100, Heidolph Instruments
qPCR cycler	StepOnePlus, Applied Biosystems
Rocker	Compact Digital Rocker, Thermo Scientific Compact Digital Waving Rotator, Thermo Scientific Titramax101, Heidolph
Scalpel and blade	F.S.T. (Fine Science Tools)
Scissors	F.S.T. (Fine Science Tools)
Seahorse Flux Analyzer	Seahorse XFe96 Analyzer, Agilent
Spectrophotometer for DNA, RNA and protein	DS-11 Spectrophotometer, DeNovix
Vortex shaker	Vortex-Genie 2, Scientific Industries
Waterbath	Type 1013, GFL

2.2. Consumables

Table 2.2 Consumables

Item	Supplier
1.2 ml microtubes	Starlab International
CASYcups	OMNI Life Science
Cell strainer nylon, 70 µm	Sarstedt
Clear bottom, black-walled 96-well plates	Greiner bio-one
CombiTips Advanced®	Eppendorf
Conical centrifuge tubes (15 mL/ 50 mL)	Greiner bio-one
Cover slips, 12 mm, No.1	VWR
Culture plates (6-well/ 12-well/ 24-well/ 96- well, flat-bottom)	Cellstar®, Greiner bio-one
Disposable Centric Luer Two-Part Syringe (5 mL) Inject®	Braun
ELISA plates Costar® (96-well, half-area)	Corning
Gloves	Kimtech
MS columns	Miltenyi Biotec
LS columns	Miltenyi Biotec
Microscope slides (Superfrost plus)	Epredia
Needle, Microlance™ 27 G	Becton Dickinson
Omnican™ 20 U Insulin Injection Syringe	Braun
Parafilm®	Bemis®
PCR tubes, Multiply®.µStrip Pro	Sarstedt
Pipette tips	TipOne, Starlab SureOne, Fisher Brand
Plate sealer ELISA, Thermowell ™ Sealing Tape	Corning
Plate sealer qPCR, MicroAmp™ Optical Adhesive Film	Applied Biosystems, Life Technologies™
PVDF membranes, Immobilon®	Millipore®

qPCR plates, MicroAmp® Fast Optical	Applied Biosystems, Life Technologies™
Round-bottom polystyrene tubes (5 mL)	Falcon
SealSafe tubes (1.5 mL/ 2 mL/ 5 mL)	Sarstedt
Serological pipettes (2 mL/5 mL/ 10 mL/ 25 mL/ 50 mL)	Cellstar®, Greiner bio-one
V-bottom 96-well plates	Greiner bio-one

2.3. Chemicals, reagents and enzymes

Table 2.3 Chemical, reagents and enzymes

Item	Supplier
100 bp DNA ladder	New England Biolabs
4EGI-1	Merk
Agarose	Biozym
Bafilomycin A1	Sigma-Aldrich
Bicinchoninic acid	Sigma-Aldrich
Bovine serum albumin	Sigma-Aldrich
Cell Dissociation Buffer	Gibco
Cycloheximide ready made solution	Sigma-Aldrich
DNase/RNase-free water	Sigma-Aldrich
DL-Dithiothreitol, 1M aqueous solution	Sigma-Aldrich
Donkey serum	Sigma-Aldrich
Double distilled water	Sigma-Aldrich
Dulbecco's Modified Eagle Medium D5761	Sigma-Aldrich
Dulbecco’s Phosphate Buffered Saline w/o Ca^{2+}/Mg^{2+}	Sigma-Aldrich
CASY ton	OMNI Life Science
DAPI (4′,6-Diamidino-2-phenyl-indol –dihydrochloride)	Biotium
ECL	Thermo Scientific
eFT508	MedChemExpress
Ethylenediaminetetraacetic acid (EDTA), 0.5 M solution	Invitrogen

FACS Clean Solution	Becton Dickinson
FACS Flow	Becton Dickinson
FACS Rinse Solution	Becton Dickinson
Fetal calf serum	PAN
Fixable Viability Dye	Invitrogen
Goat serum	Sigma-Aldrich
GlutamaX	Gibco
Heparin sodium salt	Sigma-Aldrich
Hank's Balanced Salt Solution (HBSS), Ca^{2+}/Mg^{2+}-free	Gibco
Hank's Balanced Salt Solution (HBSS), sterile	Gibco
LPS from E. coli 0111:B4	Sigma-Aldrich
MyTaq Red 2x	Meridian Bioscience
Nonidet P 40 Substitute solution	Sigma-Aldrich
NuPage 4 – 12 % Bis-Tris gel	Invitrogen
NuPage MES SDS Running buffer (20x)	Invitrogen
Pierce Protein A/G Magnetic Beads	Invitrogen
Phosphatase Inhibitor Cocktail 2	Sigma-Aldrich
Phosphatase Inhibitor Cocktail 3	Sigma-Aldrich
Poly-L-lysine	Sigma-Aldrich
Prolong Gold Antifade Mountant	Invitrogen
Protease Inhibitor, cOmplete™ Protease Inhibitor Cocktail	Roche
Protease Inhibitor Cocktail (Ribotag)	Sigma-Aldrich
Proteinase K	Roche
Protein size marker	LI-COR
Sodium Pyruvate	Gibco
SN50	Merk
Rapamycin	Sigma-Aldrich
RIPA buffer	Sigma-Aldrich
SYBR DNA Gel Stain	Invitrogen
SYBR Green Master Mix	BioRad
TAE buffer (10x)	Invitrogen

TMB substrate	BD
Torin1	Tocris
TritonX-100	Sigma-Aldrich
Tween-20	Sigma-Aldrich
UltraComp beads	eBioscience

2.4. Solutions and buffers

Table 2.4 Solutions and buffers

Solution/buffer	Content
Biopsy lysis buffer for PCR genotyping	100 mM TRIS-HCl, pH 8.5 5 mM EDTA, pH 8 0.2% SDS 200 mM NaCl 1:100 Proteinase K
ELISA stopping solution	1M H_3PO_4
ELISA wash buffer	0.05% Tween in PBS
Histology blocking buffer	2.5% BSA in PBS + 0.5% Triton X-100
Histology staining buffer	2.5% BSA in PBS + 0.1% Triton X-100
FACS buffer	0.5% FBS + 2 mM EDTA in PBS
Western Blot Transfer buffer	25 mM TRIZMA base 192 mM Glycin pH 8
Western Blot wash buffer	TRIS-buffered saline (20 mM TRIS, 150 mM NaCl) + 0.1% Tween-20

2.5. Kits

Table 2.5 Kits

Kit	Cat. No.	Supplier
Adult Microglia Isolation Kit	130-107-677	Miltenyi Biotec
High-Capacity cDNA Reverse Transcription Kit	4368814	Applied Biosystems
SMARTer® Stranded Total RNA-Seq Kit v3 - Pico Input Mammalian Components	634491	Takara Bio
RNeasy Micro Kit	74004	Qiagen
NucleoSpin RNA Mini Kit	740955.50	Macherey-Nagel
High Sensitivity DNA ScreenTape Analysis	5067-5592	Agilent
High Sensitivity RNA ScreenTape Analysis	5067- 5579	Agilent
Qubit dsDNA HS-Assay Kit	Q32851	Invitrogen

2.6. Antibodies

Table 2.6 Antibodies for flow cytometry

Antigen	Conjugate	Clone	Company
CD11b	BUV395	M1/70	BD
CD45	BV711	30-F11	BD
HA tag	APC	16B12	Biolegend
IgG1, κ isotype control for HA	APC	MOPC-21	Biolegend

Table 2.7 Antibodies for western blot

Antigen	Cat. No.	Supplier
RHEB1	13879	Cell Signaling Technology
phospho-4EBP1 Thr37/46	2855	Cell Signaling Technology
Phospho-4EBP1 Ser65	9451	Cell Signaling Technology
phospho-4EBP1 Thr70	9455	Cell Signaling Technology
4EBP1	9644	Cell Signaling Technology
eIF4E	2067	Cell Signaling Technology
phospho-eIF4E Ser209	9741	Cell Signaling Technology

phospho-S6 ribosomal protein Ser240/244	5364	Cell Signaling Technology
S6 ribosomal protein	2217	Cell Signaling Technology
phospho-p44/42 MAPK T202/Y204 (ERK1/2)	4370	Cell Signaling Technology
p44/42 MAPK (ERK1/2)	9102	Cell Signaling Technology
phospho-eIF2α Ser51	3398	Cell Signaling Technology
eIF2α	5324	Cell Signaling Technology
eIF4GI	8701	Cell Signaling Technology
Anti-β-actin	A1978	Sigma-Aldrich
anti-LC3	L8918	Sigma-Aldrich

Table 2.8 Antibodies for histology

Antigen	Species	Cat. No.	Supplier
Iba1	Guinea pig	234 008	Synaptic system
HA	Mouse	H9658-.2ML	Sigma-Aldrich
GFP	Chicken	ab13970	Abcam

2.7. PCR genotyping primers

All primers were supplied from Sigma.

Table 2.9 PCR primers

Target		Sequence (5' to 3')	PCR products
Rheb floxed	For	GCCCAGAACATCTGTTCCAT	Wt = 653 bp; fl/fl = 850 bp
	Rev	GGTACCCACAACCTGACACC	
Csf1r-Cre	For	AGATGCCAGGACATCAGGAACCTG	Tg = 236 bp; Ctrl = 324 bp
	Rev	ATCAGCCACACCAGACACAGAGATC	
	Ctrl Cre For	CTAGGCCACAGAATTGAAAGATCT	
	Ctrl Cre Rev	GTAGGTGGAAATTCTAGCATCATCC	
Cre-mediated excision	For	ATAGCTGGAGCCACCAACAC	
	Rev	GCCTCAGCTTCTCAAGCAAC	
	For	GGGAGGCTTGCTGGATATG	Wt = 260 bp;

Ribotag floxed	Rev	TTTCCAGACACAGGCTAAGTACAC	fl/fl = 290 bp
CX3CR1-CreERT2	For	AAGACTCACGTGGACCTGCT	Wt = 695 bp; Heterozygote = ~300 bp and 695 bp
	Rev	AGGATGTTGACTTCCGAGTTG	
	Tg	CGGTTATTCAACTTGCACCA	

2.8. RT-qPCR primers

All primers were supplied from Sigma.

Table 2.10 Gene expression assays

Target		Sequence (5' to 3')
Gapdh	For	CTCCACTCACGGCAAATTCAA
	Rev	GATGACAAGCTTCCCATTCTCG
Rheb1	For	GGCAAGTTGTTGGATATGGTGGG
	Rev	CCAAGATTCTGCCAAAGCCTTTC
Rhebl1	For	GAGTTCCTGGAAGGCTACGATC
	Rev	TGCTGTGTCCACCAGATGTAGG
Il6	For	TACCACTTCACAAGTCGGAGGC
	Rev	CTGCAAGTGCATCATCGTTGTTC
Il12b	For	ATGAGAACTACAGCACCA
	Rev	AGGGAGAAGTAGGAATGG
Tnf	For	CCTGTAGCCCACGTCGTAG
	Rev	GGGAGTAGACAAGGTACAACCC

2.9. Software

Table 2.11 Software

Software	Company
7900HT Fast Real-Time PCR Program	Applied Biosystems
Adobe Illustrator 2023	Adobe

Adobe Photoshop 2023	Adobe
FACS Diva	BD
Fiji (ImageJ)	Open source scientific analysis program
FlowJo 10.7	BD
FLUOstar Software	BMG Labtech
GraphPad Prism 9	GraphPad
Mendeley	Elsevier
Microsoft Office 2016	Microsoft
XStella V1	Raytest
Zen blue	Zeiss

2.10. Mice strains

All strains are on a C57BL/6 background.

Table 2.12 Mice strains

Mouse line	Strain name	Reference
Rheb floxed	Rheb^{tm1Pfw}	(Zou et al., 2011)
Csf1r^{Cre}	Csfr1^{Cre}	(Deng et al., 2010)
Ribotag floxed	B6N.129-*Rpl22*$^{tm1.1Psam}$/J	(Sanz et al., 2009)
CX3CR1$^{CreER/+}$	B6.129P2(Cg)-C*x3cr1*$^{tm2.1(cre/ERT2)Litt}$/WganJ	(Parkhurst et al., 2013)

2.11. Animal models

Animals were housed in ventilated cages under the following conditions: 22 °C, a 12-hour light/dark cycle and free access to water and food. The Animal Research Facility (ARF) of DZNE in Bonn was responsible of the animal care. All the experiments showed in this PhD thesis were approved by the German Governmental Ethical Committee (LANUV) with the following experimental license: 81-02.04-2018.A257.

2.12. Genotyping PCR

DNA was extracted from mouse tails or ear punches in order to identify the genotype of the mouse used for all experiments. Briefly, biopsies were incubated in 500 µl of lysis buffer (table 2.4) overnight at 56 C. Lysates were then cleared up by centrifuge (10.000 rpm, 10 min, 4 C), washed with 500 µl of Isopropanol and centrifuged again. A second round of wash was done with 99% Ethanol. DNA pellets were dried out at RT for 15 min before being dissolved in DNase-free water and then subjected to PCR. For each reaction, positive and negative controls were also used.

2.13. Neonatal primary microglia

Primary microglia were obtained from P0-P3 day old neonatal animals. Mice were decapitated and heads were kept in ice-cold HBSS, supplemented with antibiotics (1% pen/strep). The skin, skull and the meninges were removed using a dissection microscope. Brains were then mechanically digested using a P1000 pipette tip in the same buffer on ice and passed through a 70 µM cell strainer in order to remove any remaining meninges. About 5 ml of ice-cold HBSS was used to wash the strainer, prior to centrifuge the cell suspension at 300 x g for 5 min at 4 C. Once carefully aspirated the supernatant, brain cells were gently resuspended in 1 ml of Dulbecco's Modified Eagle Medium (DMEM), supplemented with 20% FBS, 1% pen/strep, 1% GlutamaX, 1% Sodium Pyruvate. Each brain was placed in a T75 cm^2 flask that had been previously coated with poly-L-lysine for at least 1 h and containing 14 ml of the same medium. Each flask was then incubate overnight in a cell culture incubator at 37 C / 5% CO_2. The following day, about 7.5 ml of the media was removed and replaced with fresh cell culture medium supplemented with 20% L929 supernatant. Cells were then supplemented in a similar way every 2 d until they were harvested by shaking on a rocket at 50 rpm. Cells were then replated, incubated overnight in a cell culture incubator at 37 C / 5% CO_2 and used for the described experiment (Keane et al., 2021). For the preparation of L929 supernatant, L929 cell line was a kind gift from Michael T. Heneka group, cells were cultured as described (Weischenfeldt & Porse, 2008) for 7 d before harvesting the supernatant.

For 4EGI-1 experiments, cells were pre-treated for 90 min with 25 µM 4EGI-1 (Merck, 324517) and then stimulated with 200 ng/ml LPS. This experiment has been carried out by Lily Keane.

For the phagocytosis assay, about 50.000 cells in 96 well-plate were incubated with the indicated amount of heat-killed GFP expressing *E.coli* for 30 min in the dark at 37°C / 5% CO_2 for 30 minutes. Cells were immediately fixed in 4% PFA/PBS for 15 min at RT and subjected to immunostaining of nuclei and cell surface markers. Phagocytic uptake of *E.coli* was then analyzed using ImageJ.

For eFT508 experiment, about $1x10^6$ cells were used for western blot and cytokine measurement. Cells were treated and stimulated as indicated.

2.14. Bone marrow derived macrophage differentiation (BMDMs).

Cells were obtained from murine the bone marrow. For this purpose, mice were killed by CO_2 euthanasia and the hind legs were dissected from the hip joint. Tibia and femur were separated at the knee joint and cleaned up from muscles. Both bones were then flushed with HBSS. Cells were then strained through a 70 µm cell strainer, centrifuged at 300 x g for 10 min at RT and counted by Cell Counter CASY. About 14 x 10^6 bone marrow cells were seeded in 20 ml of DMEM, supplemented with 1% GlutamaX, 1% Sodium Pyruvate, 20% FBS, 1% penicillin/streptomycin and containing either 20% L929 supernatant (preparation: see neonatal primary microglia) into a 150 mm Petri dish. Cells were incubated at 37°C / 5% CO_2 for 6 d. On day 4, half of medium was removed and new complete medium was added. On day 6, BMDMs were carefully washed twice with PBS and incubated in Cell Dissociation Buffer for 10 min at 37°C / 5% CO2. Cells were re-plated at different concentrations in complete medium as described above, supplemented with 10% FBS without L929 supernatant for subsequent experiments and allowed to adhere at 37°C / 5% CO2 overnight. The following day, cells were treated and/or stimulated as described. For pharmacological treatments, cells were pre-treated for 90 min with either 100 nM Rapamycin or 18 µM of SN50, or for 30 min with either 100 nM or 250 nM Torin1. Cells were then stimulated with 100 ng/ml LPS from E. coli 0111:B4 or medium control for indicated time points in 6-well plates. For autophagy experiments, cells

were first stimulated with 100 ng/ml LPS for 4 h and then treated with 100 nM Bafilomycin A1 for 3 h (Keane et al., 2021).

2.15. Adult microglia isolation

Adult microglia were isolated from mouse brains using the Adult Brain Dissociation Kit from Miltenyi Biotech in accordance to the manufacturer's guidelines. Briefly, brains were freshly isolated and mechanically and enzymatically digested at 37C using the gentleMACS™ Dissociator with Heaters. The brain lysates were then strained with a 70 µm cell strainer and subjected to myelin clearance using Myelin Removal Beads and MS columns (Miltenyi Biotech). Microglia were then positively selected with CD11b MicroBeads (Miltenyi Biotech) and then processed for further analysis, such as RNA isolation or protein extraction. Only CD11b/CD45 FACS-stained microglia samples showing a purity above 95% were selected for experiments.

2.16. Tamoxifen treatment

Cre expression in $Rpl22^{HA}$:$Rheb^{fl/fl}$:$CX3CR1^{CreER/+}$ and $Rpl22^{HA}$:$Rheb^{wt/wt}$:$CX3CR1^{CreER/+}$ mice was induced by treating the animals with an intraperitoneal injection of 75 mg/kg Tamoxifen solubilized in corn oil per 7 consecutive days, as indicated in the animal experimental license.

2.17. In vivo LPS treatment

$Rheb^{wt/wt}$ and $Rheb^{fl/fl}$ mice were injected by i.p. with either PBS or 5 mg/Kg of LPS for 4 hours. Mice were then sacrificed by CO^2 anesthesia for collection.

2.18. RNA extraction and qRT-PCR.

For RNA extraction from BMDMs, the RNAeasy Mini Kit (Qiagen) or the NucleoSpin RNA Mini Kit (Macherey-Nagel) were used as recommended by the manufacturers and as indicated (Keane et al., 2021). RNA was reverse transcribed using the High Capacity cDNA Reverse Transcription kit qPCR was carried out using Fast SYBR Green Master Mix and Sigma unlabeled primers. Reactions were run with corresponding standard programs using the Step One Plus Real Time PCR Machine. Target gene computed

tomography (CT) values were normalized to CT values obtained for the housekeeping genes Hprt or Gapdh using the delta CT method (Livak & Schmittgen, 2001).

2.19. Flow cytometry staining.

For surface staining, about 1 x 10^6 cells were transferred to a v-bottom96-well plate and spun down at 300 x g for 5 min. Cells were washed twice with ice-cold PBS, incubated with a combination of surface antibodies diluted in FACS buffer and incubated in the dark for 20 min at 4 C. After two consecutive washes with ice-cold PBS, cells were then fixed with 4% paraformaldehyde (PFA) for 10 min on ice in the dark. Samples were then analyzed within 24 h on the FACSymphony A5 or stained for intracellular markers with the following protocol; cells were washed twice in 0.1% Saponin/PBS, before being incubated overnight under gentle agitation with anti-HA. The following day, cells were washed twice more in 0.1% saponin and then PBS, prior to being analyzed on FACSymphony A5 (BD Biosciences).

2.20. Preparation of protein lysates

About 1.5x10^6 Microglia or 2.0x10^6 BMDMs per 1 ml, cultured in 6-well plates, were lysed in 10 ml RIPA buffer, supplemented with 1 tablet of Complete Mini, EDTA-Free Protease Inhibitor, Phosphatase Inhibitor Cocktail 2 and Phosphatase Inhibitor Cocktail 3. Briefly, cell culture was aspirated and cells were washed twice with ice-cold PBS. Then, 70 µl ice-cold lysis buffer was added, cells were scraped vigorously, collected into a 1.5 ml tube and incubated on ice for 45 minutes. Lastly, lysates were centrifuged at 9,391 x g for 10 min at 4°C, the supernatant was then removed, snap-frozen and stored at -80°C. For Western blot analysis, protein quantification was carried out using the Bicinchoninic Acid assay (BCA).

2.21. Western blot

Samples were immunoblotted as described in (Keane et al., 2021). Briefly, samples were supplemented with β-mercaptoethanol and 4x NuPAGE LDS Sample Buffer, heated at 95°C for 5 min and loaded on either 4-12% or 12% NuPAGE Bis-Tris gel or 12% or 15% Bis-Tris hand-cast gels. Protein gels were run for 30 min at 80 V and after that at 120 V until the loading dye reached the desired height. Proteins were transferred overnight at 30

V at 4°C to PVDF membranes and blocked in Intercept® (TBS) Blocking Buffer (LI-COR) for 1 h at room temperature. Blots were incubated overnight at 4°C with antibodies recognizing the indicated targets.Membranes were washed 3 times in TBS-0.1% Tween® 20 for 5 min at room temperature and incubated with secondary antibodies diluted 1:50000 in blocking buffer for 1 h at room temperature. Image acquisition was performed with a LI-COR ODYSSEY. Sometimes membranes were incubated with horseradish peroxidase (HRP) conjugated secondary antibodies, diluted 1:10,000 in blocking buffer – for 1 h at room temperature. Then proteins were visualized using the ECL Western Blot Detection System from Amersham and the Chemidoc system from Biorad. Densitometry analysis of Western blot. Densitometry analysis of bands was carried out using the software ImageJ (Java 1.8.0_172 64-bit) and the Gel Analysis tool, measuring the area under the peak of each band. Values were then normalized to the respective loading control, β-actin detected in the same membrane (Keane et al., 2021)..

2.22. Cytokine measurements.

Cytokine levels in microglia protein lysates were determined using the Legendplex mouse inflammation 13-plex panel, as described (Keane et al., 2021) . For TNF, IL-6, IL-12p40 measurements on BMDMs or microglia culture supernatants, the BD OptEIA ELISA kits were used and the assay was carried out according to manufacturers' guidelines.

2.23. Preparation of acute brain slices.

Acute brain slices experiment and immunostaining were performed by Lily Keane as described (Keane et al., 2021)

2.24. Immunofluorescence of brain tissue

Immunostaining of brain tissue was performed as described (Keane et al., 2021). Mice were anesthetized with ketamine/xylazine according to the experimental license, and then transcardially perfused with 0.9% (w/v) saline followed by 4% (v/v) PFA/PBS. Dissected brain samples were fixed overnight with 4% (v/v) PFA/PBS, and then preserved in 30% sucrose (w/v). Sagittal brain sections were cut into 30 µm-thick sections on a VT1200S vibratome (Leica) and free-floating immunostaining was performed. In brain tissue from aged mice, auto-fluorescence was quenched by incubating the tissue in CuSO4 for 2 h at

room temperature. Sagittal brain sections were then blocked in 2.5-5% (w/v) BSA, 0.5% (v/v) Triton® X-100, and 5-10% (v/v) donkey serum in PBS for 1 h at room temperature. Primary antibodies were mixed in 2.5% (w/v) BSA, 0.1% (v/v) Triton® X-100 in PBS and incubated overnight at 4°C. Sections were washed 3 times for 15 min with PBS and primary antibody was detected by incubating the brain slices with appropriate secondary donkey anti-goat and the nuclear dye DAPI (1:10000, 4',6-diamidino-2-phenylindole) in 2.5% (w/v) BSA in PBS for 3 h at room temperature. After washing the sections 3 times for 15 min in PBS, brain slides were mounted on cover-slip with Fluoromount medium (Sigma, Cat. No. F4680) and visualized with a LSM700 confocal laser-scanning microscope (Carl Zeiss) and analyzed using Fiji software. Acute brain sections staining was performed by Nina Offermann as described (Keane et al., 2021). Images were acquired using a LSM700 confocal microscope (Zeiss) and analyzed using Fiji software. Microglia morphology analysis was permed using Fiji plugin MotiQ.

2.25. Immunofluorescence staining of cells.

About 150.000 BMDMs or microglia were seeded on coverslips in 24-well plates and allowed to adhere at 37°C / 5% CO2 overnight. The following day, cells were treated and/or stimulated as described (Keane et al., 2021). Briefly, after aspirating the medium, cells were first washed in PBS for 5 min and then fixed with 4% (v/v) PFA/PBS for 15 min on shaker. After washing 3 times in PBS-T (0.5% Tween®-X) for 5 min, cells were incubated in blocking buffer (2.5% BSA / PBS, 5% Donkey Serum) for 1 h on shaker. Primary antibodies were mixed in blocking buffer and incubated for 1 h at room temperature. Cells were washed 3 times in PBS-T for 5 min and incubated with secondary antibodies conjugated for 1 h at room temperature. After washes, nuclear dye Dapi was incubated in PBS for 5 min. Coverslips were mounted on slides with ProLong™ Gold Antifade Mountant and Images were acquired by LSM700 confocal laser-scanning microscope (Carl Zeiss) and analyzed using Fiji software.

2.26. Ribosome immunoprecipitation

Brains used for translatome analysis were snap-frozen in liquid nitrogen immediately after the in vivo LPS treatment and stored in -80C until processing. Sample processing and

immunoprecipitation of ribosome-associated mRNAs were performed according to the protocol published (Sanz et al., 2019)

2.27. Library preparation for RNA-sequencing

Prior to sequencing, isolated RNA from both microglia and immunoprecipitated ribosomes were subjected to quantity and quality control using the Agilent Bioanalyzer 2100 RNA pico chip. Only samples with a RIN > 7 were subjected to RNA sequencing. RNA libraries were prepared using SMARTer® Stranded Total RNA-Seq Kit v3 - Pico Input Mammalian Components according the manufacturer's guidelines. A total of 5 µg of RNA was used for microglia transcriptome and from immunoprecipitated ribosomes. Libraries were then purified using SRI beads and magnetic separation, and subjected to ribosomal RNA depletion according the manufacturer's guidelines of the library kit. Libraries were again purified and subjected to quantity and quality control using respectively the Qubit dsDNA HS kit and the Agilent High sensitivity DNA kit. RNA-sequencing was performed by DZNE sequencing platform PRECISE in paired-end 75 bp mode using a NovaSeq S2 200 cycles v1.5 reagent kit on the NovaSeq 6000 instrument.

2.28. Transcriptome and Translatome analysis

Bioinformatics analysis of both transcriptome and translatome was carried out under the supervision of Emilia De Caro from Dr. Anna Aschenbrenner Group at DZNE Bonn. Briefly, Illumina FASTQ output files were aligned using STAR alignment method by PRECISE. Counts were then processed according to the DESeq2 pipeline and rlog-transformed for visualization. Differentially expressed genes (DEGs) with p value adjusted (HB) < 0.05 and with log_2FoldChange (log_2FC) > |1.5| for each comparisons were used for the subsequent downstream analysis and to perform Gene Set Enrichment Analysis (GSEA).

2.29. Sample preparation for mass spectrometry analysis

Approximately 300-400.000 microglia were isolated from brains of tamoxifen-treated young (4 months) and aged (18 months) *Rpl22^{HA}:Rheb$^{fl/fl}$:CX3CR1$^{CreER/+}$* and *Rpl22^{HA}:Rheb$^{wt/wt}$:CX3CR1$^{CreER/+}$* mice and subjected to *in vivo* treatment with LPS or PBS for subsequent total protein extraction. Samples were lysed in 200 µl Lysis buffer (50 mM

HEPES (pH 7.4), 150 mM NaCl, 1 mM EDTA, 1.5 % SDS, 1 mM DTT; supplemented with: 1× protease and phosphatase inhibitor cocktail (ThermoScientific). Lysis was aided by repeated cycles of sonication in a water bath (6 cycles of 1 min sonication (35 kHz) intermitted by 2 min incubation on ice). Approximately, 10 µg of total protein extracts were reduced and alkylated prior to processing by a previously described modified protocol for Filter-aided-Sample-preparation (FASP)(Scifo et al., 2015) to generate tryptic peptides for label free quantitative liquid chromatography/tandem mass spectrometry analysis. Samples were digested overnight with Trypsin (1:20; in 50 mM ammonium bicarbonate) directly on the filters, at 37 °C and precipitated using an equal volume of 2M KCl for depletion of residual detergents. Tryptic peptides were then cleaned, desalted on C18 stage tips and re-suspended in 20 µl 1% FA for LC-MS/MS analysis. MS runs were performed with 5-8 biological replicates.

2.30. Liquid chromatography and tandem Mass Spectrometry (LC-MS/MS) analysis

Tryptic peptides were analyzed on a Dionex Ultimate 3000 RSLC nanosystem coupled to an Orbitrap Exploris 480 MS. Peptides were injected at starting conditions of 95% eluent A (0.1% FA in water) and 5% eluent B (0.1% FA in 80% ACN), with a flow rate of 300 nL/min. They were loaded onto a trap column cartridge (Acclaim PepMap C18, 100Å, 5 mm x 300 µm i.d., #160454, Thermo Scientific) and separated by reversed-phase chromatography on an Acclaim PepMap C18, 100Å, 75 µm X 25 cm (both columns from Thermo Scientific) using a 75 min linear increasing gradient from 5% to 31% of eluent B followed by a 20 min linear increase to 50% eluent B. The mass spectrometer was operated in data dependent and positive ion mode with MS1 spectra recorded at a resolution of 120K, mass scan range of 375−1550, automatic gain control (AGC) target value of 300% (3×10^6) ions, maxIT of 25 ms, charge state of 2-7, dynamic exclusion of 60 sec with exclusion after 1 time and a mass tolerance of 10 ppm. Precursor ions for MS/MS were selected using a top speed method with a cycle time of 2 sec. A decision tree was used to acquire MS2 spectra with a minimum precursor signal intensity threshold of 3×10^5 for scan priority one and an intensity range of 1×10^4 - 3×10^5 for scan priority two. Data dependent MS2 scan settings were as follows: isolation window of 2 m/z, normalized collision energy (NCE) of 30% (High-energy Collision Dissociation (HCD)), 7.5K and 15K resolution, AGC target value of 100% (1×10^5), maxIT set to 20 and 50 ms, for scan priority

one and two, respectively. Full MS data were acquired in the profile mode with fragment spectra recorded in the centroid mode.

2.31. Proteome analysis

Raw data files were processed with Proteome Discoverer™ software (v3.0 SP1, Thermo Scientific) using SEQUEST® HT search engine against the Swiss-Prot® Mus musculus database (v2022-12-14). Peptides were identified by specifying trypsin as the protease, with up to 2 missed cleavage sites allowed and restricting peptide length between 7 and 30 amino acids. Precursor mass tolerance was set to 10 ppm, and fragment mass tolerance to 0.02 Da MS2. Static modifications were set as carbamidomethylated cysteine, while dynamic modifications included methionine and N-terminal loss of methionine, for all searches. Peptide and protein FDR were set to 1% by the peptide and protein validator nodes in the Consensus workflow. Default settings of individual nodes were used if not otherwise specified. In the Spectrum Selector node, the Lowest Charge State = 2 and Highest Charge State = 6 were used. The INFERYS rescoring node was set to automatic mode and the resulting peptide hits were filtered for maximum 1% FDR using the Percolator algorithm in the Processing workflow. A second stage search was activated to identify semi-tryptic peptides. Both unique and razor peptides were selected for protein quantification. Proteins identified by site, reverse or potential contaminants were filtered out prior to analysis. Significant differentially abundant proteins (DAPs) with $p < 0.05$ and with $FC > |1.5|$ were used for Gene Set Enrichment Analysis (GSEA).

3. Results

3.1. Assessment of Rheb1 deletion in microglia and BMDMs

In order to investigate the role of the mTORC1 in translation control of inflammatory and priming genes in aging microglia, I used the *Rheb1$^{fl/fl}$:Csf1r^{Cre}* mouse line, where the GTPase *Rheb1*, an upstream positive regulator of mTORC1, is deleted in cells expressing the promoter *Csf1r*. This results in the genetic loss of RHEB1 in the whole immune system and tissues-resident macrophages, including microglia, as the expression of *Csf1r* takes already place in the early homoeotic progenitors (Gomez Perdiguero et al., 2015). Rheb1$^{fl/fl}$Csf1r^{Cre} animals, BMDMs and microglia will be referred, respectively, as Rheb Ko mice, Rheb Ko microglia and Rheb Ko BMDMs in the present text for simplicity.

A representative PCR genotyping of *Rheb1* floxed gene and of *Cre* expression is shown in Fig 10A. Recombination of *Rheb1* floxed gene has been in neonatal primary microglia as shown in Fig 10B. In both Rheb Ko BMDMs and adult microglia, *Rheb1* transcript was significantly lower compared to wild-type (Wt) counterpart (Figure 10C, left and right panels). Moreover, no difference was observed in the expression of *Rhebl1*, an important paralog gene of *Rheb1* (Figure 10C, left panel). At the protein level, no RHEB1 protein was detected in the immunoblot of Wt and Rheb Ko BMDMs and neonatal primary microglia (Figure 10D-E). Given the low yield of adult microglia that can be isolated from a mouse brain and the low expression of *Rheb1* in mammalian cells, assessing the protein level of RHEB1 in microglia was rather challenging. Therefore, *Rheb1* loss in adult microglia was confirmed through the assessment of mTORC1 signaling, measuring phosphorylation levels of the two key downstream mTORC1 effectors, the proteins 4EBP1 and S6. Both 4EBP1 and S6 phosphorylation were found to be reduced in Rheb Ko microglia compared to their Wt counterpart, (Figure 10F). Collectively, these data proved that the *Rheb1* gene is successfully recombined and deleted in adult microglia, BMDMs and neonatal primary microglia in Rheb1$^{fl/fl}$Csf1r^{Cre} mice.

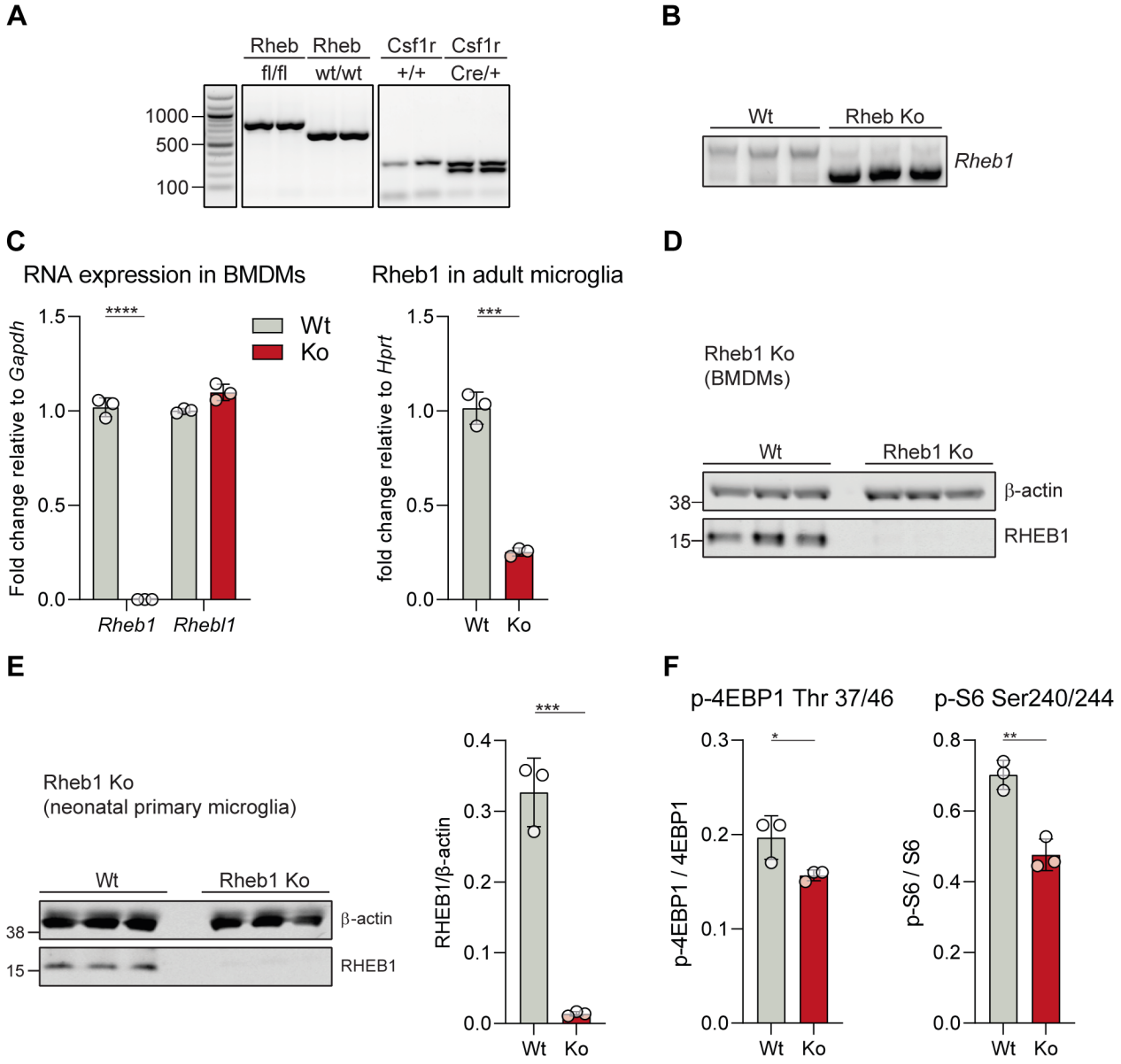

Figure 10 Characterization of Characterization of *Rheb1$^{fl/fl}$:Csf1r^{Cre} mice*.
(**A**) PCR genotyping of Rheb1 floxed gene and Csf1r-Cre with corresponding wt controls from mouse tail biopsies. (**B**) PCR on genomic DNA of neonatal primary microglia, using primers to detect Cre-excised Rheb1. (**C**) (right panel) RTqPCR of Rheb1 and Rhebl1 in Wt and Ko BMDMs at steady state. (left panel) Rheb1 expression measured by RTqPCR in adult microglia isolated from young mice. Data are shown as fold change relative to Hprt expression. (**D**) Western Blot of Rheb1 in Wt and Ko BMDMs. **(E**) (left panel) Western Blot of Rheb1 in Wt and Ko neonatal primary microglia at steady state with relative densitometry analysis normalized to β-actin as loading control (right panel). (**F**) Median Fluorescence Intensity (MFI) of phospho-4EBP1 Thr 37/46 and phospho-S6 Ser 240/244 from CD11b+CD45mid adult microglia measured by flow cytometer and isolated from young mice. Each phospho-proteins is normalized to corresponding total protein. n = 3 mice per genotype for all. (All data are represented as mean ± SD; *P < 0.05, **P < 0.01, ***P < 0.001, ****P < 0.0001;

3.2. Animal and cellular phenotype of Rheb Ko mouse

mTORC1 signaling is a central molecular node involved in cell proliferation and growth (Laplante & Sabatini, 2009; G. Y. Liu & Sabatini, 2020). In order to rule out any potential effect on organ development due to a lower mTORC1 activity in the absence of RHEB1, we conducted a general characterization of animals, in particular assessing the brain, spleen and bone marrow cells.

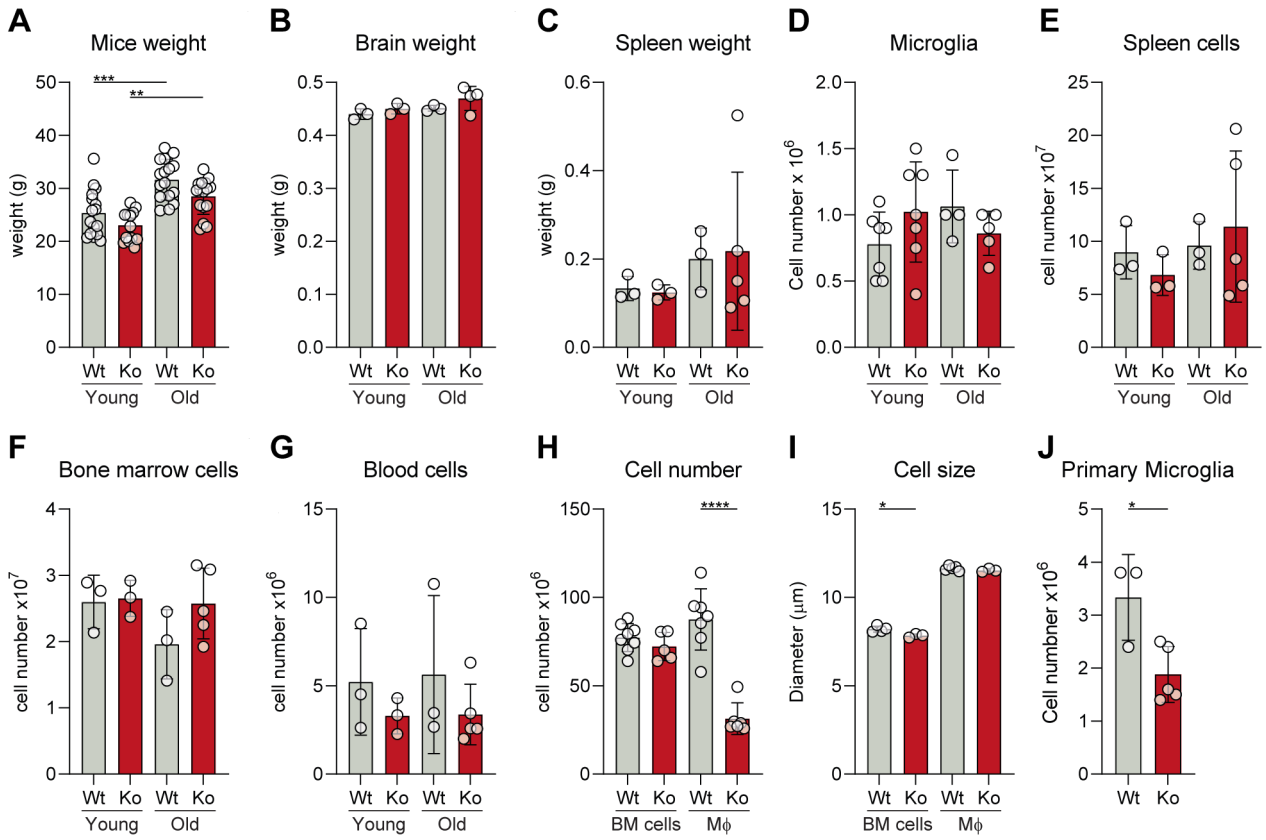

Figure 11 Animal and cellular characterization of the *Rheb1$^{fl/fl}$:Csf1r^{Cre}* mice. (**A-C**) Body, brain and spleen weight of young and old Wt and Rheb Ko animals, *n* = 3-5 mice per genotype (B-C). (**D-G**) Isolated microglia, spleen, bone marrow and blood cell numbers of young and aged Wt and Rheb Ko mice. Blood cells were counted post red-cell lysis, *n* = 3-7 mice per genotype and age group. (**H**) Number of bone marrow (BM) cells and derived BMDMs (MΦ) from Wt (*n* = 12) and Rheb Ko (*n* = 6) mice. (**I**) Cell size of bone marrow (BM) cells and BMDMs (MΦ) from Wt (*n* = 5) and Rheb Ko mice (*n* = 3). (**J**) Number of neonatal primary microglia from Wt and Rheb Ko newborns PD1. *n* = 3-5 mice per genotype. (All data are represented as mean ± SD; **P* < 0.05, ***P* < 0.01, ****P* < 0.01, *****P* < 0.0001; 2-way ANOVA (**A-I**); Student's *t*-test (**J**)). Data extracted from Keane et al., 2021

Rheb Ko animals do not show any visible abnormalities at steady-state and age normally (data not shown). Although there was a trend for a mild but not significant decrease in body weight in Ko animals with age, no difference in the brain and spleen weight was observed in young (3-6 months) and aged (18-22 months) mice compared to age-matched Wt controls (Figure 11A-C). Microglia, spleen, bone marrow and blood cells also showed a similar number, indicating that a lower mTOR activity due to RHEB1 loss does not impair cell proliferation *in vivo*, neither in young nor in aged animals (Figure 11D-G). Conversely, a defective cell proliferation *in vitro* in Ko differentiated macrophages (BMDMs) and neonatal primary microglia from P1-2 newborns was observed (Figure 11H-J).

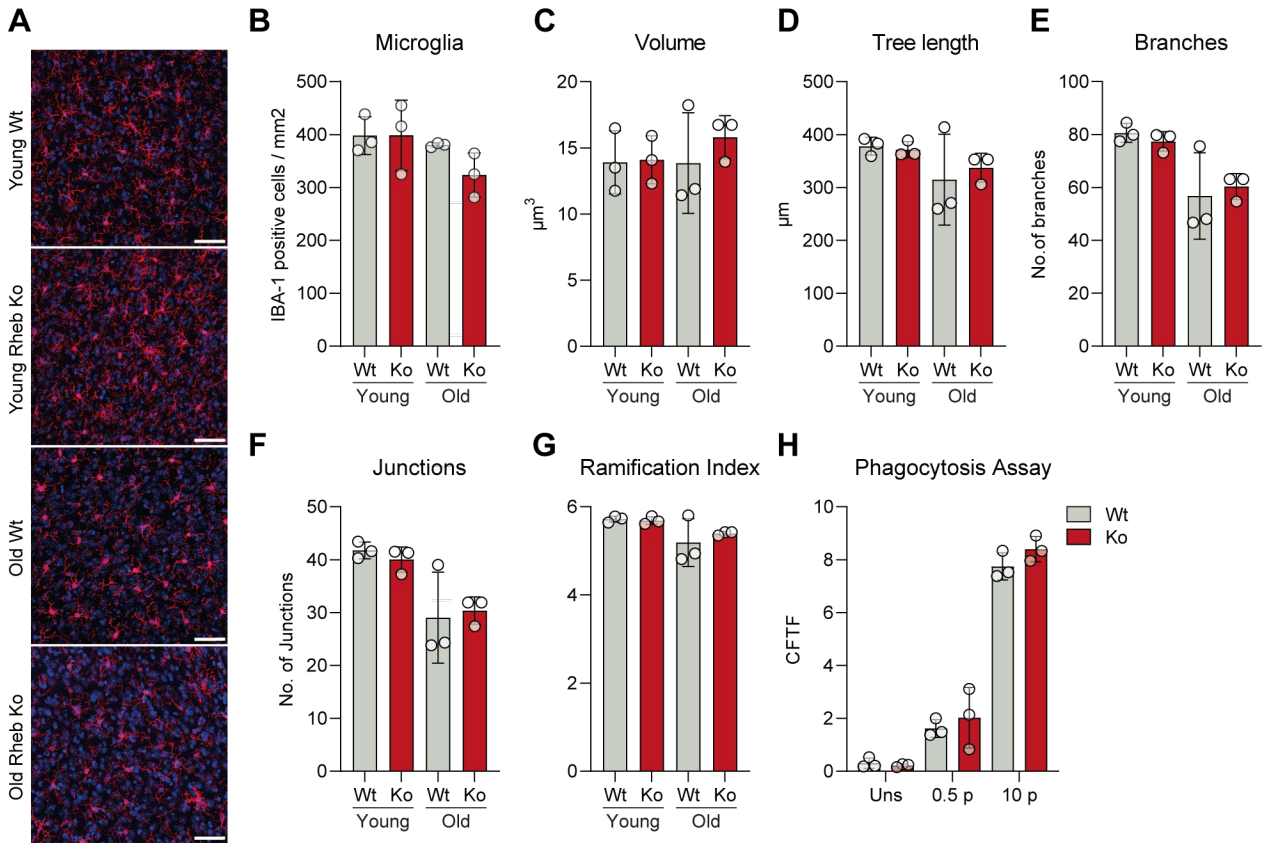

Figure 12 Rheb Ko microglia show similar morphology and no defect in phagocytosis compared to wild-type controls

(A) Immunofluorescence staining of microglia cells (IBA1, red) in the cerebral cortex of Wt and Rheb Ko brains from young (3 months) and aged mice (20 months). In Blue, DAPI-stained nuclei. *n* = 3. Scale bar= 25 µm, 40x objective. (**B**) Relative quantification of IBA1-positive microglia cell number from immunostaining described in (**A**). (**C-G**) Results of microglia morphology analysis performed using images shown in (**A**) by the plug-in MotiQ in Fiji. The sum of all branches is indicated as tree length in µm (**D**). Number of branches

is defined as total number of continuous stretches of a 3D reconstructed cell (**E**). Degree or ramification and complexity of cellular shape is shown as Ramification Index (**G**). (**H**) Phagocytosis assay in Wt and Rheb Ko BMDMs stimulated with fluorescent-conjugated E.coli particles for at indicated concentration per cell. All data are represented as mean ± SD; No significant changes observed in 2-way ANOVA statistical analysis.

As Microglia morphology is well- known to undergo radical changes in ageing as well as in response to insults and CNS pathology (Vaughan & Peters, 1974), we performed a morphological analysis in young and aged Wt and Rheb Ko brain using Fiji plug-in MotiQ (Figure 12A-G). Although aged microglia displayed the characteristic aged-induced morphology, with a lower tree length, number of branches and junctions, as well as reduced ramification, no significant changes were observed between Wt and Ko over aging (Figure 12C-G). Finally, no defect in phagocytosis was observed in Rheb Ko primary microglia treated with fluorescent-conjugated *E.coli* particles (Figure 12H). In summary, steady state organismal and cellular phenotypes are not significantly affected by mTOR inactivation in aging Rheb1 Ko mice, with the exception of a defective *in vitro* cell proliferation.

3.3. Rheb-dependent mTOR inhibition augments transcription of immune genes due to a higher nuclear translocation of the transcription factor NF-κB.

Aged microglia are phenotypically characterized by a stronger immune reactivity after challenges. Therefore, in order to investigate whether a decrease in mTORC1 activity induced by *Rheb1* loss could ameliorate microglia phenotype and responsiveness in ageing, young and old Wt and Ko animals were subjected to an intraperitoneal (i.p.) injection of either LPS or PBS for 4 hours. Microglia were then isolated and microglia priming genes were profiled by qPCR (Figure 13).

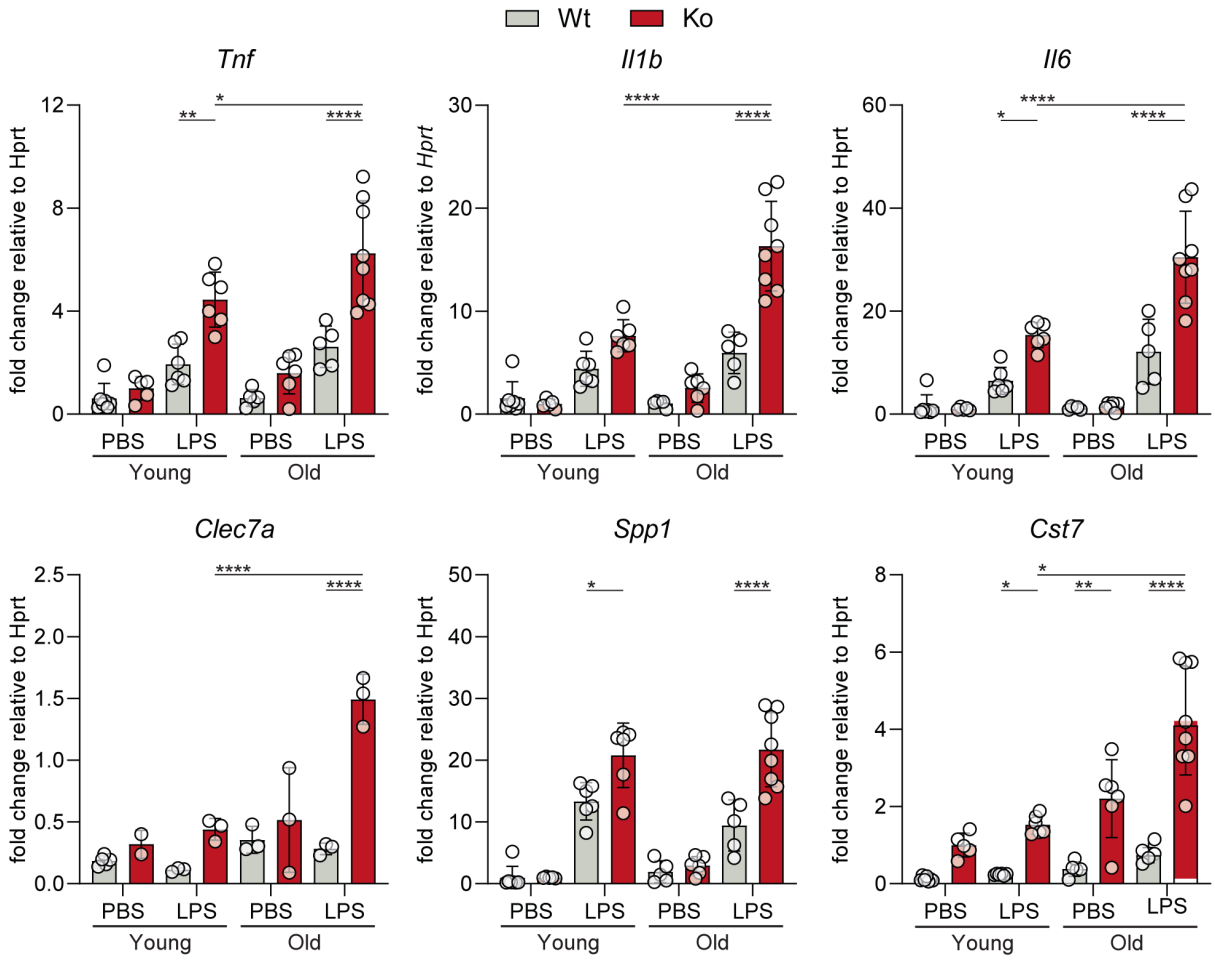

Figure 13 mTORC1 inhibition by genetic loss of Rheb1 results in an increased expression of inflammatory and priming genes after LPS challenge
Relative expression of inflammatory and age-related microglia priming genes in Wt and Rheb Ko adult microglia assessed by qPCR. Gene expression is reported as fold change relative to *Hprt* expression and normalized to young Rheb Ko microglia treated with PBS. Microglia were isolated from young (2–6 months old) and aged (15–18 months old) Wt and Rheb Ko animals, which were i.p. injected with either 5 mg/Kg LPS or PBS control and euthanized after 4 hours. Data shown were collected from 2 independent experiments

(n= 3–8). (All data are represented as mean ± SD; *P < 0.05, **P < 0.01, ****P < 0.0001; 3-way ANOVA)). Data extracted from Keane et al., 2021

Quantitative PCR of immune mediators, such as *Tnf, Il1b, Il6, Clec7a (dectin-1), Spp1, Cst7*, showed an upregulation already in PBS controls Ko microglia (Figure 13). However, these were further increased in Ko microglia after LPS treatment compared to age-matched Wt controls, suggesting a transcriptional deregulation in the expression of pro-inflammatory genes. It has been previously reported that mTORC1 inhibition by Rapamycin treatment causes an NF-κB-dependent upregulation of pro-inflammatory genes in LPS-stimulated human monocytes and mouse macrophages (Weichhart et al., 2008). To assess whether the absence of Rheb1 led to a similar NF-κB activation, nuclear translocation of NF-κB p65 subunit was assessed by immunostaining in LPS-stimulated Wt, Rheb Ko and Rapamycin-treated Wt BMDMs. As shown in Figure 14A, Rheb Ko cells showed an increased translocation of NF-κB in DAPI-stained nuclei similar to Rapamycin treatment. To further corroborate these findings, NF-κB signaling was blocked with SN50, an inhibitor that prevents NF-κB translocation to the nucleus in LPS-stimulated primary microglia. As shown in Figure 14B, SN50 effectively suppressed the increased expression of *Tnf* in Rheb Ko cells similarly to Wt cells. In summary, these results indicated that NF-κB hyperactivation was behind the augmented transcription of immune genes in the absence of RHEB1.

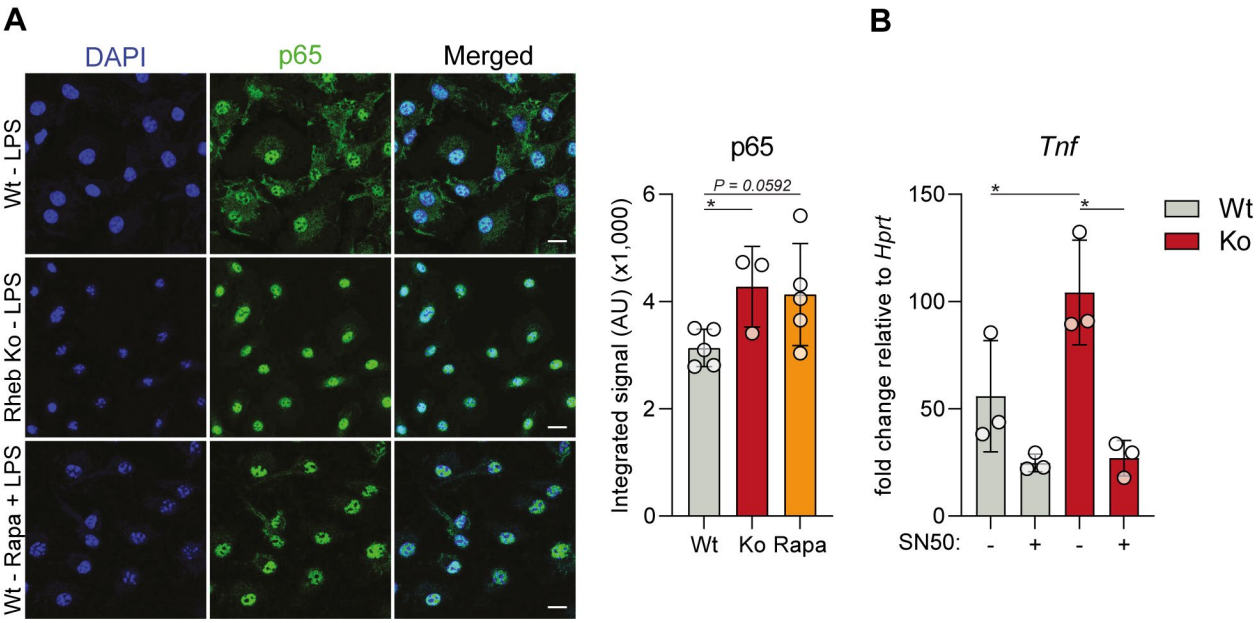

Figure 14 mTOR inhibition in Rheb Ko cells augments nuclear translocation of NF-κB.

(A) (right) Immunofluorescence staining of Wt, Rheb Ko and Rapamycin-pretreated BMDMs stimulated with 100 ng/mL LPS for 6 hours. DAPI-stained nuclei are in blue, NF-κB p65 is in green. Scale bar: 10 μm. (left) Integrated fluorescence signal of NF-κB p65 colocalized with DAPI. (n=3-5). (**B**) *Tnf* expression measured by RTqPCR from BMDMs pretreated with 18 μM of the NF-κB peptide inhibitor, SN50, for 90 minutes and then stimulated with 100 ng/mL LPS for 3 hours. Data are shown as fold change relative to *Hprt* expression (n = 3). (All data are represented as mean ± SD; *P < 0.05, **P < 0.01, ****P < 0.0001; Student's t test (**A**), and 2-way ANOVA (**B**)). Data extracted from Keane et al., 2021

3.4. Rheb1 loss leads to a decrease in expression of immune mediators at protein level.

In order to determine whether the enhanced cytokines and receptors expression at mRNA levels was translated into proteins in Rheb Ko mice, protein expression of microglia priming and activation markers was assessed in both young and aged Wt and Rheb Ko mice after i.p. injection of PBS or 5 mg/Kg LPS.

We found reduced levels of CLEC7A, CD11b, and TLR2 in contrast to their corresponding mRNA levels, both in young and aged Rheb Ko animals (Figure 15AB). Additionally, plasma levels of TNF, IL12p70, IL-1B, IL-1A and GM-CSF were also found to be markedly decreased in aged Rheb Ko compared to age-matched Wt control (Keane et al., 2021). To determine the microglia immune response independently of a systemic inflammation, acute brain slices from aged Wt and Rheb Ko mice were stimulated with LPS. Our findings indicated a significant decrease in TNF protein levels in response to LPS treatment when RHEB1 was absent in microglia, as measured by ELISA of the culture supernatant (Figure 15C), and corroborated by immunostaining of TNF in IBA1-positive microglia. Consequently, a lower systemic inflammation also resulted in an amelioration of the sickness behavior in both males and females Rheb Ko mice (Keane et al., 2021). In summary, these results demonstrate that Rheb1 loss, and subsequent mTORC1 inactivation, led to decreased protein expression of inflammatory mediators in microglial cells, despite higher mRNA levels, due to a defect in protein synthesis (Figure 15E) with an amelioration of the aged microglia phenotype.

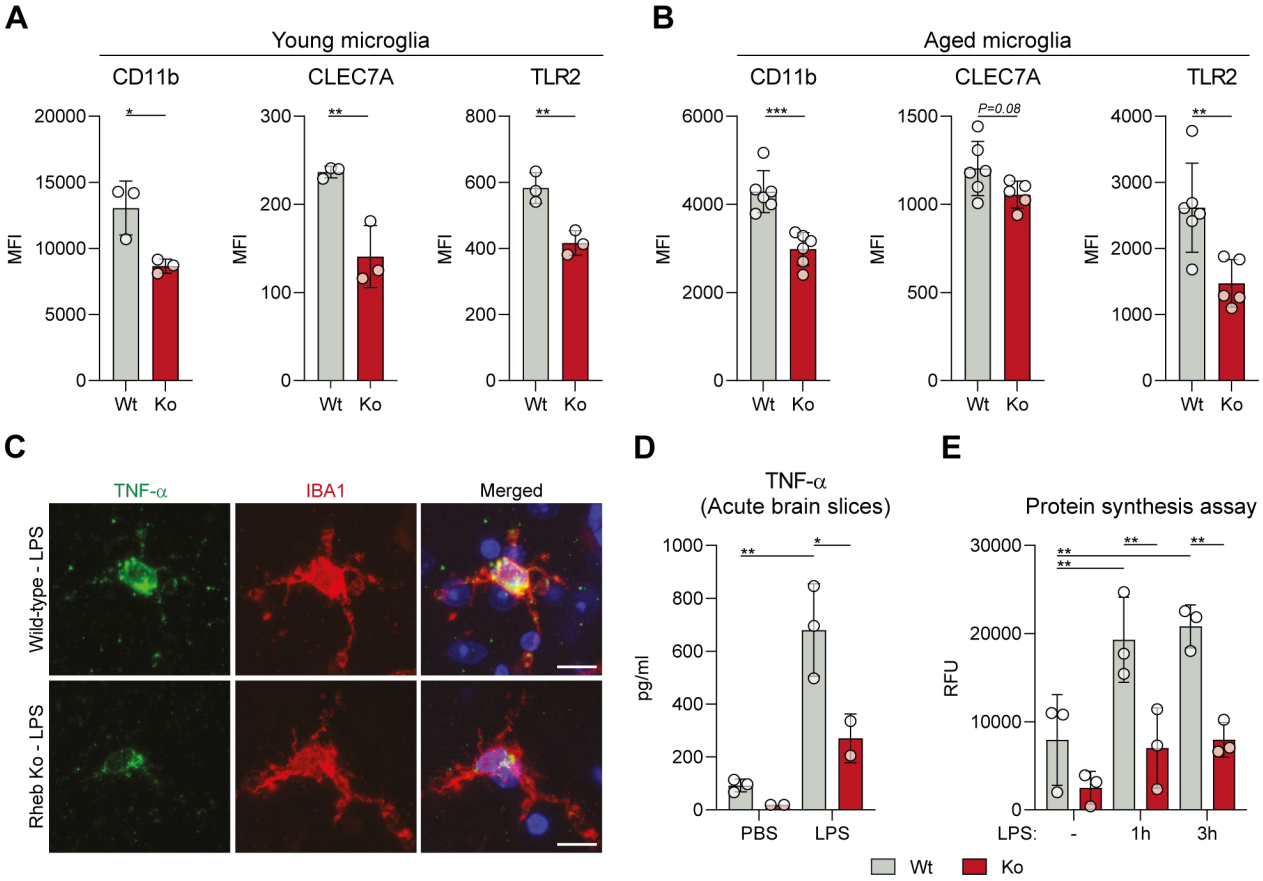

Figure 15 mTORC1 exerts a stronger control over the inflammatory response through translation.

(**A-B**) Microglia activation markers as assessed by flow cytometry of microglia from young (**A**) and old (**B**) Wt and Rheb-Ko mice. Data are shown as MFI (*n* = 3). (**C**) Immunofluorescence staining of acute brain slices from Wt and Rheb Ko mice treated with 2 µg/mL LPS for 6 hours. Green: TNF, red: IBA1 (microglia marker); Scale bar: 10 µm (objective 40X). (**D**) TNF-α levels measured by ELISA from cell culture supernatants of acute brain slices from Wt and Rheb Ko mice, after 6 hours of stimulation with 2 µg/mL LPS (*n* = 3).(E) Relative fluorescence intensity (RFU) of proteins synthesized in WT and Rheb-KO BMDMs at the steady state and after stimulation with 100 ng/mL LPS (*n* = 3). (All data are represented as mean ± SD; **P* < 0.05, ***P* < 0.01, ****P* < 0.001; Student's *t* test (**A** and **B**) and 2-way ANOVA (**D**)). Data extracted from Keane et al., 2021

3.5. 4EBP1 phosphorylation is reduced in Rheb Ko cells, but not after Rapamycin treatment

Our results indicated that mTORC1 inhibition by Rheb1 genetic loss reduces translation of inflammatory mediators in aging microglia. As mTORC1 signaling tightly regulates protein synthesis at the initiation stage, these effects could be related to a differential regulation in the phosphorylation of 4EBP1, a downstream mTORC1 effector. To this end, we examined the impact of RHEB1 loss (Figure 16A), Rapamycin (Figure 16B), and the ATP-competitive inhibitor Torin1 (Figure 17A), a more potent mTOR inhibitor (Thoreen et al., 2009), on primary phosphorylation sites of 4EBP1 by Western Blot in LPS-stimulated BMDMs. Phosphorylation of Thr37/46 is considered a priming event, followed then by phosphorylation at Thr70 and Ser65, respectively (Gingras et al., 1999, 2001). Although all phosphorylation sites are believed to be substrates of mTOR kinase, Thr-70 phosphorylation has been shown to be mTOR-independent (Thoreen et al., 2009) and is likely targeted by another kinase, such as Erk2 (Herbert et al., 2002). Furthermore, a different sensitiveness of the different phosphorylation sites to Rapamycin and Torin1 has been shown, which appears to differ based on the investigated cell-types (Thoreen et al., 2009, 2012).

Western blot and relative densitometry analysis showed a significant reduction of Thr37/46 phosphorylation in Rheb Ko cells at all investigated time points (Figure 16A and C), whereas Rapamycin did not significantly cause any alternation (Figure 16B and G). Thr70 phosphorylation was slightly downregulated in Rheb Ko cells (Figure 16D), while it was not affected by Rapamycin treatment (Figure 16H). On the other hand, Ser65 phosphorylation was strongly suppressed in both conditions (Figure 16E and I).

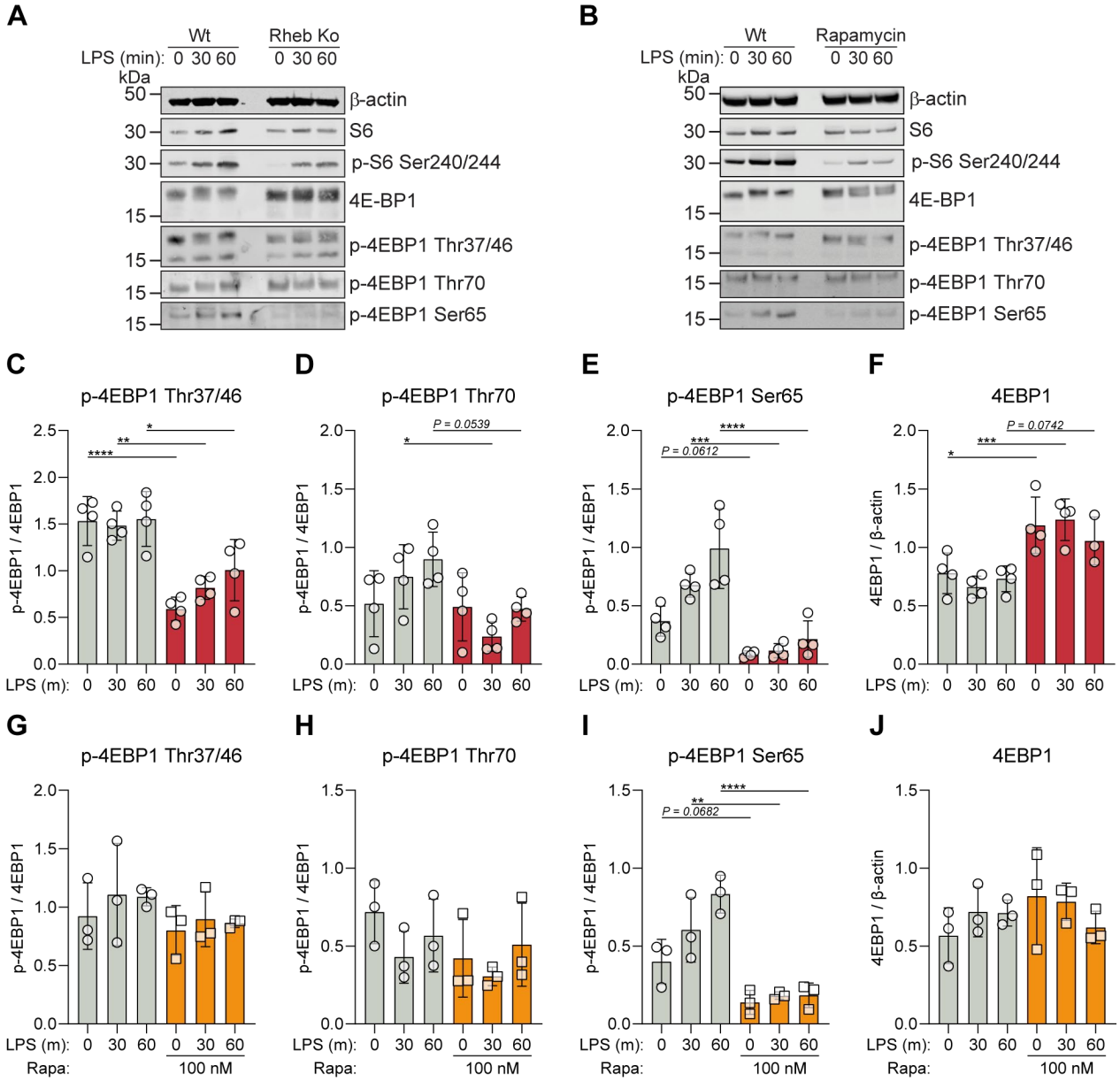

Figure 16 4EBP1 phosphorylation is impaired in Rheb Ko, but not after Rapamycin treatment in LPS-stimulated BMDMs

(**A**) Western blot of Wt and Rheb Ko stimulated with 100 ng/mL LPS for the indicated durations.

(**B**) Western blot of Wt BMDMs pre-treated with 100 nM rapamycin for 90 min and then stimulated with 100 ng/ml LPS for the indicated time points.

(**C-F**) Densitometry analysis of (**C**) p-4EBP1 Thr37/46, (**D**) p-4EBP1 Thr70, (**E**) p-4EBP1 Ser65, and (**F**) 4EBP1 from Rheb Ko experiment (**A**) (Wt in grey, Rheb Ko in red) (n = 4).

(**G-J**) Densitometry analysis of (**G**) p-4EBP1 Thr37/46, (**H**) p-4EBP1 Thr70, (**I**) p-4EBP1 Ser65, and (**J**) 4EBP1 from Rapamycin experiment (**B**) (Wt in grey, Rapamycin-treated Wt in orange) (n = 3).

(All data are represented as mean ± SD; *P < 0.05, **P <0.01, ***P < 0.001, ****P < 0.0001; 2-way ANOVA). Data extracted from Keane et al., 2021

Treatment with Torin1 reduced Thr37/46 phosphorylation more strongly than Rheb Ko (Figure 17A and B). Whereas Thr70 phosphorylation remained largely unaffected by the treatment (Figure 17C), Ser65 phosphorylation was strongly inhibited (Figure 17D), as also observed in Rheb Ko and Rapamycin-treated BMDMs (Figure 16E and I).

Finally, the increase of 4EBP1 phosphorylation in Rheb Ko positively correlated with an upregulation of total 4EPB1 in Rheb Ko and Torin1-treated cells (Figure 17E, Figure 16F), whereas no difference was observed in Rapamycin-treated cells (Figure 16J).

To summarize, mTOR inhibition by Rheb1 loss and with Torin1 treatment led to qualitatively similar changes in 4EBP1 phosphorylation, both followed by an increase of 4EPB1 levels. On the other hand, Rapamycin treatment did not cause any significant change neither in the phosphorylation of 4EPB1 at Thr37/46 and Thr70, nor in 4EBP1 levels.

It has been reported that Rapamycin treatment augments cytokines expression not only at mRNA but also at protein level in LPS-stimulated monocytes, a finding we confirmed in BMDMs (Keane et al., 2021). This could be due to Rapamycin only causing a moderate inhibition of global translation compared to Torin1, which fully blocks mTOR and strongly suppresses protein synthesis (Thoreen et al., 2012). Therefore, in order to determine the effect of mTOR inhibition on cytokines production, we assessed their expression at mRNA and protein level in Torin1-treated Wt BMDMs after LPS challenge. Similarly to Rheb Ko and Rapamycin-treated cells, mTOR inhibition with Torin1 treatment strongly upregulated cytokines transcription (Figure 17F). However, these changes were not translated into protein (Figure 17G). Indeed, Torin1 strongly suppressed protein expression of the investigated cytokines, as also observed in Rheb Ko cells.

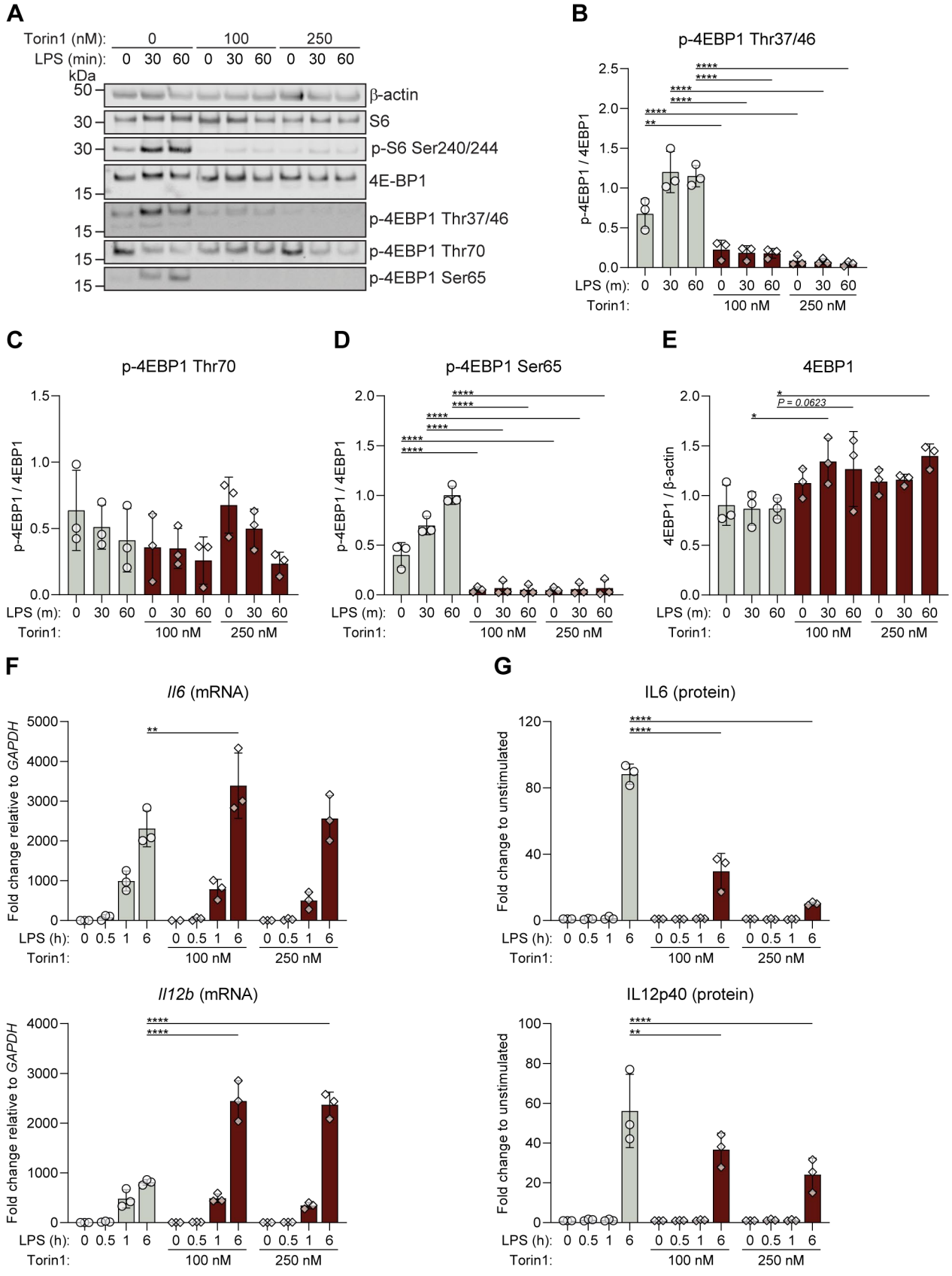
A
Torin1 (nM): 0 100 250
LPS (min): 0 30 60 0 30 60 0 30 60
kDa
50
β-actin
30
S6
30
p-S6 Ser240/244
4E-BP1
15
p-4EBP1 Thr37/46
15
p-4EBP1 Thr70
15
p-4EBP1 Ser65
15
B
p-4EBP1 Thr37/46
p-4EBP1 / 4EBP1
LPS (m): 0 30 60 0 30 60 0 30 60
Torin1: 100 nM 250 nM
C
p-4EBP1 Thr70
p-4EBP1 / 4EBP1
D
p-4EBP1 Ser65
p-4EBP1 / 4EBP1
E
4EBP1
4EBP1 / β-actin
P = 0.0623
F
Il6 (mRNA)
Fold change relative to GAPDH
LPS (h): 0 0.5 1 6 0 0.5 1 6 0 0.5 1 6
Torin1: 100 nM 250 nM
Il12b (mRNA)
Fold change relative to GAPDH
G
IL6 (protein)
Fold change to unstimulated
IL12p40 (protein)
Fold change to unstimulated

Figure 17 Inhibition of mTOR with Torin1 strongly impairs 4EBP1 phosphorylation and cytokine production.
(**A**) Western blot of Wt BMDMs pre-treated with 100 nM or 250 nM Torin1 for 30 min and then stimulated with 100 ng/mL LPS for the indicated durations. Densitometry analysis of (**B**) p-4EBP1 Thr37/46, (**C**) p-4EBP1 Thr70, (**D**) p-4EBP1 Ser65, and (**E**) 4EBP1 (n = 4) in the indicated conditions (Wt in grey, Torin1-treated Wt in dark brown) (**F**) RTqPCR of cytokine mRNAs and (G) ELISA of culture supernatants of Torin1-treated WT BMDMs as described in (**A**) (Wt in grey, Torin1-treated Wt in dark brown). *n*=3. Data are reported as fold change to change relative to Gapdh expression for RTqPCR, and as fold change to unstimulated Wt control for ELISA. n = 3 collected in 3 independent experiments. (All data are represented as mean ± SD; *P < 0.05, **P <0.01, ***P < 0.001, ****P < 0.0001; 2-way ANOVA). Data extracted from Keane et al., 2021

3.6. mTOR inhibition by Rheb1 loss impairs 4EBP1 phosphorylation

The phosphorylation of 4EBP1 is crucial for initiating translation through the release of the cap-mRNA binding protein eIF4E. The decreased 4EBP1 phosphorylation at Thr37/46 and elevated protein levels indicated that the reduced cytokine production in Rheb Ko cells was a result of a persistent binding between 4EBP1 and eIF4E, which prevents its interaction with eIF4G and consequently inhibits translation initiation. To determine whether the binding of eIF4E to eIF4G was impaired in Rheb1 Ko, a proximity ligation assay (PLA) targeting the two binding partners was performed in LPS-stimulated Wt and Rheb Ko primary microglia. A representative scheme of the PLA experiment is represented in Figure 18A (left panel). Immunostaining for eIF4E and eIF4G displayed a significant fewer PLA dots per cell in Rheb Ko microglia compared to Wt cells, indicating a reduced interaction between eIF4E and eIF4G in absence of RHEB1 (Figure 18A). However, this decrease could not be attributed to differences of expression levels of eIF4E and eIF4G, which were similarly expressed in both Wt and Rheb Ko microglia and BMDMs cells (Figure 18B-C). To further corroborate if eIF4E:eIF4G binding was determinant for the Rheb Ko phenotype, we performed experiments with 4EG-I, a pharmacological inhibitor which disrupts the interaction of eIF4G with eIF4E and promotes the binding of 4EBP1 to eIF4E (Figure 18D, left panel) (Sekiyama et al., 2015). As a result, the treatment leads to an inhibition of translation initiation. Pre-treatment of Wt microglia with 4EG-I followed by LPS stimulation causes a reduction in TNF protein levels to an extent comparable to Ko microglia (Figure 18D, right panel). Notably, 4EG-I did not reduce

further TNF level in Rheb Ko microglia, corroborating our initial finding that eIF4E-eIF4G binding was already impaired in the absence of Rheb and was responsible for the observed effect on cytokine translation.

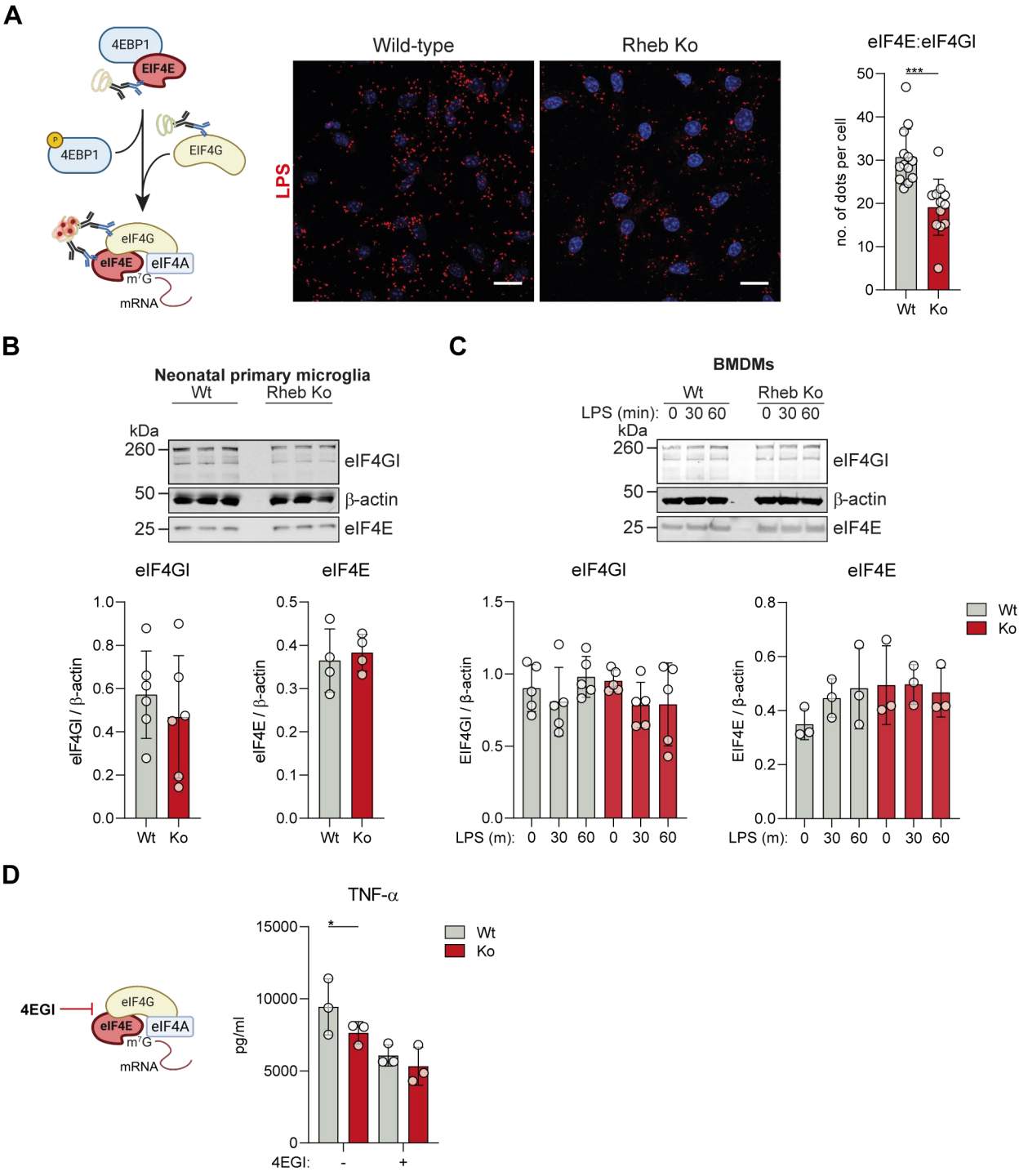

Figure 18 In Rheb-KO cells, diminished binding of eIF4E to its partner eIF4G results in diminished translation of cytokines.

(**A**) (Left) Schematic representing the mTOR downstream signaling cascade of translation initiation and the principle of proximity ligation (PLA) assay. (Middle) PLA of eIF4E and eIF4G1 in neonatal primary microglia cultures from Wt and Rheb Ko brains. (Right) relative quantification of eIF4E/eIF4G binding (PLA events, red dots). Scale bar: 25 µm (objective 40×). *n* = 3 biological replicates, each with 4 technical replicates. (**B**) Western blot and relative densitometry analysis of eIF4E and eIF4G1 from Wt and Rheb Ko neonatal primary microglia culture (*n* = 6 for eIF4G1, *n* = 4 for eIF4E) and (**C**) from Wt and Rheb Ko BMDMs stimulated with 100 ng/mL LPS for the indicated time points (*n* = 5 for eIF4G1, *n* = 3 eIF4E). (**D**) TNF measured by ELISA of cell culture supernatant from Wt and Rheb Ko primary microglia. Cells were pretreated for 90 minutes with 25 µM of the eIF4E/eIF4G inhibitor 4EGI-1 and then stimulated with 200 ng/mL LPS for 3 hours (*n* = 3). (All data are represented as mean ± SD; **P* < 0.05, ***P* < 0.01, ****P* < 0.001; Student's *t* test (**A**, **B**); 2-way ANOVA (**C**, **D**)). Data extracted from Keane et al., 2021.

3.7. Rheb1 Ko cells display lower eIF4E phosphorylation

The cap-mRNA binding protein eIF4E represents a rate-limiting determinant of protein synthesis (Yanagiya et al., 2012). As a proto-oncogene, higher protein levels are commonly associated with cancer models (Carroll & Borden, 2013). Moreover, its activity is regulated by the phosphorylation of Ser209, which is critical for mRNA translation but also cell transformation (De Benedetti & Graff, 2004; Furic et al., 2010; X. Yang et al., 2020). Ser209 phosphorylation is catalyzed by MNK-1 and MNK-2 kinases, both substrates of p38 MAPK and ERK1/2 signaling pathways, and it only occurs when eIF4E interacts with eIF4G, which functions as docking site for MNK-1 (Figure 19A) (Fukunaga & Hunter, 1997; Pyronnet et al., 1999; Waskiewicz et al., 1997). These features make Ser209 phosphorylation a valuable indicator for translation induction as well as the involvement of p38 MAPK and ERK1/2 pathways in regulating protein synthesis through eIF4E activity (Piccirillo et al., 2014). To address whether a reduction of immune genes translation corresponded to a different regulation in eIF4E phosphorylation in Rheb Ko cells, we assessed Ser209 phosphorylation by immunoblot in both Wt and Rheb Ko BMDMs. Interestingly, we noticed a time-dependent increase of Ser209 phosphorylation in LPS-treated Wt cell (Figure 19B). Conversely, eIF4E phosphorylation was reduced in LPS-stimulated Rheb Ko cells at all investigated time-points (Figure 19B). Furthermore, the defect of Ser209 phosphorylation correlated with a reduction of ERK1/2 activation (Figure 19C), which predominantly regulates MNK-1 and MNK-2 activation over p38 MAPK (Proud, 2015). Collectively, these data demonstrated that the effect of Rheb1 loss

were due also to an impairment of MAPK-MNK1/2-phospho-eIF4E cascade, which, together with the inhibition of mTOR-dependent 4EBP1 phosphorylation, further resulted in a decreased translational activity.

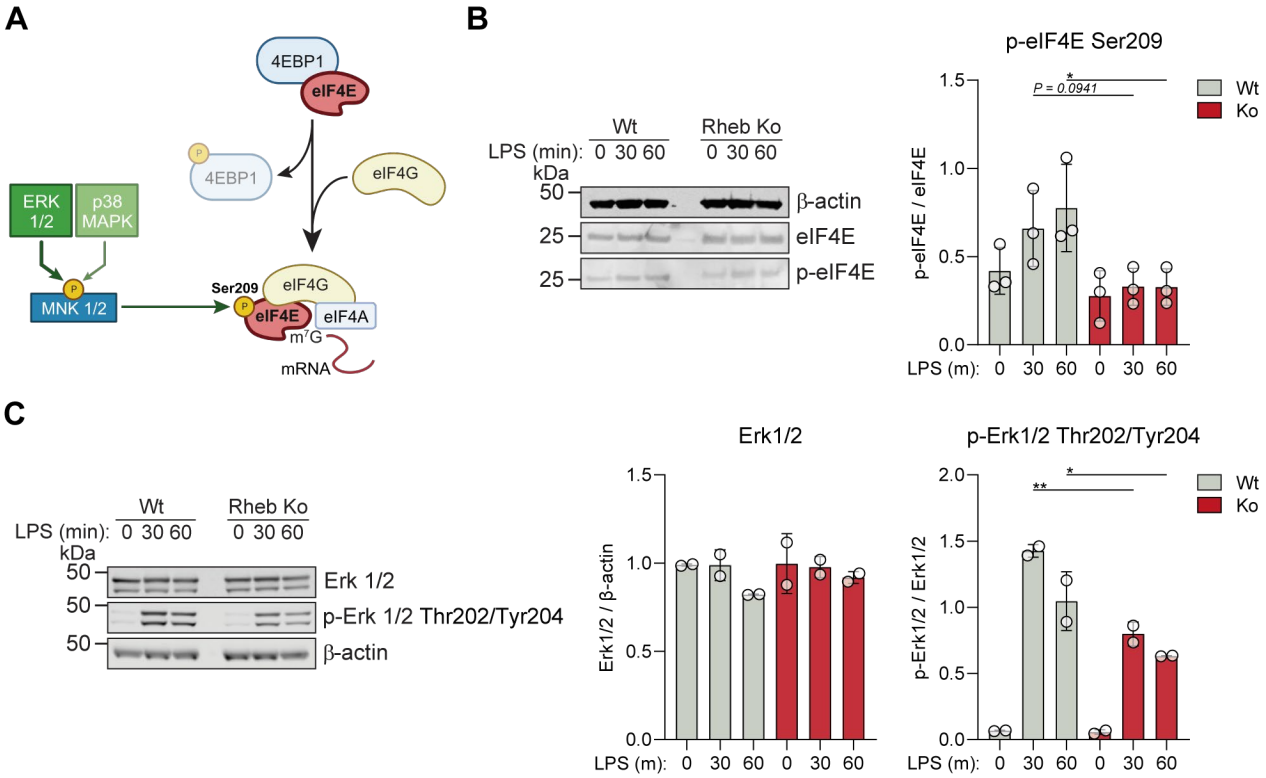

Figure 19 Phosphorylation of eIF4E at Ser209 is impaired in Rheb Ko cells.
(**A**) Schematic of mTOR-4EBP1-eIF4E signaling and crosstalk with p38 MAPK and ERK1/2 kinases, upstream regulators of MNK1/2 kinases, which phosphorylate eIF4E at Ser209 (**B**) Western blot of eIF4E and phospho-eIF4E Ser209 from Wt and Rheb Ko BMDMs stimulated with 100 ng/mL LPS for the indicated time points. Right panel, densitometry analysis of phospho-eIF4E Ser209, n = 3 biological replicates. (**C**) (left panel) Western Blot of ERK1/2 and phospho-ERK1/2 Thr202/Tyr204 from Wt and Rheb KO BMDMs stimulated with 100 ng/mL LPS for the indicated durations. (right panels) Densitometry analysis of total Erk1/2 and phospho-Erk1/2 Thr202/Tyr204, n = 3 biological replicates. (*: p-value <0.05, **: p-value <0.01; two-way ANOVA). Data showed in (**B**) are extracted from Keane et al., 2021

3.8. Inhibition of eIF4E phosphorylation exerts a limited effect over translation of inflammatory mediators.

As eIF4E phosphorylation increased upon LPS challenge in Wt, whereas it was largely suppressed in Rheb Ko cells, we sought to determine whether interfering with this event could modulate microglia immune response, in order to offer a potential therapeutic intervention. To test this hypothesis, we employed the MNK1/2 inhibitor Tomivosertib, also known as eFT508 (Figure 20A), a more potent and selective compound which does not interfere with 4EBP1 and ERK pathway and it is currently under phase II clinical trial for the treatment of several tumors (Dreas et al., 2017; Reich et al., 2018; Y. Xu et al., 2019). For this aim, primary microglia were pretreated with an increasing concentration of eFT508 and stimulated with LPS for 4 hours. The inhibition of eIF4E phosphorylation was assessed by immunoblotting, whereas cell culture supernatant was collected for quantification of TNF-α, IL-12p40 and IL-6 by ELISA. Western blot and relative densitometry analysis showed a concentration-dependent decrease of Ser206 phosphorylation, which was largely suppressed at 100 nM, corresponding to the highest dose investigated (Figure 20B-C). A reduction of TNF-α production was also observed in a dose-dependent manner (Figure 20D), whereas protein level of IL-12p40 were found already reduced at a lower concentration (20 nM), which slightly decreased at higher ones (Figure 20E). On the other hand, IL-6 levels were unaffected, independently of the doses investigated (Figure 20F). Overall, eFT508 treatment only led to a partial decrease of microglia immune response, with IL-12p40 being the most affected. The differential effect on cytokine expression might be explained by an innate sensitiveness of certain mRNA subsets to eIF4E. Indeed, a more pronounced reduction of TNF was observed in LPS-treated acute brain slices from aged animals pretreated with Ribavirin, an antiviral inhibitor competing with eIF4E for the cap-mRNA binding (Keane et al., 2021).

Collectively, these results indicated that despite a slight decrease of cytokine levels, eIF4E inhibition only exerted a limited effect over translation of inflammatory mediators.

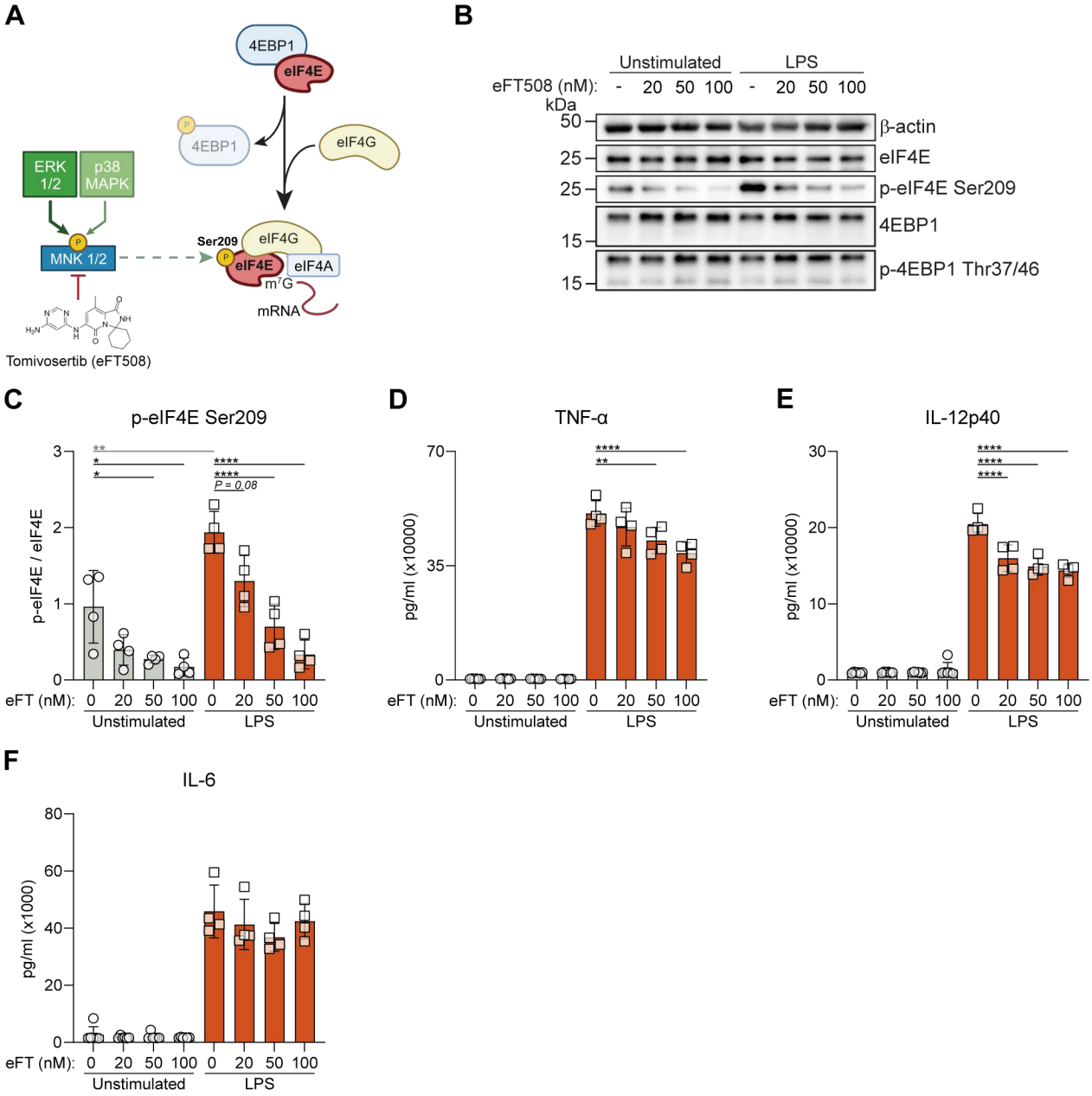

Figure 20 Inhibition of eIF4E phosphorylation by eFT508 mildly affect cytokines translation in primary microglia

(**A**) Schematic representing the mechanism of action of Tomovosertib (eFT508), which reduces eIF4E phosphorylation by inhibiting MNK1/2 kinases. (**B**) Western blot of neonatal primary microglia pre-treated for 1 hour with increasing concentrations (20-100nM) of eFT508 and stimulated with LPS 100 ng/mL for 4 hours. (**C**) Relative densitometry analysis of phospho-eIF4E from immunoblot shown in (**B**). Data is shown as fold change to total eIF4E. Both phospho- and total eIF4E are normalized to β-actin. (**D-F**) Relative cytokines abundance quantified by ELISA from cell culture supernatant of experiment described in (**B**). (All data are represented as mean ± SD; *P < 0.05, **P <0.01, ***P < 0.001, ****P < 0.0001; 2-way ANOVA).

3.9. eIF2 signaling is not impaired in Rheb Ko cells

eIF2 is a translation initiation factor which deliver the initiator methionyl transfer RNA (Met-tRNA$_i$) to 40S ribosomes, in order to catalyze the formation of the preinitiation complex (PIC) and to promote translation initiation (Merrick & Pavitt, 2018). The affinity of Met-tRNAi for eIF2 is regulated by the exchange of guanine nucleotides, which is the highest only when eIF2 is bound to GTP. The recognition of the AUG codon within a mature 48S initiation complex triggers the GTP hydrolysis mediated by the GTPase-activating protein eIF5, which results in eIF2 release. To participate in a further round, eIF2 is re-engaged with GTP by eIF2B, which functions as a guanine nucleotide exchange factor (GEF). Finally, eIF2/GTP interacts again with Met-tRNA$_i$. This critical step in translation initiation is heavily regulated, indeed, eIF2 can also block translation. In response to a wide range of stress-related signals, multiple protein kinases phosphorylate Ser51 within the eIF2α subunit. This causes the inhibition of eIF2B-mediated GEF activity, leading to a persistent binding of eIF2 with GDP and an arrest of protein synthesis (Adomavicius et al., 2019; Donnelly et al., 2013).

Based on the nature of the cellular stress, several kinases have been described to phosphorylate eIF2. Among these, the activation of the kinase PERK seems to be promoted by RHEB1 upon ER stress (Figure 21A) (X. Wang et al., 2016). Therefore, we determined whether the eIF2α phosphorylation was reduced due to Rheb1 loss in LPS-stimulated BMDMs. Interestingly, both Wt and Rheb Ko cells showed a low level of eIF2α phosphorylation already at steady state, which further decreased in response to LPS challenge. Notably, no significant changes were observed between Wt and Rheb Ko BMDMs (Figure 21B)

In summary, eIF2 signaling is not involved in the Rheb Ko-mediated effect we observed, which is primarily involved in mTOR signaling.

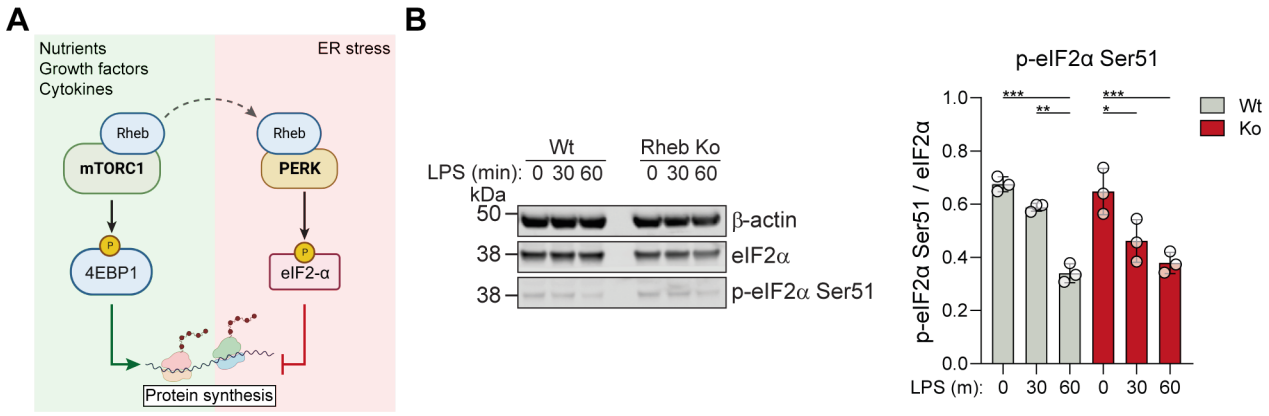

Figure 21 eIF2α phosphorylation is not induced in Rheb Ko cells
(**A**) Schematic representing the dual mechanism of Rheb1 based on cellular cues. (**B**) Western blot of eIF2α and phospho-eIF2α Ser51 in Wt and Rheb Ko BMDMs stimulated with LPS 100 ng/mL for the indicated time points. Right panel: densitometry analysis of phospho-eIF2α. Data is shown as fold change to total eIF2α, *n* = 3 biological replicates. (All data are represented as mean ± SD; *P < 0.05, **P <0.01, ***P < 0.001; 2-way ANOVA). Data showed in (**B**) are extracted from Keane et al., 2021

3.10. Lower cytokine levels in Rheb KO cells are not due to autophagy.

The mTORC1 pathway suppresses autophagy and favors anabolic over catabolic processes when activated (Laplante & Sabatini, 2009). As Rheb1 loss led to a downregulation of mTORC1 activity, a potential activation of the autophagy flux could be expected in Rheb Ko cells. Therefore, to rule out that the lower production of immune mediators in Rheb Ko mice were the results of an increased protein degradation promoted by autophagy, LPS-stimulated Wt and Rheb Ko BMDMs were cultured in the presence of Bafilomycin A1, a dual inhibitor of autophagy flux. Bafilomycin A1 increases lysosomal pH by inhibiting the v-ATPase, a proton ion pump responsible for lysosomal acidification, which is an indispensable condition for lysosomal enzyme activation and cargo degradation (R. Wang et al., 2021). Furthermore, Bafilomycin A1 also prevents the autophagosome-lysosome fusion, a function that occurs independently of v-ATPase inhibition (Klionsky et al., 2008; Mauvezin & Neufeld, 2015).

Upon Bafilomycin A1 treatment, we did not observe any increase of cytokine protein levels, rather a reduction in both LPS-stimulated Wt and Rheb Ko cells (Figure 22A). Besides, mTORC1 inhibition by Rheb1 loss did not cause any accumulation of the autophagy marker LC3-II compared to Wt controls, also in the presence of Bafilomycin

A1. On the contrary, it seemed that Rheb KO cells showed reduced autophagy activation compared Wt counterparts (Figure 22B-C).

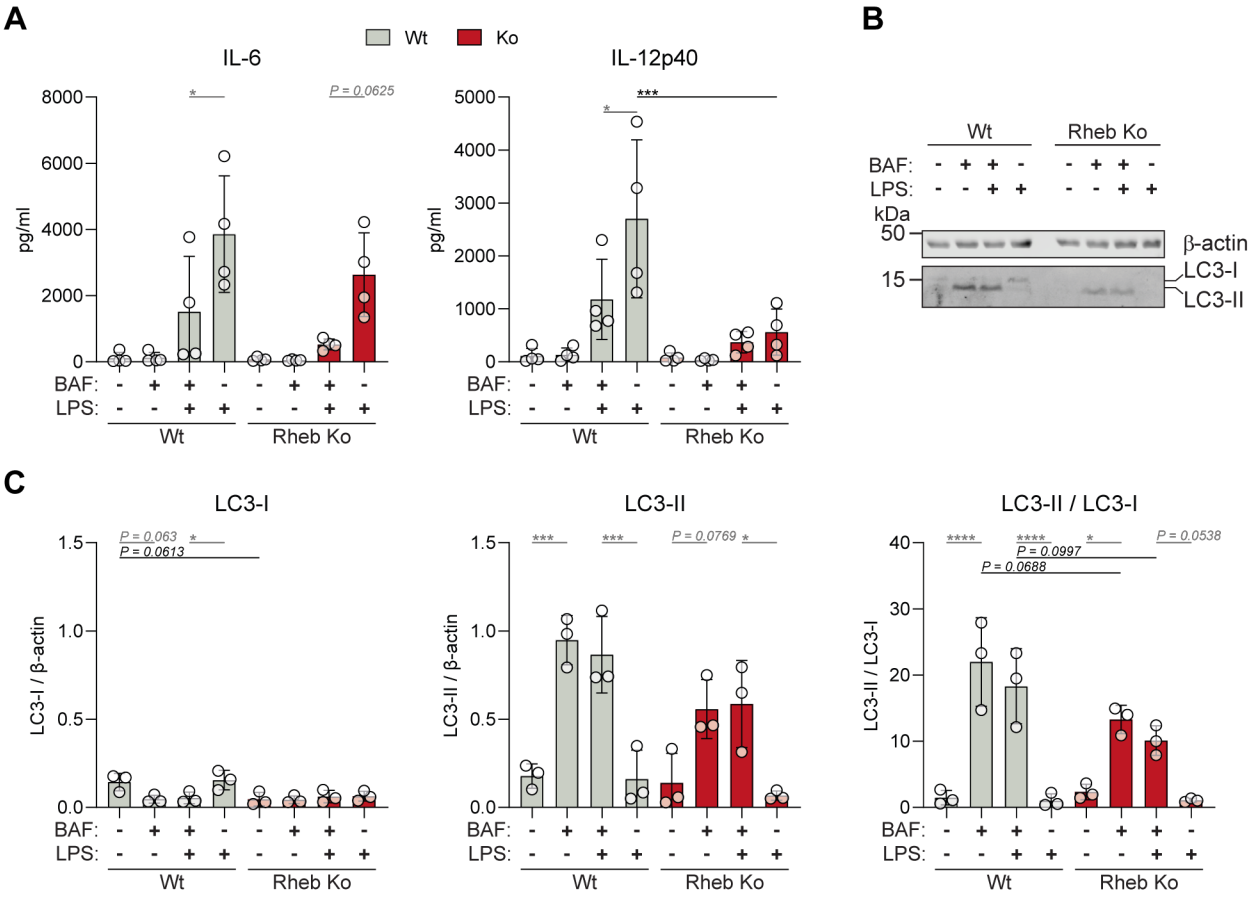

Figure 22 Autophagy is not upregulated in Rheb KO cells, nor plays a role in cytokine degradation.
(**A**) IL12p40 and IL6 measured by ELISA of culture supernatant from WT and Rheb KO BMDMs stimulated with 100 ng/ml LPS for 4 h and treated with 100 nM Bafilomycin A1 or DMSO control, for the last 3 h, n=4 mice in 4 independent experiments. (**B**) Western blot of LC3 in Wt and Rheb Ko BMDMs. Lysates were obtained from the same experiments described above. (**C**) Densitometry analysis of LC3-I (left panel), LC3-II (middle panel), and LC3-II/LC3-I ratio (right panel). (All data are represented as mean ± SD; *: p-value <0.05, **: p-value <0.01, ***: p-value <0.001, ****: p-value <0.0001; 3-way ANOVA for **A** and **C**)). Data extracted from Keane et al., 2021

3.11. Multi-omics analysis in aging microglia using *Rpl22^{HA}:Rheb$^{fl/fl}$:CX3CR1^{CreER}* mouse line

The results showed earlier, along with cumulative evidence of translationally regulated immune genes (Carpenter et al., 2014; Guillemin et al., 2022; Piccirillo et al., 2014; Schott et al., 2014; Y. Zhang et al., 2023), suggested that a similar scenario might also take place in aging microglia. Whether these features could affect the translation of global mRNAs or selective transcripts remains to be explored. These hypotheses can be specifically addressed by performing a translatome analysis, a method that allows to isolate ribosome-associated mRNAs that are being actively translated into protein. In parallel, transcriptomics and proteomics are also needed, respectively to be used as a reference for translatomics, in order to measure translational efficiency, and to confirm whether ribosome-associated mRNAs are actually translated into proteins. A summary of the strategy is represented in Figure 23.

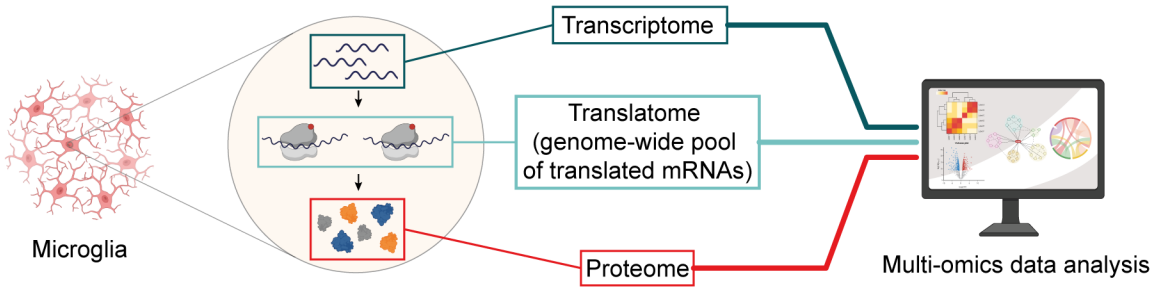

Figure 23 Schematic representing the strategy for performing a multi-omics data analysis in microglia

3.12. Establishment and characterization of *Rpl22^{HA}:Rheb$^{fl/fl}$:CX3CR1^{CreER}* mouse line

To investigate how microglia translatome changes with age and in response to LPS in Wt and Rheb Ko animals, the *RiboTag* mouse model was used. This model carries a modified ribosomal protein *Rpl22, which* possess a duplicated hemagglutinin (HA)-tagged exon 4, preceded by wild-type exon 4 flanked by loxP sites (Figure 24A, top left panel) (Sanz et al., 2009). When *RiboTag* mouse is crossed to a cell-type-specific Cre recombinase-

expressing animal, Cre recombinase leads to the expression of RPL22^{HA} and incorporation into actively translating polyribosomes only in specific tissues/cells (Sanz et al., 2009). The mRNA transcripts associated with HA-tagged ribosomes are then immunoprecipitated with an HA antibody and sequenced for translatome analysis (Sanz et al., 2009). *Rheb$^{fl/fl}$:CX$_3$CR1$^{CreER/+}$* animals were crossed with *RiboTag* mice to generate a Cre-expressing mouse line targeting specifically microglia. As a result, the newly established *Rpl22^{HA}:Rheb$^{fl/fl}$:CX$_3$CR1$^{CreER/+}$* mouse line expressed a tamoxifen-inducible Cre recombinase under the control of the endogenous *CX$_3$CR1* promoter, leading to the selective rearrangement of the *Rheb1 and Rpl22* genomic loci in microglia and tissue-resident macrophages, after tamoxifen treatment. (Figure 24A). Also bone-marrow derived monocytes express the Cre recombinase, leading to Rheb1 loss also in circulating monocytes, however, new monocytes are replaced by CX3CR1-negative hemopoietic stem cells within a month of Cre induction, ensuring that only microglia and other longer-lived tissue resident macrophages carry the genetic modification (Parkhurst et al., 2013). Prior to using these animals for in-vivo experiments, three relevant points had to be addressed: 1) the estimation of the Cre recombinase leakage in microglia from tamoxifen-untreated *CX$_3$CR1$^{CreER/+}$* animals (Figure 24B-C); 2) the time needed for Cre-mediated Rheb1 deletion to become apparent in microglia and 3) the time needed to reach good RPL22^{HA} expression in microglia after tamoxifen treatment (Figure 25A-C).

To address these points, microglia were isolated from adult mice and RPL22^{HA} expression was measured by flow cytometry. In addition to point 3, RPL22^{HA} was also used as a proxy for assessing point 1 and 2. This approach was chosen due to the RPL22^{HA}-dependent expression on Cre recombinase activity and could, indirectly, indicate if mTORC1 activity in microglia from tamoxifen-treated *Rpl22^{HA}:Rheb$^{fl/fl}$:CX3CR1$^{CreER/+}$* animals was impaired. Since the expression of ribosomal proteins is transcriptionally and translationally controlled by mTORC1 (G. Y. Liu & Sabatini, 2020), it was expected that Rheb Ko microglia from tamoxifen-treated animals would show a lower expression of RPL22^{HA}.

3.13. Assessment of the Cre expression in *Rpl22^{HA}:Rheb$^{fl/fl}$:CX$_3$CR1$^{CreER/+}$* mice in absence of tamoxifen

Concerning the leakiness of our inducible Cre line, CD11b^{high}CD45^{mid} microglia isolated from tamoxifen-untreated *Rpl22^{HA}:Rheb$^{wt/wt}$:CX$_3$CR1$^{CreER/+}$* mice were assessed by flow cytometry and showed approximately 5-8% of RPL22^{HA} positive cells compared to *CX$_3$CR1$^{+/+}$* controls (Figure 24B, left panel). For the analysis, adult microglia isolated from *Rpl22^{HA}:Rheb$^{wt/wt}$:Csf1r^{Cre}*, which constitutively expressed Cre recombinase under the control of the *Csf1r* promoter, were used as positive control (Figure 24B, right panel). Furthermore, these findings were corroborated by immunostaining of brain sections derived from tamoxifen-untreated *Rpl22^{HA}:Rheb$^{wt/wt}$:CX3CR1$^{CreER/+}$* mice, which actually showed no IBA1^{+}EYFP^{+} microglia expressing the HA tag (Figure 24C).The different results in HA expression might be related to the higher sensitiveness of flow cytometry vs microscopy. Indeed, as shown in Figure 24B, steady-state leakiness of Cre activity led to relatively low HA expression levels when compared to *Rpl22^{HA}:Rheb$^{wt/wt}$:Csf1r^{Cre}* controls, as also suggested previously by others (Parkhurst et al., 2013).

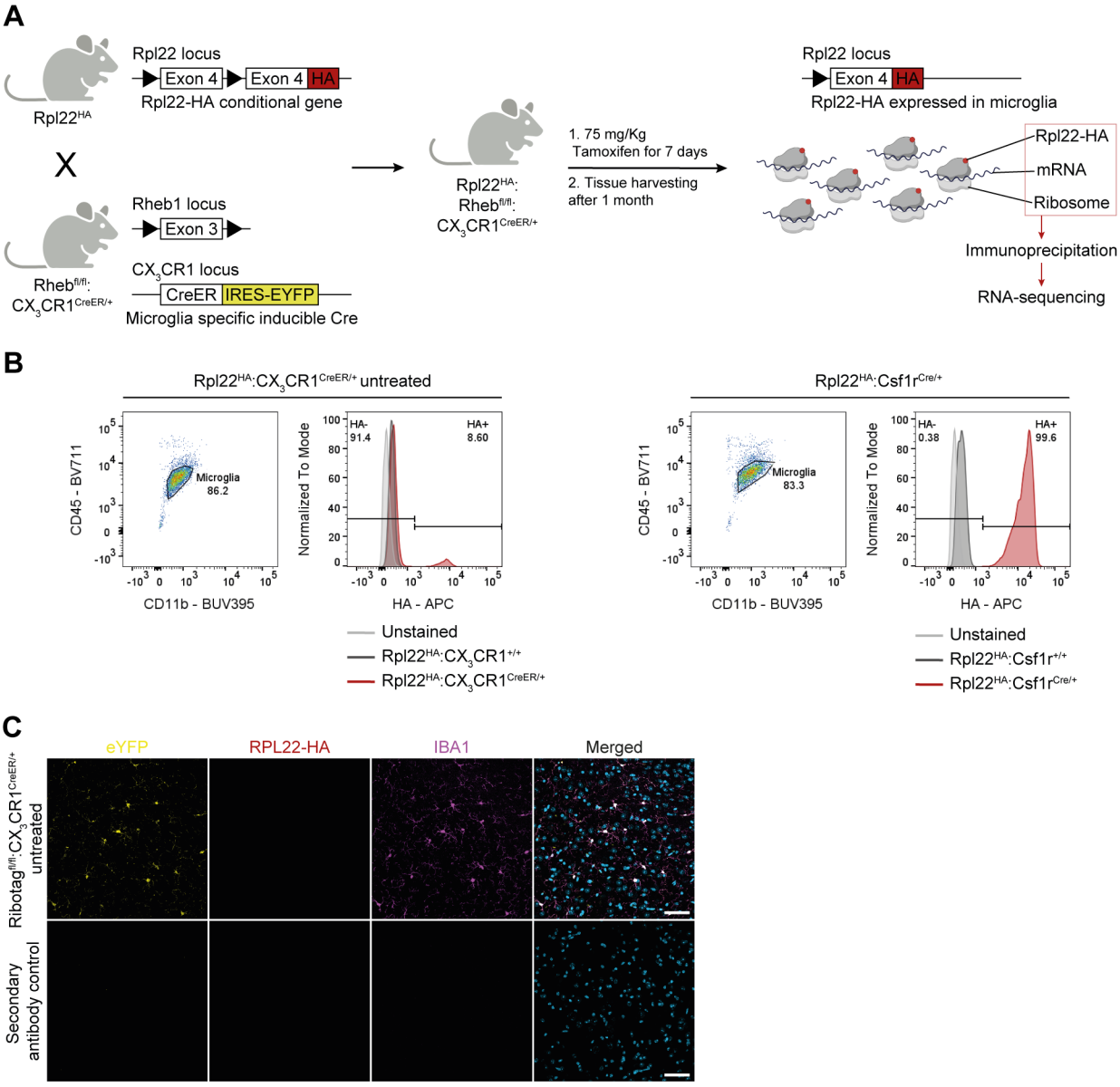

Figure 24 Establishment of Rpl22HA:Rhebfl/fl:CX3CR1CreER mouse line and its characterization in the absence of tamoxifen.
(**A**) Schematic representation of the breeding strategyto establish *the* Rpl22^{HA}:Rheb$^{fl/fl}$:CX3CR1$^{CreER/+}$ mouse line. (**B**) (left panel) Representative FACS plot and histogram showing HA tag expression from gated CD11b^{high}CD45^{mid} microglia isolated from 2 months old Rpl22^{HA}:Rheb$^{wt/wt}$:CX3CR1$^{CreER/+}$ and Rpl22^{HA}:Rheb$^{wt/wt}$:CX3CR1$^{+/+}$ animals without tamoxifen treatment. (right panel) Similar strategy applied for *Rpl22^{HA}:Rheb$^{wt/wt}$:Csf1r$^{Cre/+}$* and *Rpl22^{HA}:Rheb$^{wt/wt}$:Csf1r$^{+/+}$* used as positive control for HA *expression* (*N* = 3) (**C**). Representative images obtained by the immunostaining of EYFP (yellow), HA (red), IBA1 (microglia marker, violet), nuclei (DAPI, blu) in sagittal brain sections derived by Rpl22^{HA}:Rheb$^{wt/wt}$:CX3CR1$^{CreER/+}$ mice. (*n* = 2).

3.14. Characterization of *Rpl22^{HA}:Rheb$^{fl/fl}$:CX$_3$CR1$^{CreER/+}$* mouse line after tamoxifen treatment

To assess *Rheb1* deletion and RPL22^{HA} expression in microglia, young *Rpl22^{HA}:Rheb$^{fl/fl}$:CX3CR1$^{CreER/+}$* and *Rpl22^{HA}:Rheb$^{wt/wt}$:CX3CR1$^{CreER/+}$* mice were evaluated at 1 and 2 months post-treatment with tamoxifen (Figure 25A). While a slight reduction of *Rheb1* expression was already observed by RTqPCR in *Rheb$^{fl/fl}$* microglia at 1 month compared to *Rheb$^{wt/wt}$* counterparts, its level was strongly reduced only at 2 months (Figure 25B). Assessment of RHEB1 protein levels by western blot were attempted, however, the low yield of microglia combined with the low expression of RHEB1 in these cells, made the measurement challenging. Therefore, as indirect evidence that RHEB1 was lost and therefore mTORC1-dependent translation was reduced, RPL22^{HA} expression was also measured by flow cytometry in CD11b^{high}CD45^{mid} microglia, at 1 and 2 months-post tamoxifen treatment (Figure 25C). The progressively lower expression of RPL22^{HA} confirmed that microglia cells had a reduced mTORC1 activity, indicating sufficient downregulation of RHEB1 protein levels.

Based on these evidence, we concluded that 2 months post-tamoxifen treatment was a suitable time-point to isolate microglia, in order to assess differences in Wt vs Ko animals.

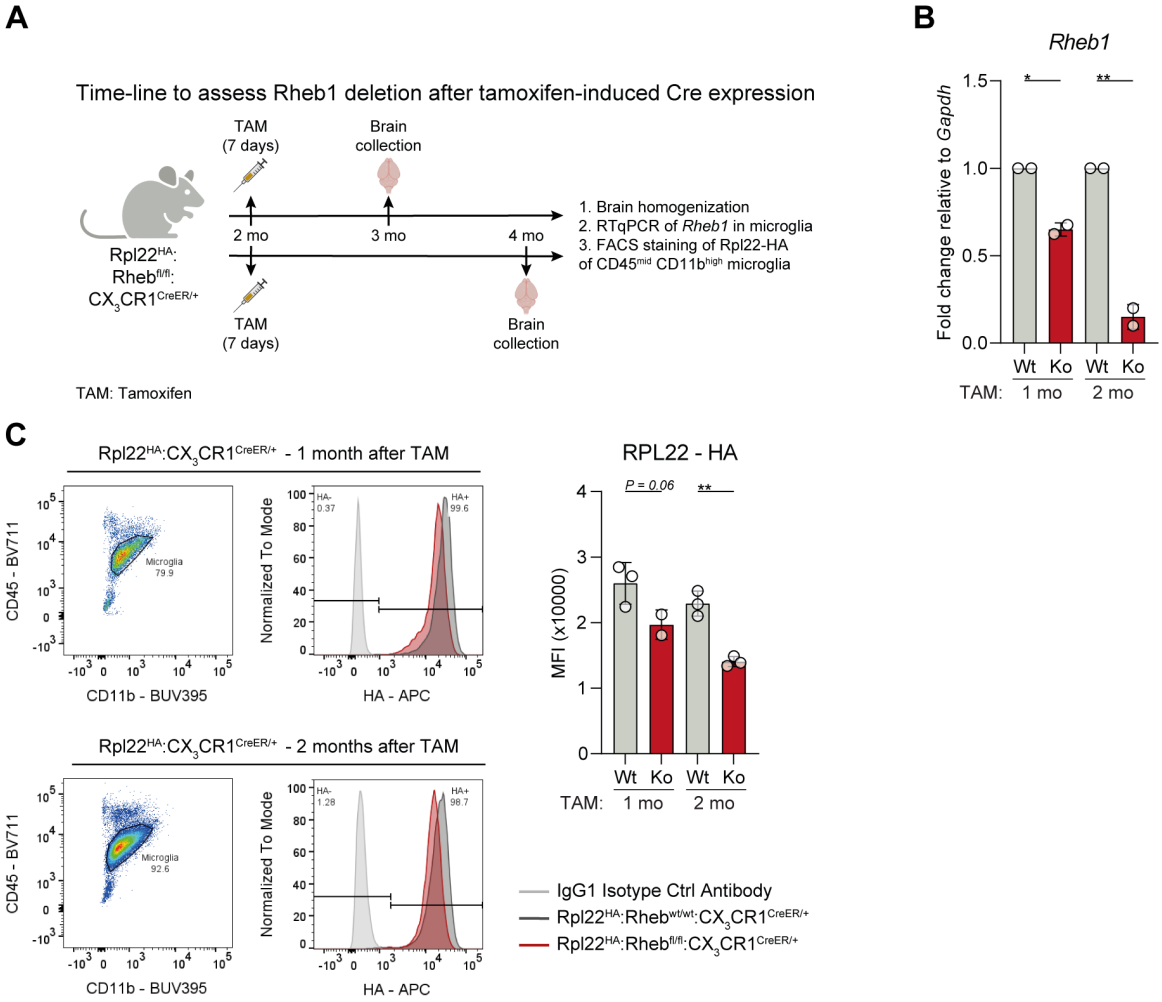

Figure 25 Characterization of Rpl22HA:Rhebfl/fl:CX3CR1CreER after treatment with tamoxifen.

(**A**). Representative schematic on the time-line used for assessing Rheb1 deletion and RPL22^{HA} expression in Rpl22^{HA}:Rheb$^{fl/fl}$:CX$_3$CR1^{CreER} mice. (**B**). RTqPCR of Rheb1 performed in isolated microglia from Rpl22^{HA}:Rheb$^{wt/wt}$:CX$_3$CR1^{CreER} and Rpl22^{HA}:Rheb$^{fl/fl}$:CX$_3$CR1^{CreER} animal at 1 and 2 month post-tamoxifen treatment. N = 2 per condition. (**C**). Flow cytometry plot of HA expression in CD11b^{high}CD45^{mid} microglia; (right panel) relative quantification of HA expression, shown as Median Fluorescence Intensity (MFI).

3.15. In-vivo experiment design and bioinformatics strategy

Since we aimed to assess transcriptional, translational and proteome changes through a multi-omics approach in aging microglia at steady state and in response to LPS, the in-vivo experiment was designed to minimize sources of variation for bioinformatics analysis. Specifically, cohorts of 2 and 16 months old *Rheb*$^{fl/fl}$ and *Rheb*$^{wt/wt}$ animals were treated at the same time with tamoxifen via i.p. injections for 7 consecutive days. Due to the higher number of animals involved (*N* = 6 biological replicates for the two genotypes, two age points and two treatments, in total 48 mice) and the long procedure for microglia isolation, animals were split in 5 cohorts, where each investigated condition was paired with its corresponding age-, treatment-, genotype-matched controls. At two months post-tamoxifen treatment, mice were challenged via i.p. injection of either PBS or 5 mg/Kg LPS and culled after 4 hours. Brains were immediately extracted from heads in an RNase-free environment (for further details, refer to Material and Methods). In particular, right hemispheres were rapidly collected and snap-frozen in liquid nitrogen to be used for HA-tagged microglia ribosomes immunoprecipitation ("Ribotag IP"); on the other hand, left hemispheres were processed to isolate microglia for proteome and transcriptome analysis. mRNAs from transcriptomics and translatomics were extracted and isolated in the same day. A brief description of the in-vivo experiment design and of bioinformatics strategy is illustrated in Figure 26.

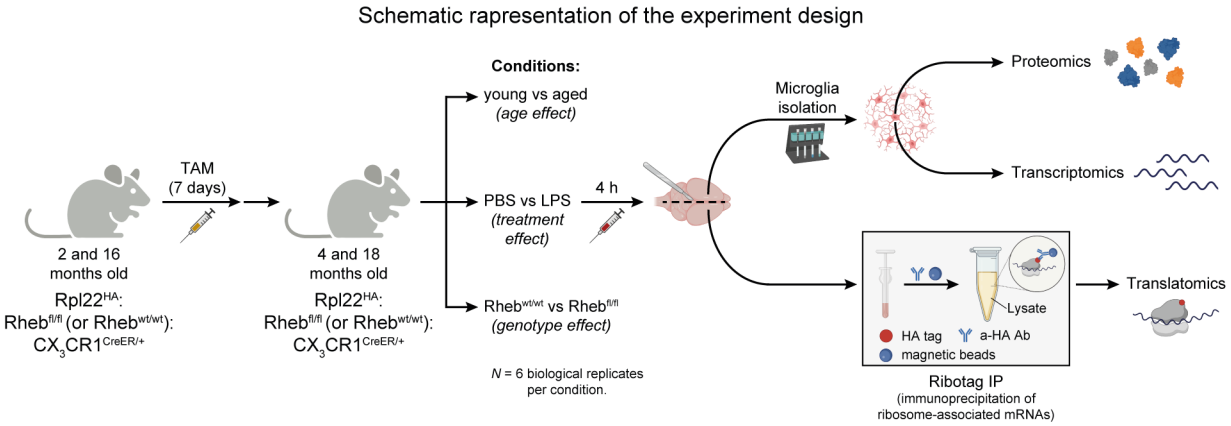

Figure 26. Schematic representing the in-vivo experiment design using Rpl22^{HA}: Rheb$^{fl/fl}$:CX$_3$CR1^{CreER} mouse model.

3.16. Exploratory data analysis of the transcriptome and translatome: LPS-induced immune response is the main driving factor in both transcriptomics and translatomics

After vst transformation of the raw counts, the expression table was first used for an exploratory data analysis (EDA) to identify general patterns in the data (i.e. outliers or unexpected features). Carefully looking at hierarchical clustering heatmaps showing the 1% of the most variable genes in both transcriptome and translatome (Figure 27A-B), it was clear that samples mainly separated in two major clusters representing microglia immune response to the *in-vivo* treatment (LPS on the left, PBS on the right). Within these two clusters, we could still observe that the greatest changes were determined by genotype-related differences in the LPS-treated sample group, whereas the age effect was more predominant in the PBS group (Figure 27A-B). This was also confirmed in the exploratory data analysis taking into account sample groups with either PBS or LPS treatment (data not shown). In order to discover which condition of our metadata contributed to the highest variance in both methods, we performed a principal component regression (PCR) analysis (Figure 27C-D). For both microglia transcriptome and translatome, the highest variance described by principal component (PC) 1 was shown by the treatment, whereas genotype effect was largely represented by PC4 (Figure 27C-D). On the other hand, age-related differences were shown by PC2 for the transcriptome and PC3 for the translatome (Figure 27C-D).

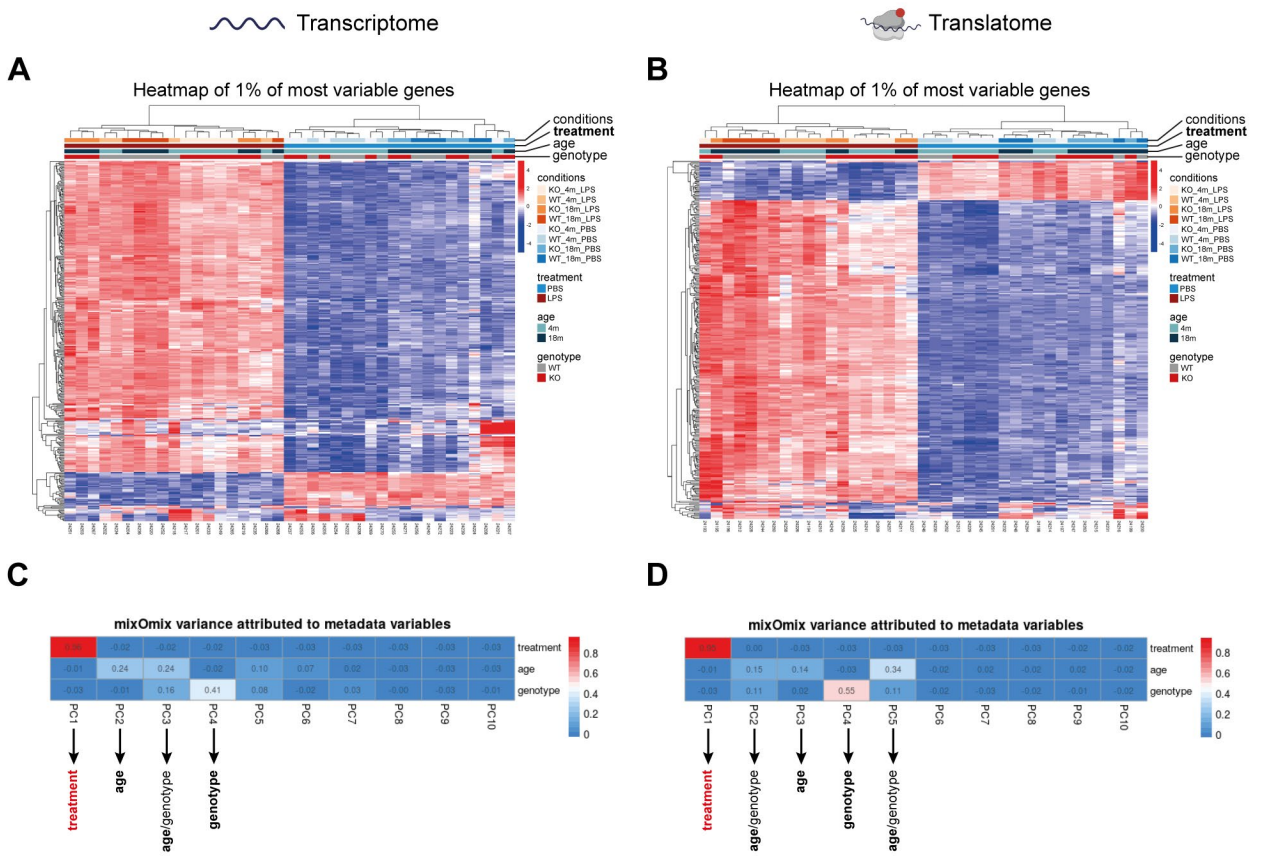

Figure 27 Exploratory data analysis from microglia transcriptome and translatome indicated that the major driving effect in both datasets is represented by LPS response.
A-B. Heatmap showing 1% of most variable genes in microglia transcriptome (**A**) and translatome (**B**) across all investigated conditions. **C-D**. Principal component regression (PCR) analysis representing the highest variance contribution attributed to each condition (treatment, age, and genotype) in (**C**) microglia transcriptome and (**D**) translatome.

As expected, samples mainly separated in two major groups in PC1, which represented about 36.5% and 37.4% of the variance for the transcriptome and the translatome, respectively (Figure 28A-B), and corresponded to either LPS- or PBS-treated samples (Figure 28C-D). Despite a lower variance due to a much greater effect of the treatment, a separation of sample groups based on genotype- and age-related differences was still visible in both methods (Figure 28E-H). Overall, these data indicated a high robustness of the two methods and reliability of data.

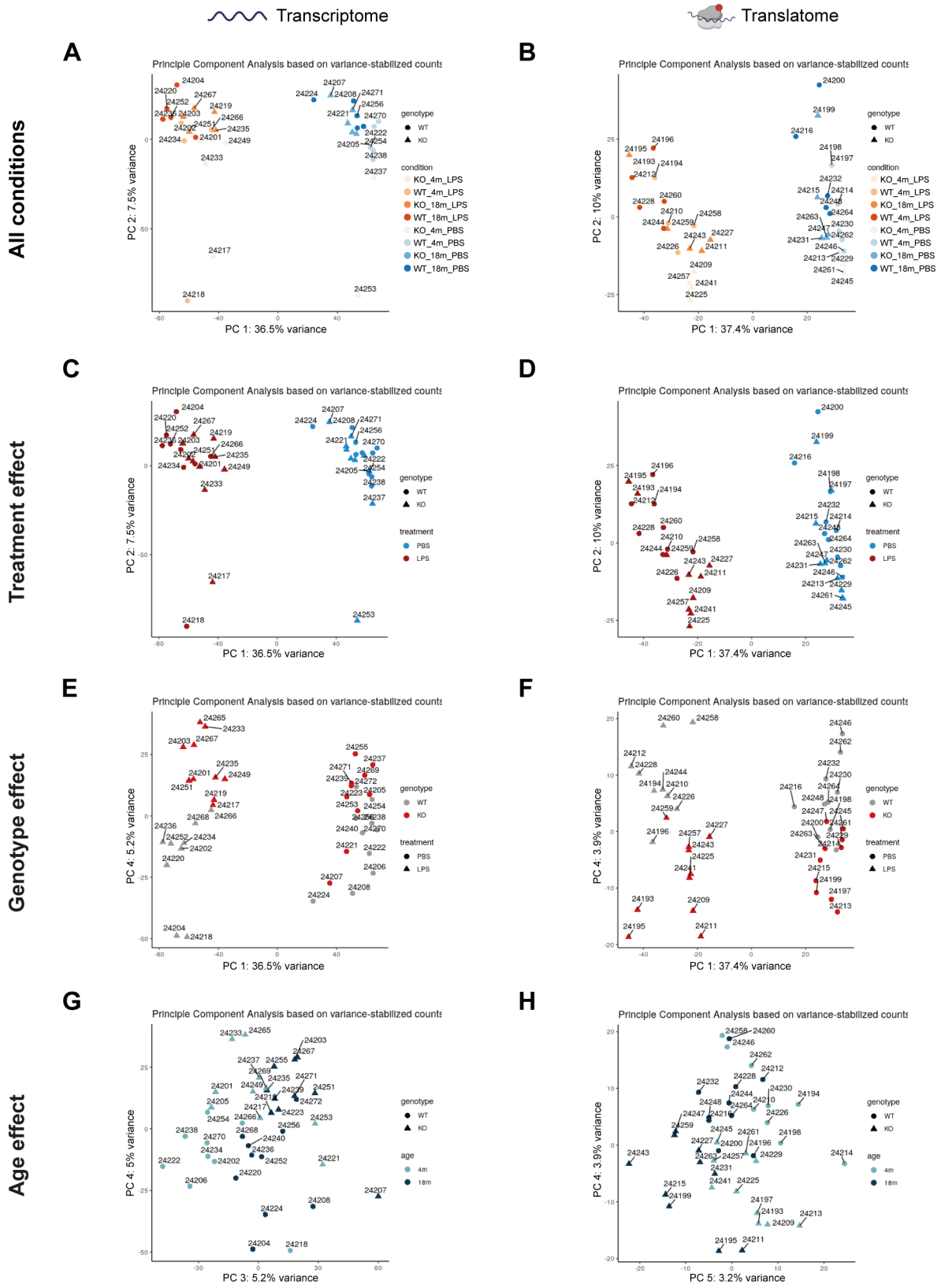

Figure 28. Principal component analysis of microglia transcriptome and translatome across all the conditions investigated.

(**A-B**) PCA of transcriptome (**A**) and translatome (**B**) for all conditions. (**C-H**) PCA to assess treatment, genotype and age effect in the transcriptome (**C**,**E**,**G**) and translatome (**D**,**F**,**H**) dataset.

3.17. Experimental setup: which comparisons were investigated

To understand which set of genes are predominantly upregulated and downregulated in microglia transcriptome, translatome and proteome, Gene Set Enrichment Analysis (GSEA) was performed using significant differentially expressed genes (DEGs) In this regard, the top 10 terms of gene ontology aspects relative to Molecular Function (MF), Cellular Component (CC) and Biological Process (BP) were taken into account. As the aim of this PhD thesis was to define which changes microglia underwent with age, in response to LPS and in absence of Rheb1, I focused on the following comparison (C):

- PBS-treated aged wildtype vs PBS-treated young wildtype, defined as C1;
- LPS-treated aged wildtype vs PBS-treated young wildtype, defined as C2;
- LPS-treated aged Rheb1 Ko vs LPS-treated aged Rheb1 Ko, defined as C3

3.18. Aging microglia show a higher immune sensitiveness at the transcriptome level (comparison C1)

In aging wild-type microglia at steady state (C1), 716 significant differentially expressed genes (DEG) were detected, of which 229 were downregulated and 487 were upregulated, when compared to younger counterparts at the transcriptome level (Figure 29A). Relative to GSEA, aged microglia mainly downregulated genes that were involved in cytoskeleton organization, indicative of defects in cellular organization, and constituents of Glutamate receptors. The latter are expressed in microglia and are known to participate in the regulation of the inflammatory response (Antignano et al., 2023; H. Liu et al., 2016) . Therefore, one possibility is that aged microglia may downregulate glutamate receptors to counteract their own immune activation due to an increased ability to sense an inflamed brain environment. Indeed, the terms upregulated by aging microglia were associated to cytokines and chemokines activities and receptors, which indicated an overall increase in aged microglia of an immune-alert state (Figure 29B), in line with the current literature (Antignano et al., 2023).

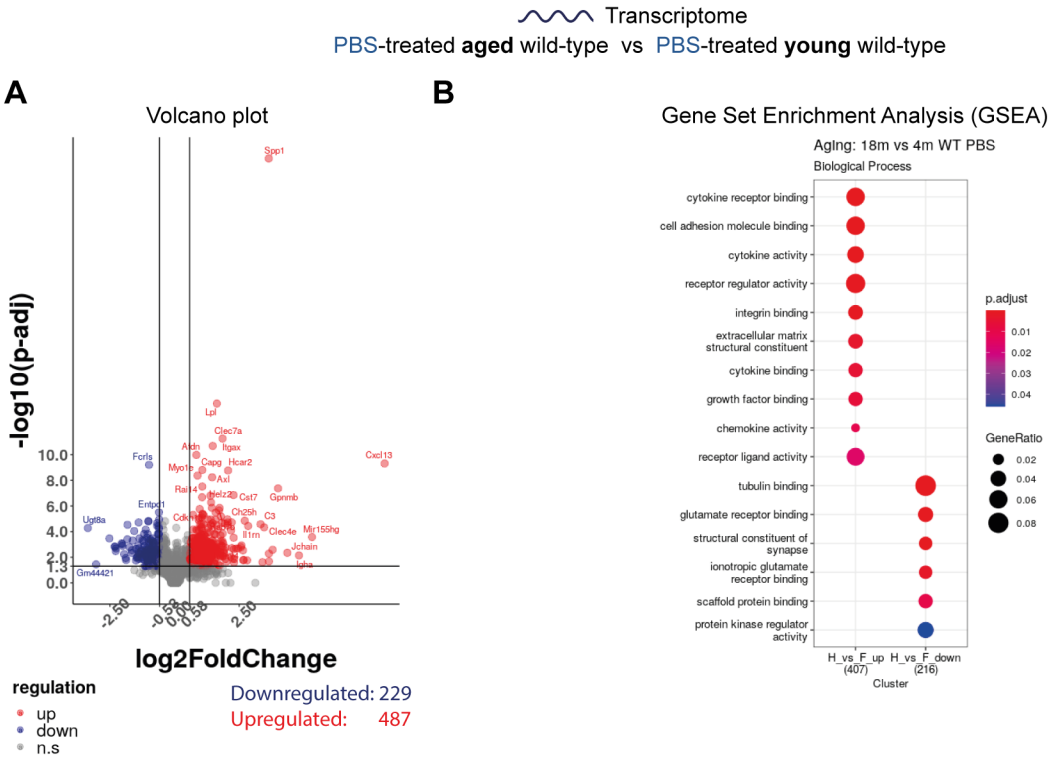

Figure 29 Microglia upregulates immune-sensing genes with age at transcriptome level.
(**A**) Volcano plot showing significant differentially expressed genes (DEGs) between aged vs young microglia isolated from PBS-treated animals at transcriptome level. (**B**) Gene Set Enrichment Analysis (GSEA) of significant DEGs derived from the same comparison.

Regarding the microglia translatome at steady state, nearly all the DEGs were upregulated (121 against 7 downregulated) (Figure 30A), and were associated to increased cytokine-mediated signaling pathways, regulation of immune response to stimuli and activation of adaptive immunity (Figure 30B). The latter might be explained due to an upregulation of MHC class I molecules that we found highly enriched as biological process and cellular component (Figure 30B). This increased expression might lead to a greater antigen presentation in order to activate T cells, which are known to accumulate in the aged brain (Dulken et al., 2019; Groh et al., 2021; Krishnarajah et al., 2021). Even considering the low number of genes downregulated at the translatome level, we could observe that aged microglia lowered the expression of genes that counteract oxidative stress and cell death-induced programs, therefore indicating a general dysregulation of homeostatic mechanisms with age (Figure 30B).

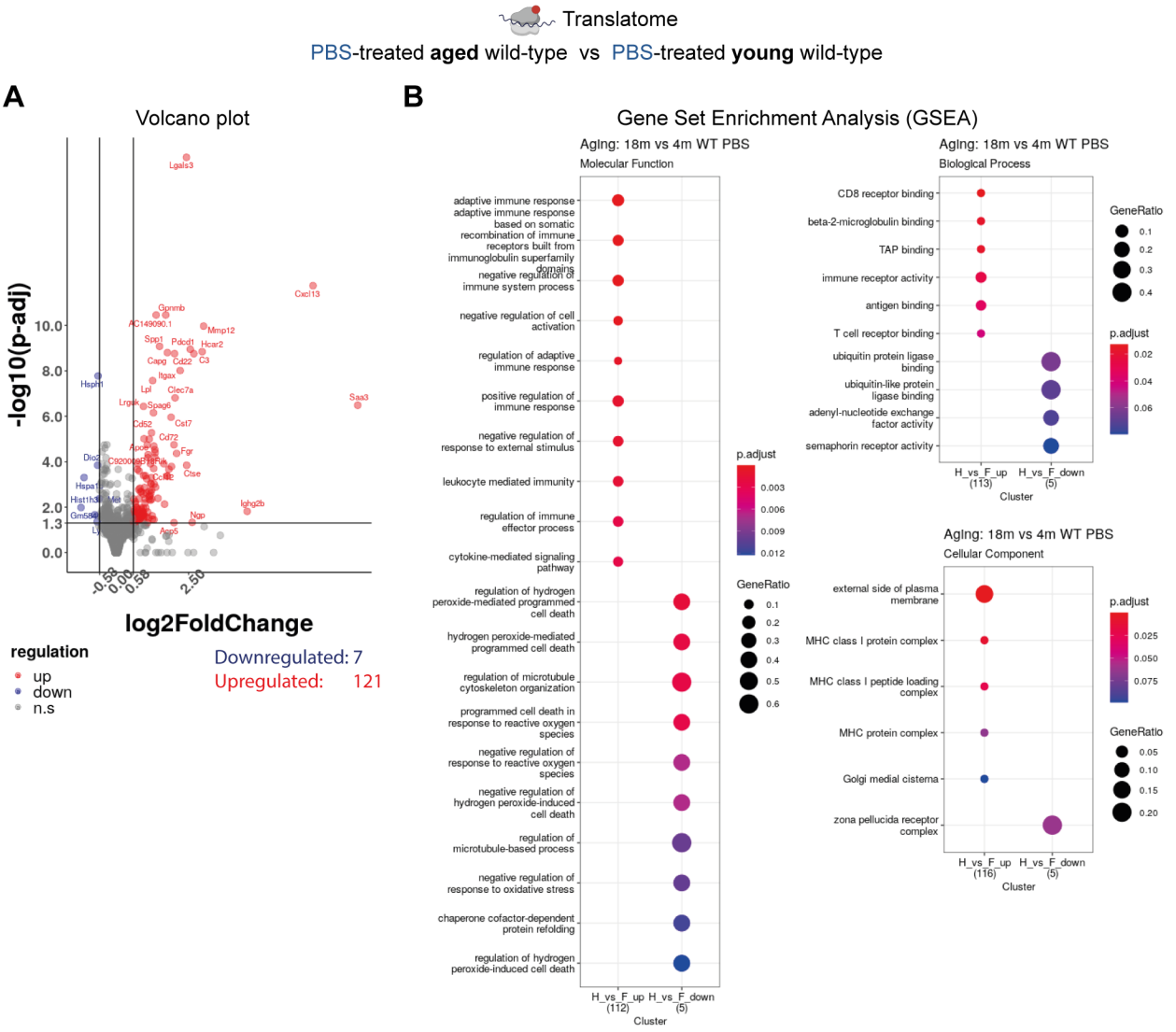

Figure 30 Immune-sensing genes are more translated in aged microglia translatome (**A**) Volcano plot showing significant differentially expressed genes (DEGs) between aged vs young microglia isolated from PBS-treated animals at translatome level. (**B**) Gene Set Enrichment Analysis (GSEA) of significant DEGs derived from the same comparison.

3.19. Translation is a major component upregulated in LPS aged microglia vs young counterparts (comparison C2).

About 6651 significant DEGs were detected from aged microglia isolated from LPS-challenged wild-type animals compared to PBS controls at transcriptome level. Specifically, 3583 were downregulated and 3068 were upregulated as shown in the volcano plot (Figure 31A). Interestingly, the first upregulated terms were related to

ribosome biogenesis and translation regulatory activity of initiation factors (Figure 31B), indicating an overall increased expression of protein synthesis machinery needed to amplify microglia immune response. Indeed, immune-related terms (i.e. positive regulation of cytokine production, response to INF-β and INF-γ) were among the most upregulated biological processes in the enrichment analysis (Figure 31B). In parallel, an increased expression of genes encoding for ubiquitin ligase proteins was also observed (Figure 31B). This might be due to a higher translation rate and unbalanced protein synthesis quality control, leading to an overall excess of misfolded proteins targeted by the proteasome. About the downregulated terms, we observed a reduced expression of genes involved in DNA replication (Figure 31B), which might suggest a differentiation program induced by LPS stimulation or maybe it reflects the reduction in the pool of homeostatic microglia upon systemic inflammation. Further investigations will clarify the role of these genes belonging to this group.

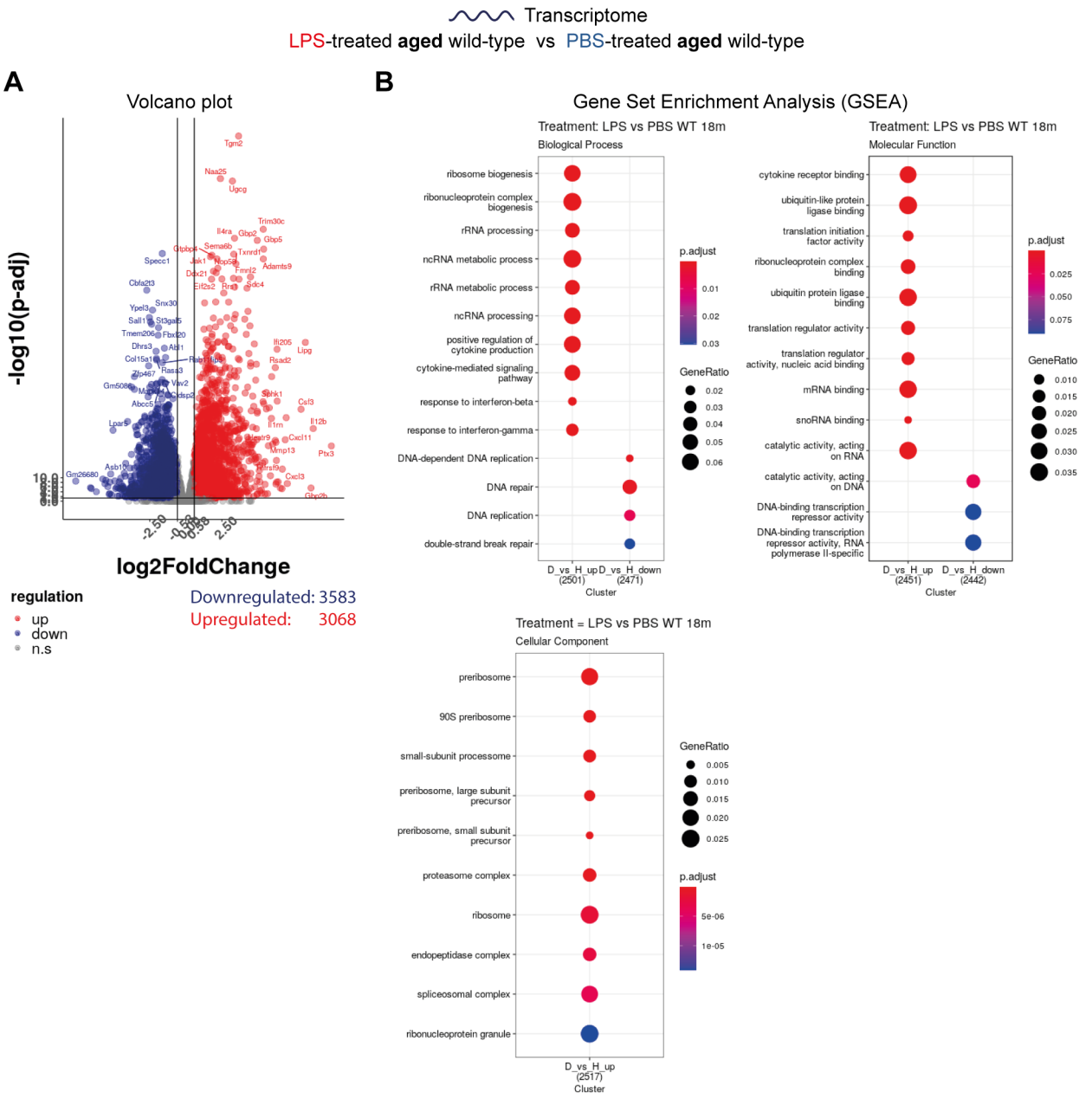

Figure 31 Constituents of protein synthesis machinery are strongly upregulated by aged microglia in response to in vivo LPS-treatment at transcriptome level
(**A**) Volcano plot showing significant differentially expressed genes (DEGs) between microglia isolated from LPS-treated vs PBS-treated wild-type at transcriptome level. (**B**) Gene Set Enrichment Analysis (GSEA) of significant DEGs derived from the same comparison.

Interestingly, DEG analysis of upregulated genes in microglia translatome yielded a more pronounced expression of genes involved in the immune response (Figure 32A-B), clearly indicating that these genes were associated with ribosomes, therefore more translated by aged microglia in response to LPS. This evidence was also supported by an increased

protein expression of protein synthesis constituents that we found in the proteomics, as explained later in paragraph 3.23. Of note, some of these immune-related terms were found both upregulated and downregulated at translatome level (Figure 32B). This would suggest that certain subsets of genes belonging to the same gene ontology terms might undergo a different gene expression regulation occurring at translatome level.

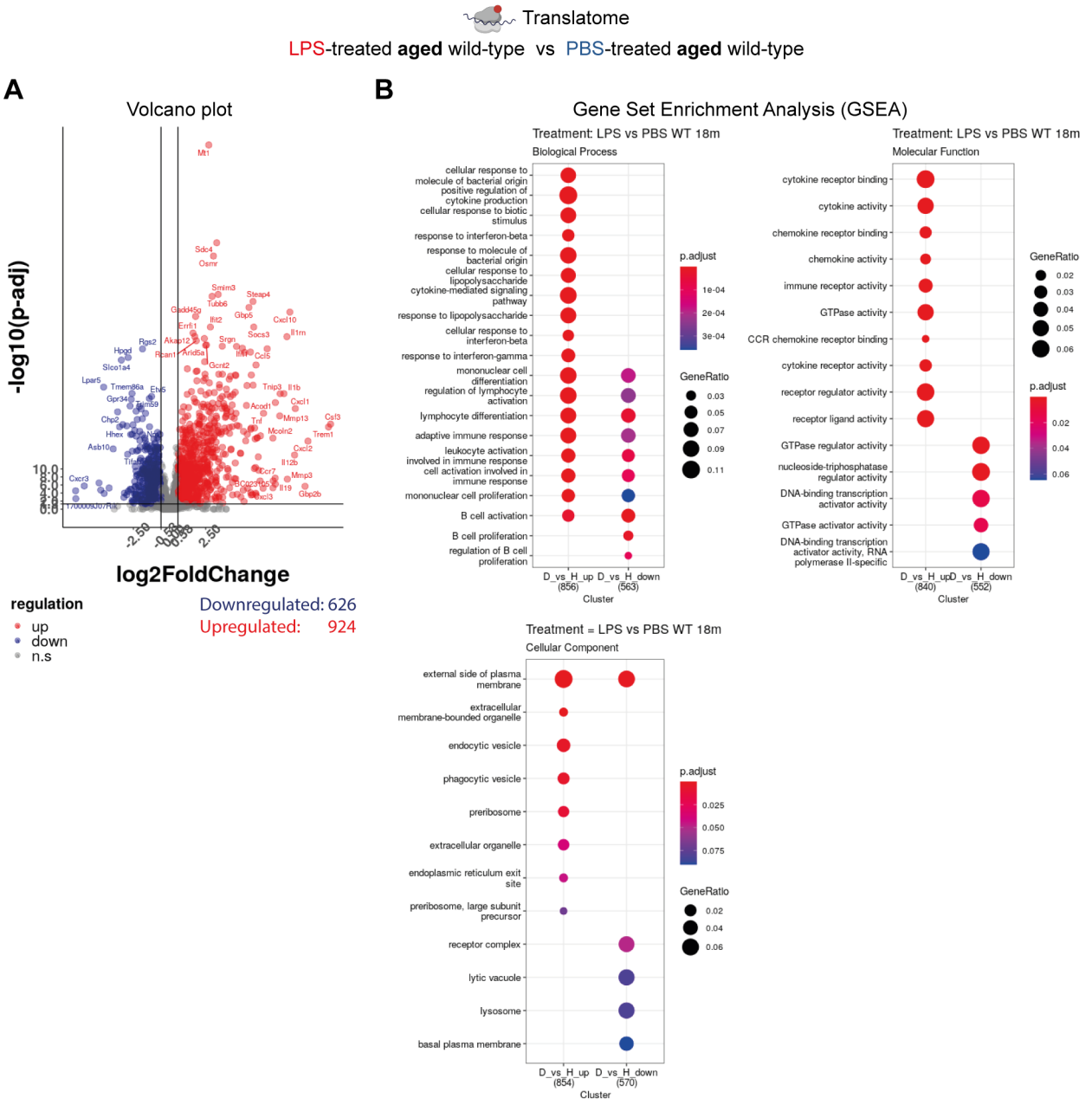

Figure 32 Immune-related genes are more translated by aged microglia in response to in vivo LPS treatment

(**A**) Volcano plot showing significant differentially expressed genes (DEGs) between microglia isolated from LPS-treated vs PBS-treated wild-type at translatome level. (**B**)

Gene Set Enrichment Analysis (GSEA) of significant DEGs derived from the same comparison.

3.20. Rheb1 loss impairs translation of immune-related genes despite the increased expression at mRNA level (comparison C3)

In order to understand if Rheb1 loss decreased the excessive immune response of aged microglia in LPS-challenged mice, we compared Rheb Ko aged microglia vs Wt aged microglia upon LPS treatment.

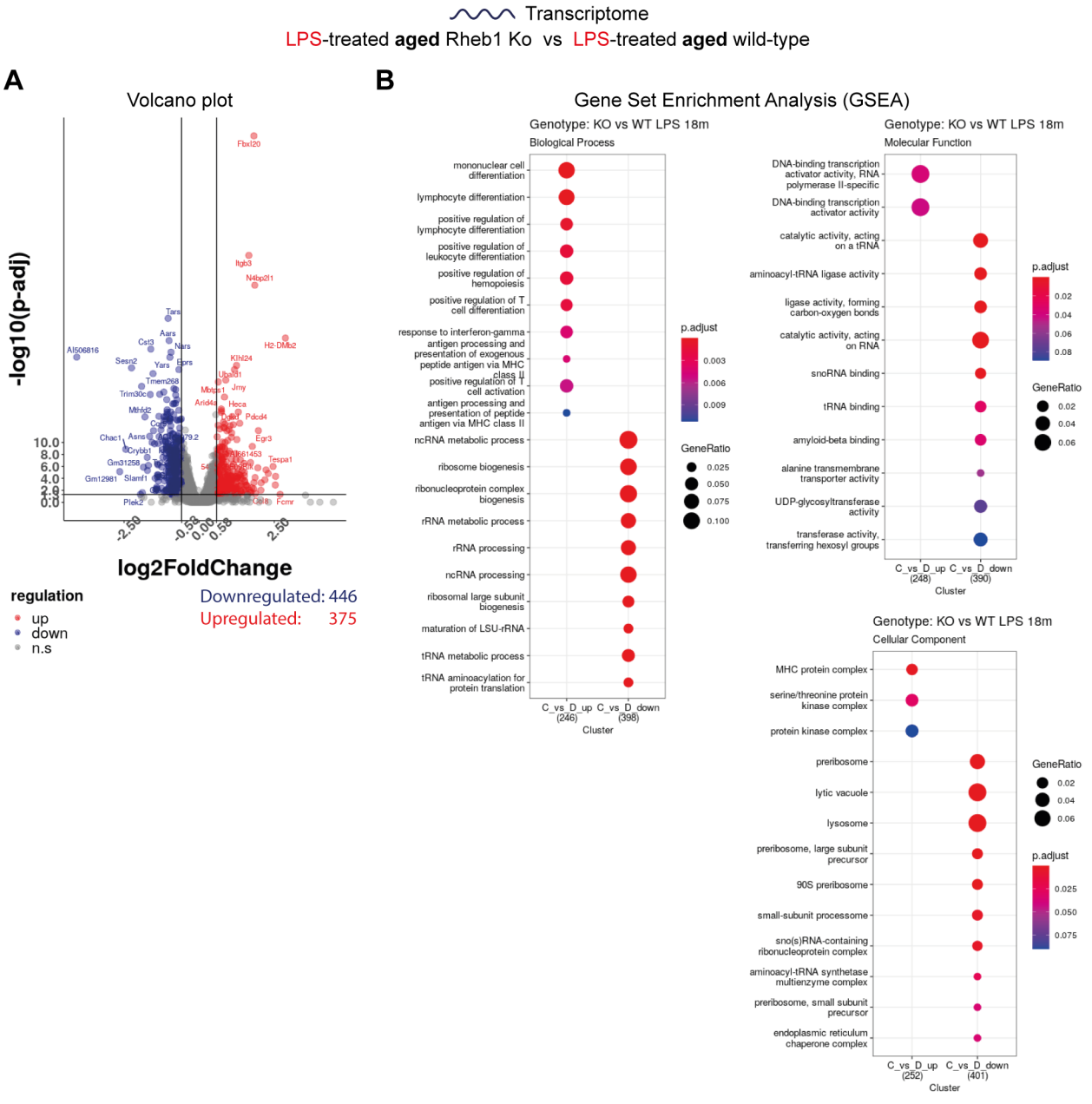

Figure 33 mTORC1 inhibition by Rheb loss severely impairs the transcription of protein synthesis-related genes, but not immune genes

(**A**) Volcano plot showing significant differentially expressed genes (DEGs) between Ko vs Wt microglia isolated from LPS-treated animals at transcriptome level. (**B**) Gene Set Enrichment Analysis (GSEA) of significant DEGs derived from the same comparison.

In contrast to aged Wt, Rheb deletion led to a strong downregulation of genes encoding for components of protein synthesis, in particular genes involved in ribosome biogenesis, tRNA binding and aminoacylation (Figure 33A-B). This indicated a defect of protein synthesis, as we expected due to mTOR inhibition by Rheb loss. Of note, genes related to immune response were even found more upregulated at the transcriptome level in Rheb Ko, such as genes involved in antigen presentation through MHC class II and in response to INF-γ (Figure 33A-B). Most likely, this effect was due to an overall increase of DNA transcription activity that we observed to be the only upregulated GO term among the altered molecular functions in Rheb Ko.

With regard to the translatome, one of the most striking results was the low number of DEGs, where the majority, 120 genes, were downregulated, while 32 were found upregulated (Figure 34A). Interestingly, the 10 top pathways associated with downregulated genes upon LPS treatment in Rheb Ko aged microglia were related to immune regulation of pro-inflammatory cytokines, in particular to TNF production and NF-κB signaling (Figure 34B). This indicated a potential role of the mTORC1-dependent translation pathway to translationally regulate the expression of certain subsets of immune response-related genes, as we initially hypothesized (Keane et al., 2021). However, not all immune genes were influenced by Rheb1 loss. Some of these, which were involved in the formation of “MHC protein complex” or encoding for “cytokine receptor” were indeed found upregulated in aged Rheb Ko microglia (Figure 34B). This suggested that, as far as protein synthesis was impaired, as confirmed by the proteome analysis (Paragraph 3.24), certain mRNA subsets were still translated, possibly through a Rheb1-mTORC1-independent mechanisms.

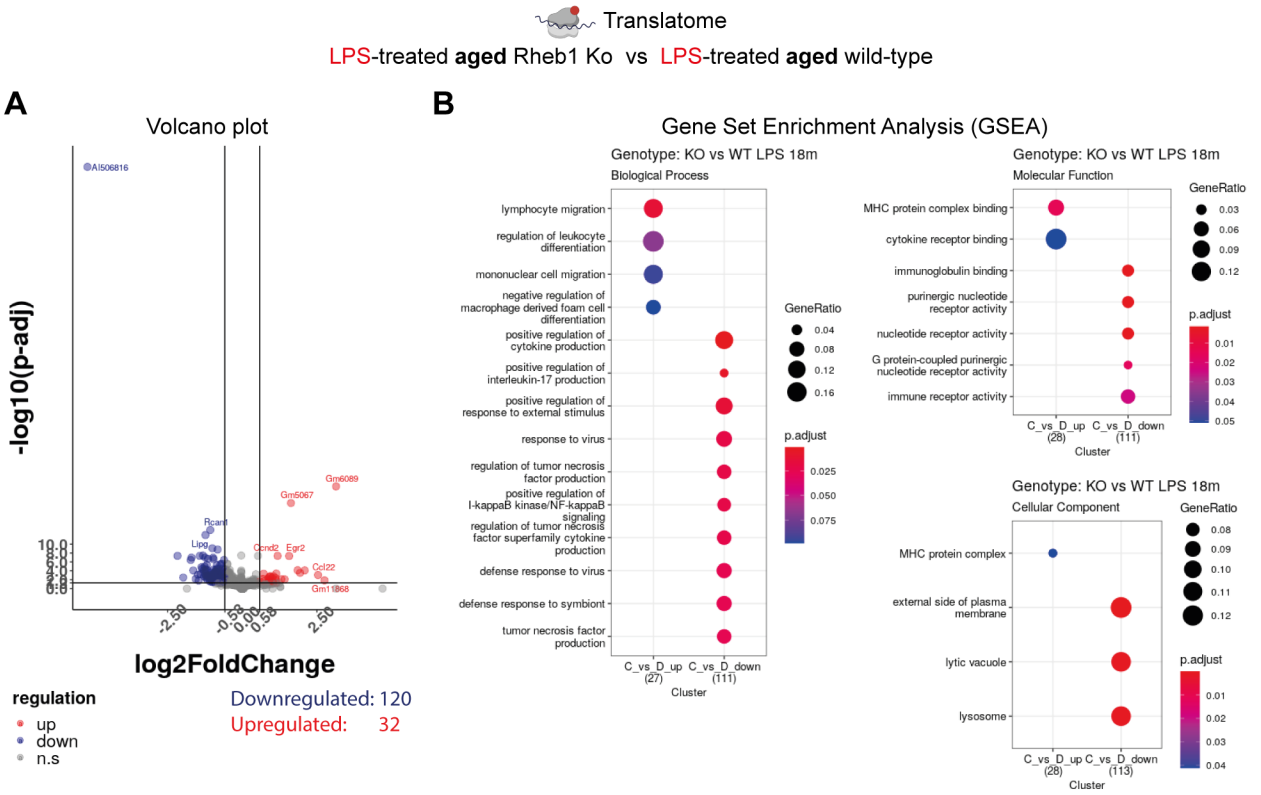

Figure 34 Translation of immune-related genes are downregulated in Rheb Ko microglia

(**A**) Volcano plot showing significant differentially expressed genes (DEGs) between Ko vs Wt microglia from LPS-treated animals at translatome level. (**B**) Gene Set Enrichment Analysis (GSEA) of significant DEGs derived from the same comparison.

3.21. Proteome analysis on aging microglia

As explained earlier in the experimental design, an aliquot of microglia cells were subjected to proteomics analysis, which was performed in collaboration with Dr. Enzo Scifo in Dr. Dan Ehninger group at DZNE, Bonn.

Raw data from the LC-MS/MS experiment were processed with Proteome Discoverer™ software, using SEQUEST® HT search engine against the Swiss-Prot® *Mus musculus* database for protein identification. All samples successfully passed selected quality control metrics, showing high instrument performance and optimal enzyme digestion efficiency (refer to Materials and Method). Prior to the analysis, raw MS peptide intensities were normalized based on total peptide amounts. Finally, protein identified as contaminants (i.e. keratin) and with low confidence score were filtered out.

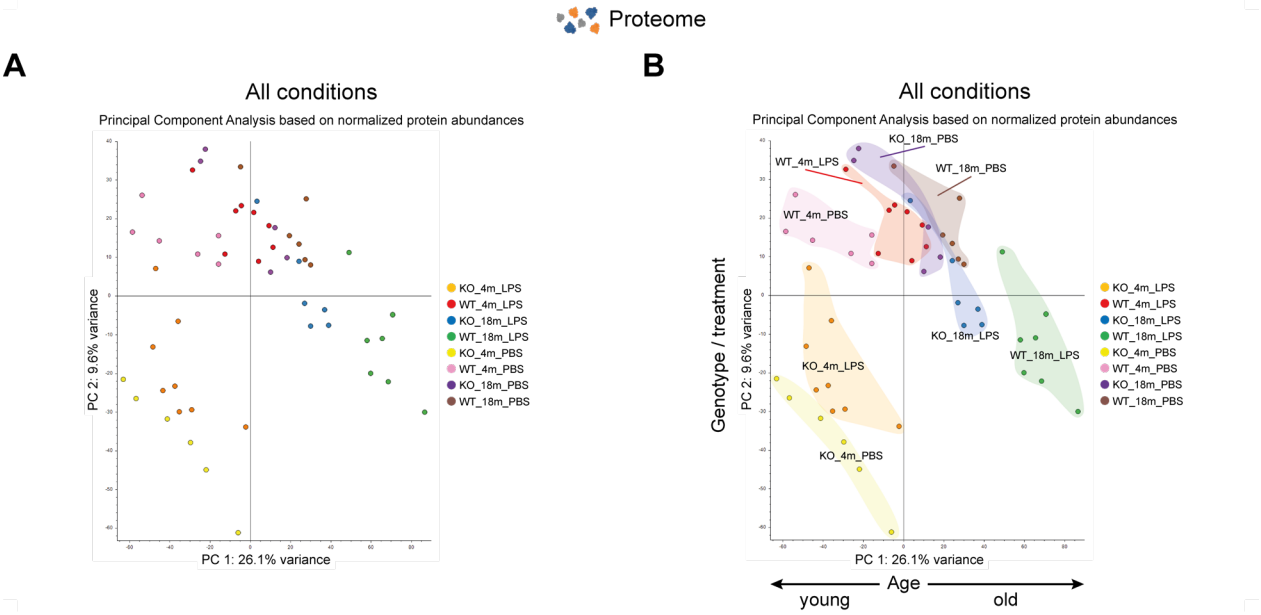

Figure 35 Principal component analysis of microglia proteome in the conditions investigated.
(**A**) Principal component analysis (PCA) of microglia isolated from young and old tamoxifen-treated *Rpl22^{HA}:Rheb$^{fl/fl}$:CX3CR1$^{CreER/+}$* and *Rpl22^{HA}:Rheb$^{wt/wt}$:CX3CR1$^{CreER/+}$* animals and subjected to PBS or LPS *in vivo* treatment. (**B**) Same representation of the PCA described in (**A**) with the indicated conditions highlighted in different colors for a better visualization of the sample groups.

Principal component analysis based on normalized protein abundances clearly showed that sample groups were mainly separated based on the age as shown in PC1, where most of the variance was identified (Figure 35A-B, young group on the left, old group on the right in PC1). On the other hand, groups displayed by PC2 represented a contribution derived from both genotype and treatment effects (Figure 35A-B).

More generally, we could observe at least three major clusters: the first was represented by young Rheb Ko; the second, much larger, contained most of the conditions investigated; and a third group was represented by LPS-treated aged wild-type samples. (Figure 35B). In particular, with regard to the aged groups, it was interesting to note that Rheb Ko microglia from LPS-treated animals (in blue) remained relatively close to PBS groups (in violet and brown), but it was clearly separated from the LPS Wt cluster (in green). This suggested that changes induced in aging upon stimulation are regulated by Rheb and its loss rendered microglia less responsive to LPS.

3.22. Microglia upregulate components of protein synthesis machinery in aging (Comparison 1)

In aging wild-type microglia at steady state (C1), 1197 significant differently abundant proteins (DAPs) were detected, of which 398 were downregulated and 798 were upregulated, when compared to younger counterparts (Figure 36A). Relative to the enrichment analysis, aged microglia mainly downregulated proteins that were involved in cytoskeleton organization, endocytosis and ATPase-coupled transmembrane transporter activity, indicative of a defective cell migration and cellular communication (Figure 36B and Figure 37). On the other hand, the terms found over-represented in aged microglia were related to increased protein synthesis, such as structural components of ribosomes (i.e. ribosomal proteins), translation regulatory activity as well as aminoacyl-tRNA ligases promoting aminoacylation of tRNAs during translation elongation (Figure 36B and Figure 37).Moreover, proteins involved in Endoplasmatic-reticulum-associated-protein degradation (ERAD) pathway were also found (Figure 36B and Figure 37). This was indicative of an increased mRNA translation, most likely coupled to this degradative pathway, which is typically found upregulated in response to age-dependent accumulation

of misfolded proteins. Finally, aged microglia also upregulated proteins involved in the regulation of immune response, indicative of a shift towards a more immune-alert state, in line with the transcriptome and translatome results (Figure 36B and Figure 37)..

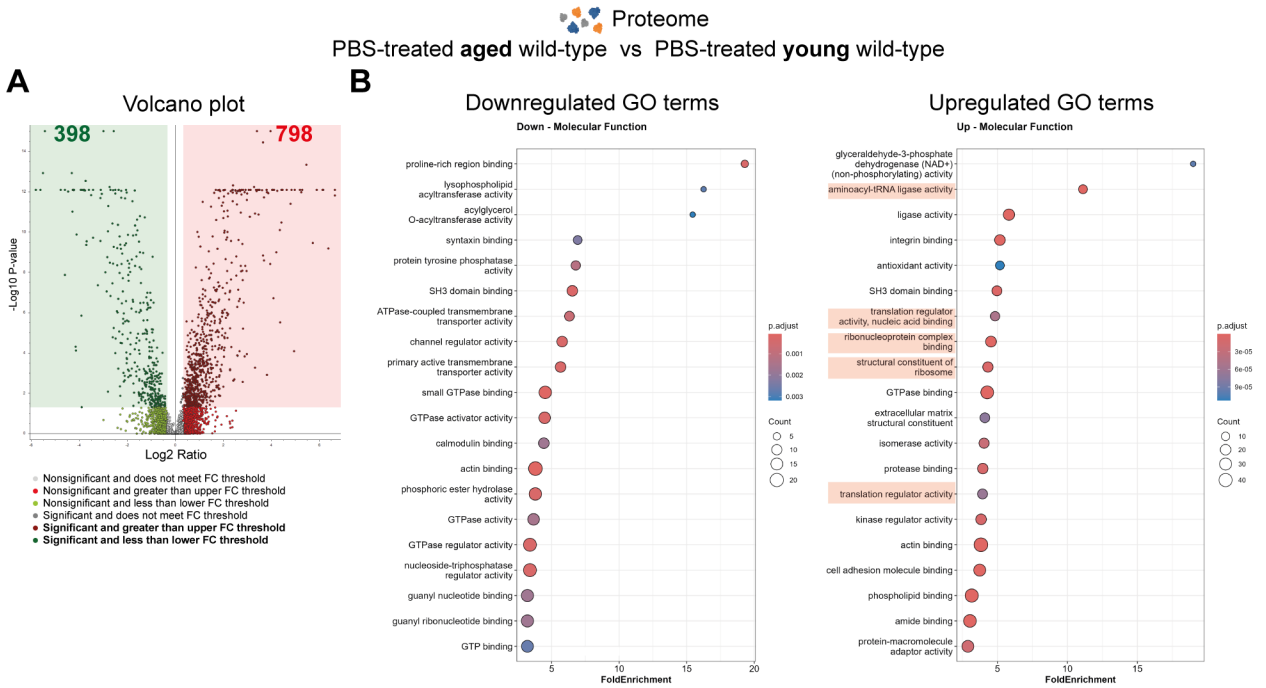

Figure 36 Protein synthesis machinery is upregulated in aging wild-type microglia at steady state
(**A**) Volcano plot showing significant differently ambundant proteins (DAPs) between aged vs young microglia isolated from PBS-treated animals. (**B**) Gene Set Enrichment Analysis (GSEA) of significant DAPs derived from the same comparison.

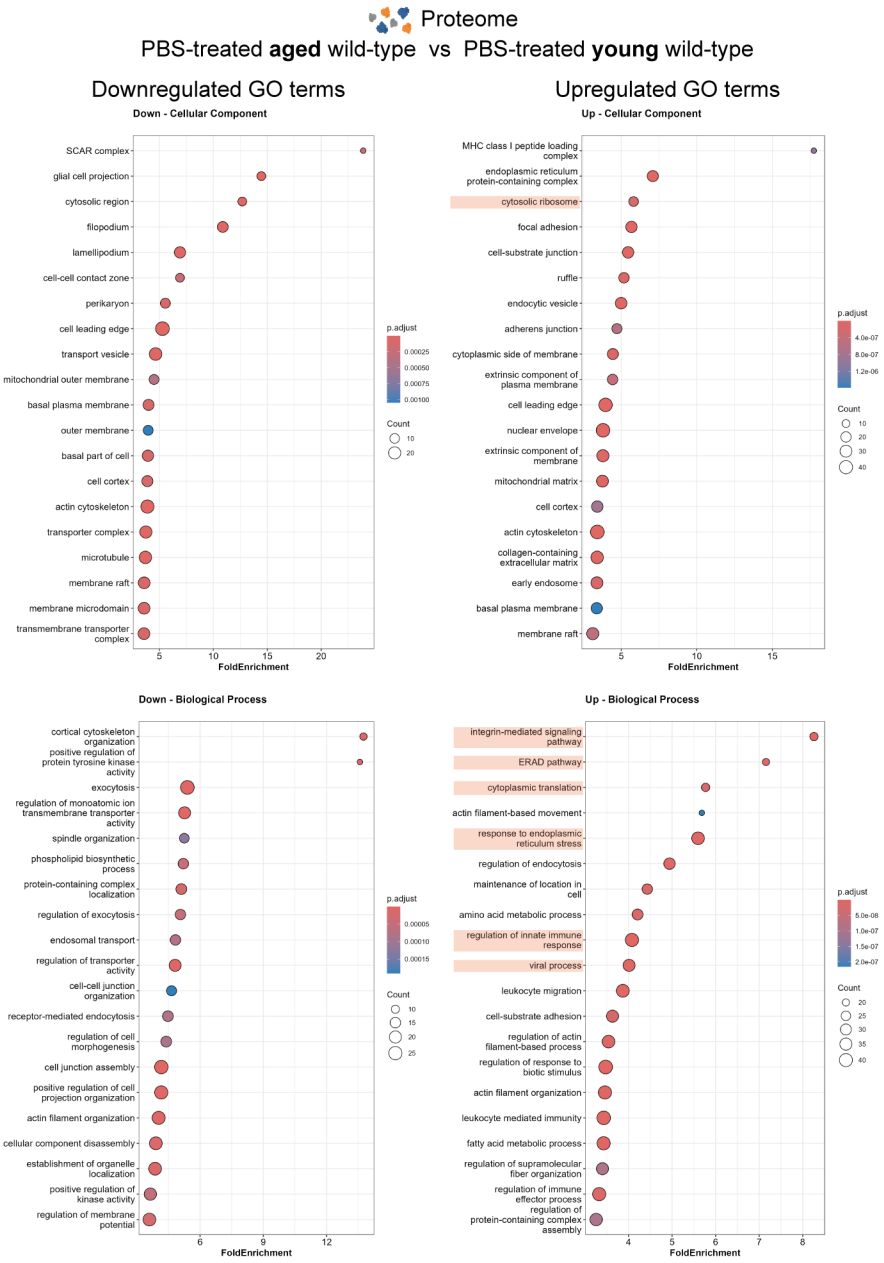

Figure 37 Additional GO aspects derived from proteome analysis of aging wild-type microglia

Gene Set Enrichment Analysis (GSEA) of significant DAPs derived from aging wild-type proteme and related to Figure 36B

3.23. Protein synthesis machinery is further upregulated by aged microglia in response to LPS (Comparison 2)

About 966 significant DAPs were detected from aged microglia isolated from LPS-challenged wild-type animals compared to PBS controls. Specifically, 489 were downregulated and 476 were upregulated (Figure 38A). By similarity, aged microglia in response to LPS also downregulated terms previously shown in Figure 36 and 37, nevertheless, vacuolar ATPase (V-ATPase) proteins belonging to the ATP6V family were the most downregulated, indicating a potential defect in the acidification of intracellular organelles responsible for recycling and degrading molecules or an overall reduction of endolysosomes (Figure 38B and Figure 39). Interestingly, protein synthesis was the first top represented term as biological process in response to LPS (Figure 38B and Figure 39). In this regard, the main components of the translation machinery represented were: tRNA aminoacylation enzymes (TARS2, SARS2, LRRC47, HARS, MARS1, CARS, FARSB, TARS), subunits of eIF3 complex (EIF3A, EIF3K, EIF3H, EIF3I), initiation and elongation translation factors (EIF4A1, EIF4G1, EIF2S1, EIF1A, EEF2, EEF1B2), as well as ribosomal proteins. Additionally, aged microglia also displayed a more inflammatory profile with an increased expression of protein involved in the immune response, specifically in the regulation of IL-6 and viral response (Figure 38B and Figure 39). Taken together, these data further corroborate our previous findings (Keane et al., 2021), that protein synthesis is upregulated in aged microglia and contributes to a stronger immune response.

Figure 38 Protein synthesis is further upregulated by aged microglia in response to LPS.

(**A**) Volcano plot showing significant differently ambundant proteins (DAPs) between LPS vs PBS microglia isolated from aged wild-type animals. (**B**) Gene Set Enrichment Analysis (GSEA) of significant DAPs derived from the same comparison.

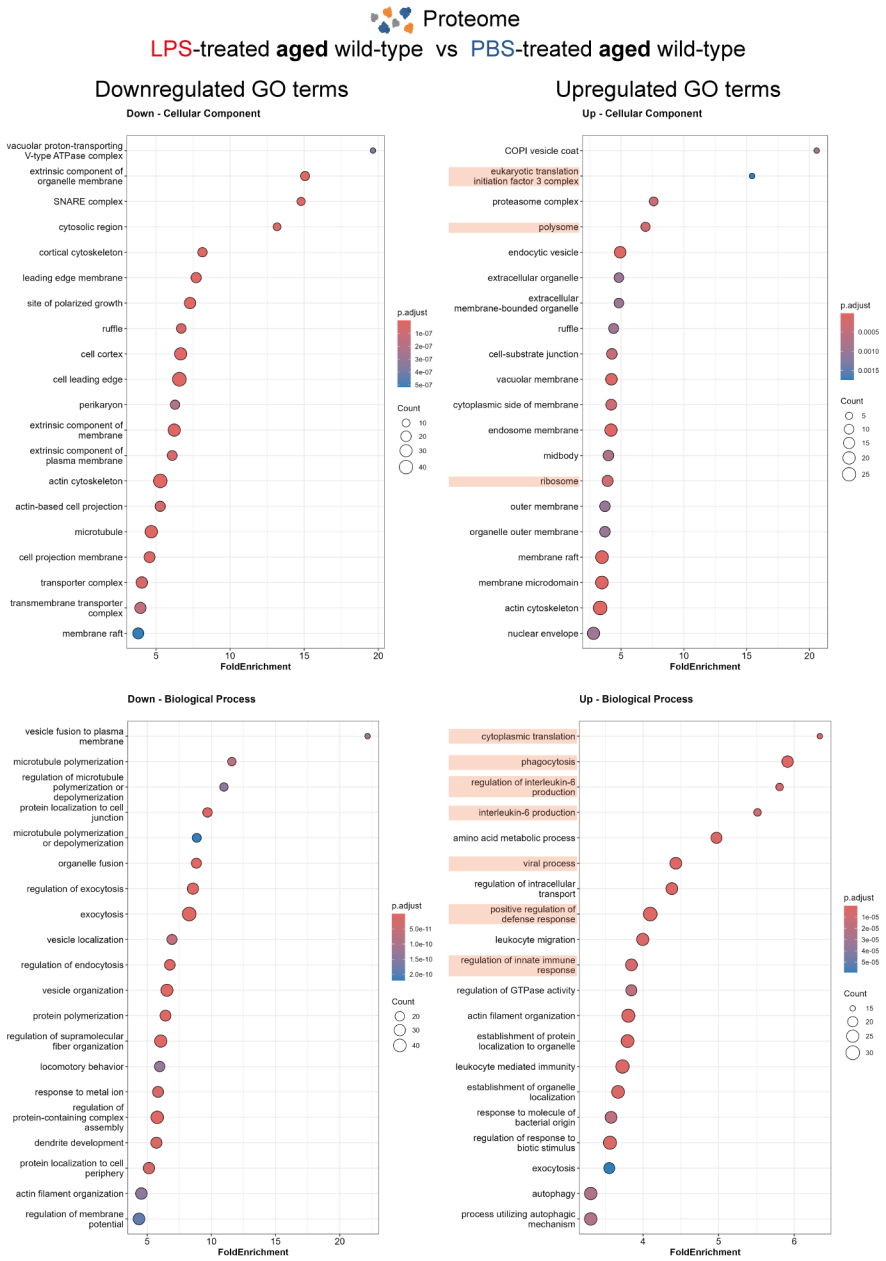

Figure 39 Additional GO aspects derived from proteome analysis of microglia from LPS vs PBS-treated wild-type animals

Gene Set Enrichment Analysis (GSEA) of significant DAPs between LPS vs PBS microglia isolated from aged wild-type animals and related to Figure 38B

3.24. Genetic loss of Rheb1 in aged microglia downregulates constituents of the proteins synthesis machinery and pro-inflammatory mediators in response to LPS (Comparison 3)

In order to understand if Rheb1 loss was indeed dampening the immune response of aged microglia in LPS-challenged mice, confirming our hypothesis that translation its a critical amplifier of aged immune responses, we compared Rheb KO aged microglia vs WT aged microglia proteome upon LPS treatment.

As shown in the volcano plot (Figure 40A), about 920 significant DAPs were found in aged Rheb Ko microglia in response to LPS compared to Wt counterparts. Of these, 500 proteins were found downregulated, and 419 upregulated. In contrast to aged Wt and the previous comparisons, components of protein synthesis, which were upregulated in aged microglia vs young microglia (Figure 38B and 39), were the most de-enriched terms in aged Rheb1 Ko in response to LPS (Figure 40B and 41). Among these, proteins involved in tRNA aminoacylation (TARS, FARSB, NARS, CARS2, HARS, QARS, MARS1, SARS2, LARS2, TARS2), subunits of the EIF3 complex (EIF3K, EIF3I, EIF3H, EIF3A and DDX3X), translation regulatory factors (EIF2S1, EEF1B2, EEF2, EEF1G, ABCF1, GTPPB1), as well as ribosomal proteins were significantly downregulated. As the expression of these proteins is tightly regulated by mTORC1 (G. Y. Liu & Sabatini, 2020), these data further corroborated our previous findings on the role of mTORC1-dependent translation in boosting inflammatory responses in aged microglia (Keane et al., 2021a). Additionally, aged Rheb Ko microglia downregulated proteins involved in mechanisms for correct protein folding and in the regulation of ER stress (Figure 40B and 41). Most probably, this effect was due to a lower translation rate in Rheb Ko microglia, which decreased the chance of protein misfolding.

Although they were not showed among the first 20 terms, aged Rheb Ko microglia also downregulated immune response-related proteins, such as DDX3X, PYCARD, NLRC4, required for the inflammasome complex formation, and proteins involved in IL-6 signaling.

On the other hand, the most upregulated over-represented terms were related to proteins involved in cytoskeleton organization, of which some displayed GTPase regulatory

activities, and in cell-to-cell and intracellular communication, potentially indicating an amelioration of the aged microglia phenotype (Figure 40B and Figure 41)

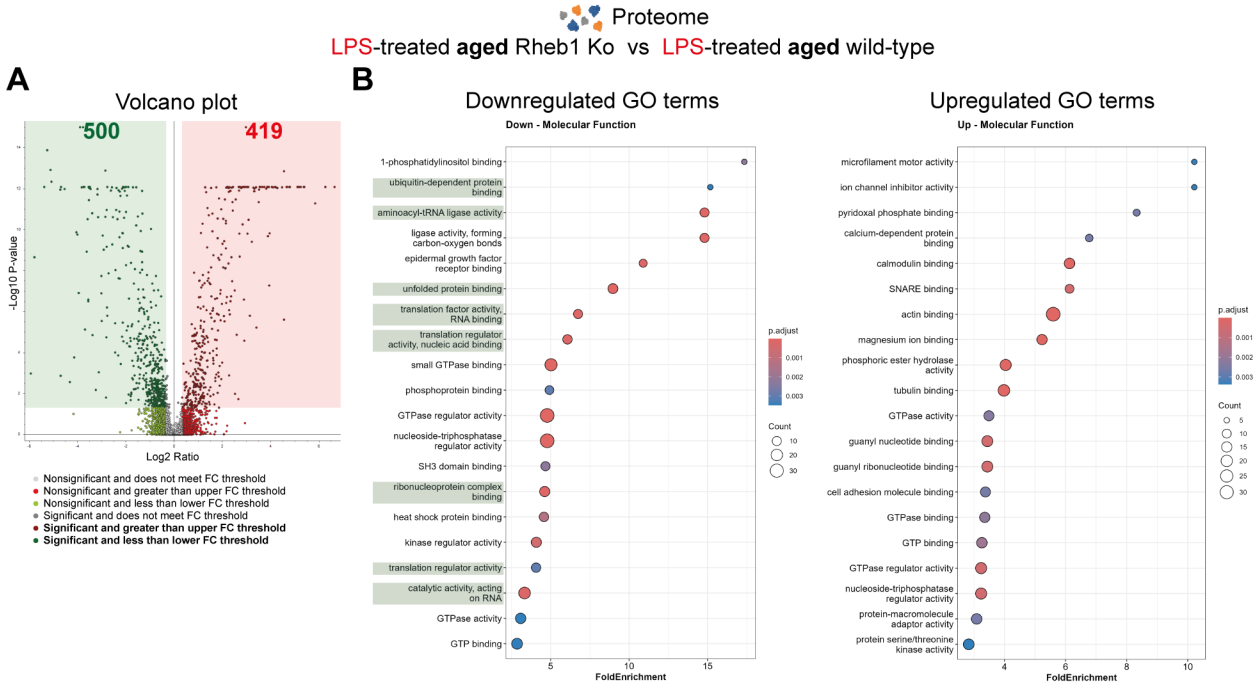

Figure 40 Genetic loss of Rheb1 in aged microglia downregulates constituents of the proteins synthesis machinery in response to LPS.
(**A**) Volcano plot showing significant differently ambundant proteins (DAPs) between Ko vs Wt microglia from LPS-treated aged animals. (**B**) Gene Set Enrichment Analysis (GSEA) of significant DAPs derived from the same comparison.

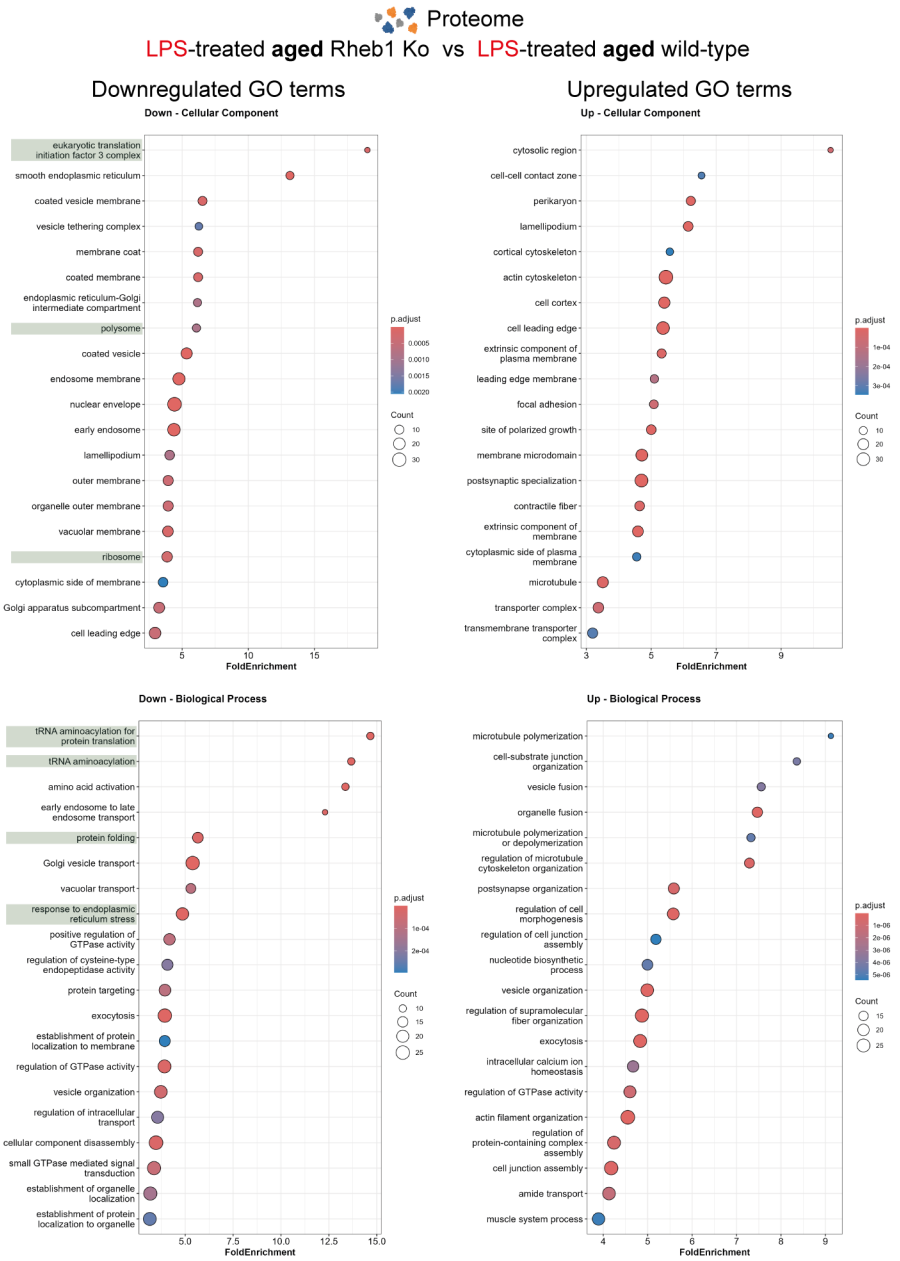

Figure 41 Additional GO aspects derived from proteome analysis of Ko vs Wt microglia isolated from LPS-treated aged animals

Gene Set Enrichment Analysis (GSEA) of significant DAPs between LPS vs PBS microglia isolated from aged wild-type animals and related to Figure 40B

4. Discussion

In my PhD, I investigated the role of mTORC1-dependent translation pathway in the regulation of aged microglia immune response. Microglia are the innate immune cells of CNS, a tissue-resident macrophage population supporting CNS environment and health (Helmut et al., 2011; R. C. Paolicelli et al., 2022); however, with age, they alter their functions and morphology (Norden & Godbout, 2013). Cumulative evidences over the years corroborated the idea that aged microglia have a “primed” phenotype, which is referred to a propensity to respond more strongly to stimulation due to a higher immune sensitiveness (Niraula et al., 2017). Several studied attempted to define the aged microglia phenotype, as we reviewed in Antignano et al., 2023; however, few of these have explored the molecular pathway(s) contributing to these changes (Gulen et al., 2023; Keane et al., 2021; Minhas et al., 2021).

4.1. Aged microglia upregulate mTORC1-dependent translation pathway

Our first transcriptome analysis of isolated microglia over the mouse lifespan suggested that mTORC1-dependent translation pathway is dysregulated in aging. This evidence was supported by an increased expression of ribosomal proteins, as it was similarly found in an earlier report (Holtman et al., 2015). However, we also observed a higher expression of key translation factors involved at the initiation stage of translation (i.e. *eIF4EBP1*, also known as *4EBP1*, *eIF3h*, *eiF3k*, *eIF3e*, *Pabpc1*) (Keane et al., 2021a) . Of note, these genes are tightly regulated by mTORC1-dependent transcriptional and translation programs (Chauvin et al., 2013; G. Y. Liu & Sabatini, 2020; Thoreen et al., 2009b, 2012). A clear indication of mTORC1 signaling upregulation in microglia came from the age-dependent increase in the phosphorylation levels of its two key downstream effectors: 4EBP1, which controls the initiation of cap-dependent translation; and RPS6, which regulates ribosome biogenesis, and supports protein synthesis during initiation and elongation (Sonenberg & Hinnebusch, 2009). While we observed only a milder increase in p-RPS6, p-4EPB1 was instead more strongly upregulated in aged microglia compared to younger counterparts, indicating a stronger age-related effect. Interestingly, both p-4EBP1 and p-RPS6 levels were further augmented in aged microglia following *in vivo* LPS treatment. These changes correlated with a greater expression of pro-inflammatory

cytokines (IL1-β, TNF-α, IL-6) exclusively at protein level, whereas their corresponding mRNAs resulted unchanged in both LPS-challenged young and aged microglia. The increase in cytokine production we observed may be caused by an overall upregulation of protein synthesis, as suggested by our RNA-seq analysis. Alternatively, selective translation control of immune genes might also take place (Carpenter et al., 2014; Guillemin et al., 2022; Piccirillo et al., 2014; Schott et al., 2014; Y. Zhang et al., 2023).

4.2. mTORC1 inhibition by Rheb1 loss ameliorated aged microglia phenotype and sickness behavior by reducing translation of inflammatory immune genes

To investigate why mTORC1 pathway promoted an increased translation of immune genes, I used the *Rheb*$^{fl/fl}$*;Csf1r*^{Cre} mouse model, which leads to a genetic deletion of *Rheb1*, a positive regulator of mTORC1, under the control of *Csf1r* promoter. As *Csf1r* is active at embryonic day (E) 8.5 in hemopoietic stem cells (Gomez Perdiguero et al., 2015), *Rheb1* is deleted in both tissue-resident and circulating immune cells, including macrophages and microglia. Despite a deficiency in Rheb-mediated mTORC1 activation, no sign of abnormalities was shown in Rheb Ko animals. They breed, developd and aged normally; furthermore, they displayed comparable organs and body weight to wild-type counterparts. Bone marrow, blood and spleen cells, as well as isolated microglia from both young and old Ko mice also showed similar numbers compared to the Wt controls. Additionally, no differences were observed in both microglia morphology and *in vitro* phagocytosis of E.coli-embedded particles. A previous report with *Rheb*$^{fl/fl}$;*ROSA26*$^{\text{CreER}}$ have indicated that *Rheb1* is dispensable for in vivo hemopoietic stem cell proliferation and self-renewal (Peng et al., 2018). On the other hand, in contrast to *Rheb1* deletion, loss of *Raptor* – a constituent of mTOR complex 1 – caused a more severe phenotype, suggesting that residual mTORC1 activation could still take place in the absence of *Rheb1*, although the mechanism remains to be elucidated. Our results support this conclusion, since we do not observe a complete inhibition of p-4EBP1 and p-S6 in Rheb Ko cells. This represented a positive feature of *Rheb*$^{fl/fl}$*;Csf1r*^{Cre} model, since the downregulation of mTORC1 signaling rather than complete inhibition allow to assess mTORC1 role in microglia in vivo and also in aging. On the other hand, we did observe a defect in cell proliferation *in vitro,* in both BMDMs and neonatal primary microglia, as previously reported in *Rheb*$^{fl/fl}$; *Vav1*^{Cre} macrophages (X. Wang et al., 2016). The reason

behind the discrepancy between *in vivo* and *in vitro* proliferation in the *Rheb*$^{fl/fl}$*;Csf1r*^{Cre} model remains to be clarified. One hypothesis is that proliferation *in vivo* could rely more on compensatory signaling pathways due to the reduced mTORC1 signaling by Rheb1 loss, whereas *in vitro* proliferation, supported by CSF1 as growth factor, relies more strictly on the RHEB1-mTOR axis.

As we aimed to investigate the immune-regulatory role of mTORC1-dependent translation pathway in microglia, we next exanimated their immune response followed by *in vivo* LPS treatment in aging animals. In this scenario, *Rheb1* loss caused an NF-κB-dependent upregulation of priming genes at transcript level (*Tnf*, *Il1b*, *Il6*, *Clec7a*, *Spp1* and *Cst7*), which was further increased in older Ko animals. These results are consistent with a previous report where mTORC1 inhibition by Rapamycin caused an increase of pro-inflammatory genes transcription in LPS or SAC-treated human or mouse peripheral immune cells (Weichhart et al., 2008). More specifically, these changes were due to a greater nuclear translocation and activity of NF-κB p65 subunit (Weichhart et al., 2008), as we similarly observed in Rheb Ko cells. However, while mTOR inhibition by Rapamycin also led to a greater cytokine expression at protein level (Keane et al., 2021; Weichhart et al., 2008), this did not occur when Rheb1 was deleted in BMDMs and microglia. The reason behind this discrepancy in immune genes translation into proteins derived from a different mode of inhibiting 4EBP1 phosphorylation at Thr37/46. Both sites are considered the first to be phosphorylated by mTORC1 and this event is indispensable to initiate the cap-dependent translation that the majority of mRNAs undergoes (Gingras et al., 1999, 2001; Sonenberg & Hinnebusch, 2009). While Rapamycin did not induce any inhibition of Thr37/46 phosphorylation, as others also observed (Choo et al., 2008; Feldman et al., 2009; Gingras et al., 1999, 2001; Livingstone & Bidinosti, 2012; Mothe-Satney et al., 2000), phosphorylation at these two Threonines was significantly reduced in Rheb Ko cells, as well as in the presence of Torin1, a more potent mTOR inhibitor (Thoreen et al., 2009). This difference also led to a differential regulation of total 4EBP1 levels, which we found upregulated in Rheb Ko and with Torin1 treatment, but not with Rapamycin. High 4EBP1 phosphorylation, particularly at Thr37/46, results in its own ubiquitination and subsequent degradation (Elia et al., 2007), which could explain why translation of inflammatory genes was impaired in Rheb Ko and Torin1-treated cells but not after rapamycin treatment, in contrast to what was described by *Weichhart* et al. Additionally, it

is important to note that while Rapamycin has only modest effects on protein synthesis (Neshat et al., 2001; Pedersen et al., 1997; Shor et al., 2008), Rheb Ko cells instead impairs it more strongly, especially after LPS treatment. A similar effect on protein synthesis is also exerted by Torin1 (Thoreen et al., 2012) and, indeed, we observed a similar reduced protein expression of cytokines with Torin1.

The direct consequence of hypo-phosphorylated 4EBP1 in Rheb Ko cells was the downstream disruption of initiation of translation factor eIF4E binding to eIF4G, a step needed for translation initiation. We further confirmed that eIF4E:eIF4G interaction was impaired in Rheb Ko, and this was not due to differences in their expression levels, as both proteins were similarly expressed at steady-state and following LPS challenge. Moreover, treating cells with 4EG-I, an inhibitor that disrupts eIF4E:eIF4G binding, resulted in a similar outcome in terms of inhibition of translation. It is believed that the eIF4E phosphorylation at Ser209 increases its own activity, favoring the translation of certain immune genes (Piccirillo et al., 2014). However, this requires eIF4G binding to eIF4E, as eIF4G functions as a docking site for MNK1/2-mediated eIF4E phosphorylation (Pyronnet et al., 1999). In our Rheb Ko model, we found that eIF4E phosphorylation is impaired after LPS treatment and that this effect derived from a lower activation of ERK1/2 signaling controlling MNK1/2 activity. In light of these observations and of the role of eIF4E in translation regulation (Piccirillo et al., 2014), we tested whether the inhibition of eIF4E phosphorylation resulted in a similar phenotype of reduced cytokine expression by using eFT508, a selective inhibitor of MNK1/2 (B. Huang et al., 2023; Shukla et al., 2021). Despite the downregulation in eIF4E phosphorylation, eFT508-treated neonatal primary microglia showed only a mild decrease in cytokine production after LPS stimulation. It is possible that these effects were limited by the short time of eFT508 incubation we used or due to an uncompleted eFT508-mediated inhibition of eIF4E phosphorylation, or a combination thereof. However, contradictory evidences have recently emerged, depending on how the inhibition is achieved. Indeed, complete loss of eIF4E phosphorylation in *4Eki* mice caused LPS-induced depression-like behaviors and resulted in differential expression of a subset of genes (Amorim et al., 2018), whereas eFT508-mediated inhibition led to a rescue of the phenotype in a similar setting (Gong et al., 2023).

In addition to an increase of mTOR signaling, the eukaryotic Initiation Factor 2 (eIF2) signaling was also upregulated in our aging microglia transcriptome analysis. eIF2 in a critical component of initiation of translation, which mediates the transfer of Met-tRNAi to the 40S ribosomal subunit (Merrick & Pavitt, 2018). This important step in initiating translation is heavily regulated by cellular stress-related pathways, which can cause the phosphorylation of the small eIF2α subunit, resulting in inhibition of translation (Adomavicius et al., 2019; Donnelly et al., 2013). Based on the nature of cellular stress, several kinases have been described to inhibit eIF2α, however, it was not clear whether our RNAseq results indicated an activation of signaling leading to eIF2α phosphorylation. Based on a number of observations, we excluded that increased eIF2α phosphorylation (and therefore protein synthesis inhibition) is happening in aged microglia. First, eIF2α gene expression levels did not change with age. The genes responsible for the increase in eIF2 signaling in the IPA analysis were also genes that regulated translation and were shared by the eIF2 signaling, p70S6K and 4EBP1 signaling and mTOR signaling, like ribosomal proteins. The only gene truly specific to eIF2-α signaling was Eif2ak1, a eIF2α kinase, which appeared slightly upregulated (1.4 fold)(Keane et al., 2021). However, this transcriptional increase did not indicate that the kinase was more active. Furthermore, neither Wt nor Rheb Ko macrophages showed significant eIF2α phosphorylation at steady state, and it decreased further after LPS stimulation, corroborating the idea that more active microglia would not shut down translation through eIF2α phosphorylation.

Finally, inhibition of mTORC1 is well known to lead to autophagy activation (Laplante & Sabatini, 2009), which potentially could promote cytokine degradation in our model. However, this was not the case, as inhibition of autophagy did not rescue the decrease in cytokines observed in Rheb Ko cells. Furthermore, Rheb Ko cells did not show higher level of autophagy marker LC3-II compared to wild-type counterpart, which was in line with the previous evidence in cardiomyocytes (Tamai et al., 2013). Additional evidences that autophagy was not involved in cytokine degradation came from our experiment with rapamycin (Keane et al., 2021). BMDMs treated with rapamycin, which induces autophagy (Abdulrahman et al., 2011; Rangaraju et al., 2010), but does not significantly affect cytokine mRNA translation (Thoreen et al., 2012) showed even an increase in IL-12p40 levels (Keane et al., 2021; Weichhart et al., 2008). Lastly, changes in autophagy gene

expression did not change with age neither in our RNAseq (Keane et al., 2021), nor in other datasets (Grabert et al., 2016b; Hickman et al., 2013). In line with the current literature that autophagy is not involved in the degradation of pro-inflammatory cytokines (Saitoh et al., 2008), the effects we observed in Rheb Ko resulted exclusively from a defective protein synthesis.

4.3. Multi-omics data analysis indicates that the age-dependent increase of protein synthesis modulates microglia immune response.

Our data indicated that although mTOR is known to regulate cap-dependent translation, it does not regulate all mRNAs in the same manner (Hershey et al., 2019b; Sonenberg & Hinnebusch, 2009b; Uttam et al., 2018). Indeed, several evidences have shown different modes of translation regulations, especially for genes involved in immune functions, such as IRF7, IRF8, IκB-α, SPP1, CCL5, GATA3, IL-4 (Colina et al., 2008; Herdy et al., 2012; Piccirillo et al., 2014). It is believed that determined features in the mRNAs confer increased eIF4E (and therefore mTORC1) sensitivity, for instance, long and highly structured 5′-UTR or *cis*-regulatory elements like 5′ terminal oligopyrimidine tracts (TOPs or TOP like) and CERT, cytosine-rich 15-nucleotide motif. In light of these considerations, it is possible to speculate that priming and inflammatory genes in microglia could also share a yet unidentified consensus sequence or secondary structure, which might also involve unknown *trans*-regulatory factors (like RNA-binding proteins).

As the majority of genes we investigated did not show any consensus sequence (Keane et al., 2021), we aimed to have a more comprehensive view of what type of translation regulation is taking place in the immune response of aged microglia. This was achieved by performing a translatome analysis using the $Rpl22^{HA}$:$Rheb^{fl/fl}$:$CX3CR1^{CreER/+}$ mouse model following *in vivo* LPS treatment. The advantage of this line that I established was due to two relevant points. First, the line offers a better control of the Cre-mediated Rheb1 deletion targeting specifically microglia (Parkhurst et al., 2013; Sahasrabuddhe & Ghosh, 2022). Cre expression is only induced after tamoxifen treatment in adult animals, rather than being constitutively expressed from embryogenesis and during the entire animal lifespan as it occurs in $Rheb^{fl/fl}$:$Csf1r^{Cre}$. In this scenario, the induction of Rheb1 deletion at specific time points might also avoid to interfere with the role of mTORC1 in cell proliferation, which is important during mouse development (Saxton & Sabatini, 2017).

Secondly, a Cre-mediated RPL22^{HA} expression allows to assess the translatome more easily than ribosome profiling or other methods used for this type of analysis (Sanz et al., 2009). Indeed, in most cases, they require a higher number of cells that cannot be achieved with the available methods of microglia isolation (Q. Wang & Mao, 2023). In parallel, we also performed transcriptome and proteome analysis from the same animals, to be used as a reference for translatomics, in order to measure translational efficiency, and to confirm whether ribosome-associated mRNAs are actually translated into proteins.

Exploratory data analysis of both transcriptome and translatome did not suggest major differences between the two methodologies. The most variance was given by the LPS treatment, as it is well-known to be a potent immune stimulant. Nevertheless, we were still able to see age- and genotype-related differences. The most striking result about this point was that in both methods the age effect was prevalent within PBS-treated samples, whereas the differences induced by the genotype (Ko vs Wt) were instead predominant in LPS-treated animals. This was a further indication that Rheb1 was critical in regulating microglia immune responses but less so in their steady-state function.

For simplicity, we only addressed three biological questions that are relevant for the scope of this PhD thesis, which aimed to address microglia changes induced in aging Wt at steady state, by LPS treatment in aged Wt and by the mTORC1 downregulation in LPS-treated Rheb Ko microglia. Gene Set Enrichment Analysis (GSEA) of microglia from aged vs young animals at steady state corroborated the previous findings of an upregulation in immune-sensing genes from aged microglia at transcriptome level (Hickman et al., 2013). Importantly, these changes seemed to be more pronounced in the translatome and are mostly recapitulated in the proteome analysis, along with an upregulation of protein synthesis components and ER-associated degradative (ERAD) pathway, involved in the degradation of misfolded protein. It is possible that these two events are actually contributing together to the aged microglia phenotype. One hypothesis is that the increase in translation is also associated with a defective translation fidelity and poor quality-control mechanisms, leading to a greater burden of misfolded protein, which is typically found in aged mouse and human brain (Cuanalo-Contreras et al., 2023; Kapur & Ackerman, 2018).

In response to LPS, transcriptome of aged Wt microglia strongly upregulated components of protein synthesis machinery, along with immune-related terms (i.e. positive regulation

of cytokine production, response to INF-β and INF-γ). These changes in immune response were clearly more translated into proteins, as they were highly enriched at both translatome and proteomic level. This was further supported by an increase of translation factors in the proteomics (i.e. eIF3 complex, aminoacyl-tRNA ligase activity among others). These data are important because they confirm the relevance of translation in modulating inflammatory responses in ageing but also because they confirm that the changes observed at transcription levels are indeed “real” and correspond to changes at protein levels. Conversely, Rheb 1 loss led to an opposing scenario: as much as immune-related genes were still upregulated at the RNA level, they were downregulated in the translatome and proteome. In this regard, a severe defect of protein synthesis constituents, contrary to what we found upregulated in LPS vs PBS-treated Wt, were observed at the protein level in Rheb Ko microglia from LPS-treated animals. Despite the low number of differently expressed genes in the translatome, the majority resulted downregulated, thereby indicating a decreased protein synthesis, as we expected in the Rheb Ko. It is possible that this effect could derive from a defective loading of mRNAs onto the ribosomes and consecutive mRNA processing, as supported by the decreased protein expression of translation initiation and elongation factors from the proteome analysis. This might also occur through an unknown translation mechanism that we aim to define by integrating the three datasets. However, it also important to note that one possibility could be related to a lower $RPL22^{HA}$ expression, therefore a lower number of immune-precipitated ribosomes, in the Rheb Ko microglia versus wild-type controls. As much as translatome analysis alone could give us an indication of which mRNAs were associated with ribosomes, it is important to note that we studied it without considering the transcriptome as reference. Indeed, an additional, and more correct way to ensure that a gene is indeed being translated into protein is by assessing the so-called “translation efficiency”. Relative to this point, efforts are currently being made to perform DEG analysis of the translatome over the transcriptome by merging the two datasets.

4.4. Dataset analysis indicates an important role for eFI3 in mTORC1-mediated translation

In our proteomics dataset we could observe an increase in the expression of eIF3 complex in relation to LPS-induced inflammatory response in microglia. We found eIF3 to be

upregulated in LPS vs PBS-treated aged Wt, but, interestingly, it was downregulated in Rheb Ko vs Wt LPS-challenged animals. Of note, eIF3, a 13-subunits complex, have been recently come to the attention due to new evidences of its multiple roles in translation regulation (Gomes-Duarte et al., 2017; Lee et al., 2015a). On top of favoring translation initiation by interacting with initiation factors (i.e. eIF4E, eIF4G, PABPs) and supporting AUG recognition by 40S ribosomes, eIF3 complex also promotes translation elongation by remaining associated with the elongating 80S ribosomes (Wolf et al., 2020), at least in the early stage of the open-reading frame (ORF) scanning (Bohlen et al., 2020; Lin et al., 2020; Wagner et al., 2020). Considering this last point, eIF3 complex is now considered to cooperate with mechanisms that ensure a correct protein folding and protein quality control of the nascent polypeptide chain, both of which lead to the activation of proteasome in case of abnormalities (Pegoraro et al., 2012; Wolf et al., 2020).

Relative to this type of eIF3-mediated quality control, it was interesting to observe that proteasome-related terms were either upregulated or downregulated in Wt and Rheb Ko in response to LPS, respectively. Of note, eIF3 followed the same pattern. One hypothesis is that Rheb1 loss, which strongly reduces translation late, might cause a decrease numbers of errors in translation fidelity and protein folding, which will eventually constitute an insufficient signal to trigger proteasome activation. Additionally, with the evidence that certain eIF3 subunits differently regulate the translation of certain mRNAs subsets (Choe et al., 2018; Lee et al., 2015b; Meyer et al., 2015; X. Wang et al., 2015), and that only 4 out of 13 subunits are differently expressed in our conditions in the proteomics (EIF3K, EIF3I, EIF3H and EIF3A), it is possible that a similar scenario also occur in aging microglia. Interestingly, some of these subunits (*eif3k*, *eif3h*) were already found upregulated in aging in our earlier RNA-seq analysis (Keane et al., 2021). How microglia immune response and phenotype might be regulated by eIF3 complex in aging, potentially either by regulating specialized mRNA subsets or through specific functions, remains yet to be defined. Efforts are currently being made in our laboratory in order to unveil these questions.

4.5. Future directions

Despite the efforts to generate a multi-layered gene expression dataset in aging microglia, further experiments need to be performed in light of the strikingly novel results I reported

in my PhD thesis. In this respect, I would like to highlight the future research directions stemming from my PhD project, which are the following:

- **Determination of differential translation efficiency genes (DTEGs)** by integrative analysis of microglia translatome and transcriptome, as previously mentioned (Chothani et al., 2019).
- **Multi-omics data integration** to unveil modules of gene expression that might be either similarly or differently expressed by microglia. More broadly, we also aim to perform motif enrichment analysis to identify common or unknown *cis*-regulatory elements in 5'UTR, Open Reading Frame (ORF) and 3'UTR underlying mRNA subsets that might be translationally regulated. Regardless of this point, these aforementioned regions of interests will be also assessed by String analysis for mRNA structure analysis.
- **Investigating the role of eIF3 subunits in microglia immune response.** The upregulation of certain subunits of the eIF3 complex in our current and earlier datasets (EIF3K, EIF3I, EIF3H and EIF3A) likely plays a role in translation regulation of microglia genes, as suggested by the literature (Choe et al., 2018; Lee et al., 2015; Meyer et al., 2015; X. Wang et al., 2015) . In this regard, we will further investigate the specific upregulation of certain eIF3 subunits if this is accompanied by a specific upregulation of translation of certain mRNAs, which might further characterize aged microglia phenotype. Furthermore, we will assess whether the assembly of the whole complex is in some ways compromised in Rheb Ko cells and if this might contribute to the phenotype of Rheb Ko microglia.
- **Exploring the role of protein synthesis and translation regulations in models of neurodegenerative disorders** (i.e. APP/PS1 or 5XFAD for Alzheimer's disease). A more recent report highlighted that isolated amyloid plaque-containing microglia from 6 months old 5XFAD mice are highly enriched for ribosome constituents and protein synthesis-related processes, among others (Grubman et al., 2021). Interestingly, this signature strongly overlapped with aged mouse microglia from the bulk RNAseq and two clusters from sc-RNAseq of AD-isolated human microglia (Grubman et al., 2021). Similarly, our mTOR translational signature was significantly enriched in damaged-associated microglia (DAM)

cluster or in aging human microglia, indicating a common mechanism that is upregulated in both mouse and human aging and in neurodegeneration (Keane et al., 2021a). In light of these considerations, the mouse line that I established, the *Rpl22^{HA}:Rheb$^{fl/fl}$:CX3CR1$^{CreER/+}$* , is being currently crossed with APP/PS1 animals in order to assess microglia translatome from these animals. An alternative idea would be to profile microglia cells using the newly established single-cell translatome analysis approach (VanInsberghe et al., 2021b).

4.6. List of publications

- **Keane L**, **Antignano I**, Riechers SP, et al. mTOR-dependent translation amplifies microglia priming in aging mice *J Clin Invest*. **2021**;131(1):e132727. doi:10.1172/JCI132727

  (co-first authorship)

- **Antignano I**, Liu Y, Offermann N, Capasso M. Aging microglia. *Cell Mol Life Sci*. 2023;80(5):126. Published **2023** Apr 21. doi:10.1007/s00018-023-04775-y

  (Literature review article based on the current state of art about aging microglia)

- **Antignano I**, Keane L, Capasso M. Assessing mRNA translation in mouse adult microglia and bone-marrow-derived macrophages. *STAR Protoc*. Published online September 13, **2023**. doi:10.1016/j.xpro.2023.102559

  (Optimization of the methodologies used for assessing mRNA translation rate by flow cytometry and fluorescent plate reader, both in use in the laboratory)

- Kapellos TS, Baßler K, Fujii W, Nalkurthi C, Schaar AC, Bonaguro L, Pecht T, Galvao I, Agrawal S, Saglam A, Dudkin E, Frishberg A, de Domenico E, Horne A, Donovan C, Kim RY, Gallego-Ortega D, Gillett TE, Ansari M, Schulte-Schrepping J, Offermann N, **Antignano I**, Sivri B, Lu W, Eapen MS, van Uelft M, Osei-Sarpong C, van den Berge M, Donker HC, Groen HJM, Sohal SS, Klein J, Schreiber T, Feißt A, Yildirim AÖ, Schiller HB, Nawijn MC, Becker M, Händler

K, Beyer M, Capasso M, Ulas T, Hasenauer J, Pizarro C, Theis FJ, Hansbro PM, Skowasch D, Schultze JL. Systemic alterations in neutrophils and their precursors in early-stage chronic obstructive pulmonary disease. Cell Rep. **2023** Jun 27;42(6):112525. doi: 10.1016/j.celrep.2023.112525. Epub 2023 May 26.

5. Abstract

Aged microglia are known to become primed, acquiring the ability to respond more strongly to immune stimuli. By RNAseq, we discovered an upregulation of pathways controlling translation depending on mTORC1 signaling. Indeed, mTOR-dependent phosphorylation of 4EBP1 and S6 were increased in aged microglia, as assessed by phospho flow cytometry, and this correlated with an increase in inflammatory cytokines upon *in vivo* LPS challenge only at protein level. Attenuation of mTOR signaling through deletion of Rheb1, specifically in microglia and immune cells in *Rheb1$^{fl/fl}$;Csf1r^{Cre}*, showed two opposing effects on microglia priming genes: an NF-κB–dependent upregulation at mRNA level but a downregulation at protein level. Indeed, *Rheb1$^{fl/fl}$;Csf1r^{Cre}* mice showed milder symptoms of inflammation upon *in vivo* LPS injection, including milder sickness behavior. Mechanistically, the decrease in protein levels of inflammatory mediators in aged microglia were due to a reduction of the mTOR-eIF4E-dependent protein synthesis. In particular, Rheb1 loss caused diminished phosphorylation of 4EBP1, which resulted in decreased binding of eIF4E to eIF4G, a step required for the formation of the initiation complex eIF4F. Similar changes were also present in aged human microglia and in damage-associated microglia (DAM), a subset of microglia identified in neurodegeneration, indicating that the upregulation of mTOR-dependent translation is an essential aspect of microglia priming in aging and neurodegeneration. Whether translation regulatory elements play a role in regulating microglia immune gene expression in aging remains unclear. To address this point, we conducted a comprehensive multi-omics approach by analyzing the transcriptome, translatome and proteome of microglia upon *in vivo* LPS challenge from *Rpl22^{HA}:Rheb$^{fl/fl}$:CX$_3$CR1$^{CreER/+}$* animals. We confirmed our previous evidences that aging microglia upregulated components of protein synthesis machinery to boost their immune response to LPS. Further analysis will be carried out by integrating the datasets in order to discover *cis*-regulatory elements that might be underlying to translation regulation of immune genes. These findings will offer potential avenues for therapeutic interventions by targeting mTOR-dependent translation to alleviate age-related neuro-inflammatory diseases in the elderly.

6. List of figures

7. List of tables

8. References

Abdulrahman, B. A., Khweek, A. A., Akhter, A., Caution, K., Kotrange, S., Abdelaziz, D. H. A., Newland, C., Rosales-Reyes, R., Kopp, B., McCoy, K., Montione, R., Schlesinger, L. S., Gavrilin, M. A., Wewers, M. D., Valvano, M. A., & Amer, A. O. (2011). Autophagy stimulation by rapamycin suppresses lung inflammation and infection by Burkholderia cenocepacia in a model of cystic fibrosis. *Autophagy*, *7*(11), 1359. https://doi.org/10.4161/AUTO.7.11.17660

Adomavicius, T., Guaita, M., Zhou, Y., Jennings, M. D., Latif, Z., Roseman, A. M., & Pavitt, G. D. (2019). The structural basis of translational control by eIF2 phosphorylation. *Nature Communications 2019 10:1*, *10*(1), 1–10. https://doi.org/10.1038/s41467-019-10167-3

Aires, V., Coulon-bainier, C., Pavlovic, A., Ebeling, M., Schmucki, R., Schweitzer, C., Kueng, E., Gutbier, S., & Harde, E. (2021). *CD22 Blockage Restores Age- Related Impairments of Microglia Surveillance Capacity*. *12*(June), 1–16. https://doi.org/10.3389/fimmu.2021.684430

Amorim, I. S., Kedia, S., Kouloulia, S., Simbriger, K., Gantois, I., Jafarnejad, S. M., Li, Y., Kampaite, A., Pooters, T., Romanò, N., & Gkogkas, C. G. (2018). Loss of eIF4E Phosphorylation Engenders Depression-like Behaviors via Selective mRNA Translation. *Journal of Neuroscience*, *38*(8), 2118–2133. https://doi.org/10.1523/JNEUROSCI.2673-17.2018

Antignano, I., Liu, Y., Offermann, N., & Capasso, M. (2023). Aging microglia. *Cellular and Molecular Life Sciences : CMLS*, *80*(5). https://doi.org/10.1007/S00018-023-04775-Y

Baker, D. J., Wijshake, T., Tchkonia, T., Lebrasseur, N. K., Childs, B. G., Van De Sluis, B., Kirkland, J. L., & Van Deursen, J. M. (2011). Clearance of p16Ink4a-positive senescent cells delays ageing-associated disorders. *Nature*, *479*(7372), 232–236. https://doi.org/10.1038/NATURE10600

Bohlen, J., Fenzl, K., Kramer, G., Bukau, B., & Teleman, A. A. (2020). Selective 40S Footprinting Reveals Cap-Tethered Ribosome Scanning in Human Cells. *Molecular Cell*, *79*(4), 561-574.e5. https://doi.org/10.1016/J.MOLCEL.2020.06.005

Borst, K., Dumas, A. A., & Prinz, M. (2021). Microglia: Immune and non-immune functions. *Immunity*, *54*, 2194–2208. https://doi.org/10.1016/j.immuni.2021.09.014

Buttgereit, F., & Brand, M. D. (1995). A hierarchy of ATP-consuming processes in mammalian cells. *The Biochemical Journal*, *312 (Pt 1)*(Pt 1), 163–167. https://doi.org/10.1042/BJ3120163

Cangalaya, C., Wegmann, S., Sun, W., Diez, L., Gottfried, A., Richter, K., Stoyanov, S., Pakan, J., Fischer, K. D., & Dityatev, A. (2023). Real-time mechanisms of exacerbated synaptic remodeling by microglia in acute models of systemic inflammation and tauopathy. *Brain, Behavior, and Immunity*, *110*, 245–259. https://doi.org/10.1016/J.BBI.2023.02.023

Carpenter, S., Ricci, E. P., Mercier, B. C., Moore, M. J., & Fitzgerald, K. A. (2014). Post-transcriptional regulation of gene expression in innate immunity. *Nature Reviews Immunology 2014 14:6*, *14*(6), 361–376. https://doi.org/10.1038/nri3682

Carroll, M., & Borden, K. L. B. (2013). The Oncogene eIF4E: Using Biochemical Insights to Target Cancer. *Journal of Interferon & Cytokine Research*, *33*(5), 227. https://doi.org/10.1089/JIR.2012.0142

Chauvin, C., Koka, V., Nouschi, A., Mieulet, V., Hoareau-Aveilla, C., Dreazen, A., Cagnard, N., Carpentier, W., Kiss, T., Meyuhas, O., & Pende, M. (2013). Ribosomal protein S6 kinase activity controls the ribosome biogenesis transcriptional program. *Oncogene 2014 33:4*, *33*(4), 474–483. https://doi.org/10.1038/onc.2012.606

Chen, W.-T., Lu, A., Craessaerts, K., Lundeberg, J., Fiers, M., De, B., & Correspondence, S. (2020). *Spatial Transcriptomics and In Situ Sequencing to Study Alzheimer's Disease*. https://doi.org/10.1016/j.cell.2020.06.038

Choe, J., Lin, S., Zhang, W., Liu, Q., Wang, L., Ramirez-Moya, J., Du, P., Kim, W., Tang, S., Sliz, P., Santisteban, P., George, R. E., Richards, W. G., Wong, K. K., Locker, N.,

Slack, F. J., & Gregory, R. I. (2018). mRNA circularization by METTL3-eIF3h enhances translation and promotes oncogenesis. *Nature*, *561*(7724), 556. https://doi.org/10.1038/S41586-018-0538-8

Choi, S. H., Veeraraghavalu, K., Lazarov, O., Marler, S., Ransohoff, R. M., Ramirez, J. M., & Sisodia, S. S. (2008). Non-cell-autonomous effects of presenilin 1 variants on enrichment-mediated hippocampal progenitor cell proliferation and differentiation. *Neuron*, *59*(4), 568–580. https://doi.org/10.1016/J.NEURON.2008.07.033

Choo, A. Y., Yoon, S. O., Sang, G. K., Roux, P. P., & Blenis, J. (2008). Rapamycin differentially inhibits S6Ks and 4E-BP1 to mediate cell-type-specific repression of mRNA translation. *Proceedings of the National Academy of Sciences of the United States of America*, *105*(45), 17414–17419. https://doi.org/10.1073/PNAS.0809136105/SUPPL_FILE/0809136105SI.PDF

Chothani, S., Adami, E., Ouyang, J. F., Viswanathan, S., Hubner, N., Cook, S. A., Schafer, S., & Rackham, O. J. L. (2019). deltaTE: Detection of Translationally Regulated Genes by Integrative Analysis of Ribo-seq and RNA-seq Data. *Current Protocols in Molecular Biology*, *129*(1). https://doi.org/10.1002/CPMB.108

Colina, R., Costa-Mattioli, M., Dowling, R. J. O., Jaramillo, M., Tai, L. H., Breitbach, C. J., Martineau, Y., Larsson, O., Rong, L., Svitkin, Y. V., Makrigiannis, A. P., Bell, J. C., & Sonenberg, N. (2008). Translational control of the innate immune response through IRF-7. *Nature*, *452*(7185), 323–328. https://doi.org/10.1038/NATURE06730

Collins, S. L., Oh, M.-H., Sun, I.-H., Chan-Li, Y., Zhao, L., Powell, J. D., & Horton, M. R. (2021). mTORC1 Signaling Regulates Proinflammatory Macrophage Function and Metabolism. *The Journal of Immunology*, *207*(3), 913–922. https://doi.org/10.4049/jimmunol.2100230

Cuanalo-Contreras, K., Schulz, J., Mukherjee, A., Park, K. W., Armijo, E., & Soto, C. (2023). Extensive accumulation of misfolded protein aggregates during natural aging and senescence. *Frontiers in Aging Neuroscience*, *14*, 1090109. https://doi.org/10.3389/FNAGI.2022.1090109/FULL

De Benedetti, A., & Graff, J. R. (2004). eIF-4E expression and its role in malignancies and metastases. *Oncogene*, *23*(18), 3189–3199. https://doi.org/10.1038/sj.onc.1207545

Deng, L., Zhou, J. F., Sellers, R. S., Li, J. F., Nguyen, A. V., Wang, Y., Orlofsky, A., Liu, Q., Hume, D. A., Pollard, J. W., Augenlicht, L., & Lin, E. Y. (2010). A novel mouse model of inflammatory bowel disease links mammalian target of rapamycin-dependent hyperproliferation of colonic epithelium to inflammation-associated tumorigenesis. *The American Journal of Pathology*, *176*(2), 952–967. https://doi.org/10.2353/AJPATH.2010.090622

Ding, X., Wang, J., Huang, M., Chen, Z., Liu, J., Zhang, Q., Zhang, C., Xiang, Y., Zen, K., & Li, L. (2021). Loss of microglial SIRPα promotes synaptic pruning in preclinical models of neurodegeneration. *Nature Communications 2021 12:1*, *12*(1), 1–17. https://doi.org/10.1038/s41467-021-22301-1

Donnelly, N., Gorman, A. M., Gupta, S., & Samali, A. (2013). The eIF2α kinases: their structures and functions. *Cellular and Molecular Life Sciences : CMLS*, *70*(19), 3493–3511. https://doi.org/10.1007/S00018-012-1252-6

Dorrello, N. V., Peschiaroli, A., Guardavaccaro, D., Colburn, N. H., Sherman, N. E., & Pagano, M. (2006). S6K1- and betaTRCP-mediated degradation of PDCD4 promotes protein translation and cell growth. *Science (New York, N.Y.)*, *314*(5798), 467–471. https://doi.org/10.1126/SCIENCE.1130276

Dreas, A., Mikulski, M., Milik, M., Fabritius, C.-H., Brzózka, K., & Rzymski, T. (2017). Mitogen-activated Protein Kinase (MAPK) Interacting Kinases 1 and 2 (MNK1 and MNK2) as Targets for Cancer Therapy: Recent Progress in the Development of MNK Inhibitors. *Current Medicinal Chemistry*, *24*(28). https://doi.org/10.2174/0929867324666170203123427

Dulken, B. W., Buckley, M. T., Navarro Negredo, P., Saligrama, N., Cayrol, R., Leeman, D. S., George, B. M., Boutet, S. C., Hebestreit, K., Pluvinage, J. V., Wyss-Coray, T., Weissman, I. L., Vogel, H., Davis, M. M., & Brunet, A. (2019). Single-cell analysis reveals T cell infiltration in old neurogenic niches. *Nature 2019 571:7764*, *571*(7764), 205–210. https://doi.org/10.1038/s41586-019-1362-5

Elia, A., Constantinou, C., & Clemens, M. J. (2007). Effects of protein phosphorylation on ubiquitination and stability of the translational inhibitor protein 4E-BP1. *Oncogene 2008 27:6*, *27*(6), 811–822. https://doi.org/10.1038/sj.onc.1210678

Faust, T. E., Gunner, G., & Schafer, D. P. (2021). Mechanisms governing activity-dependent synaptic pruning in the developing mammalian CNS. *Nature Reviews. Neuroscience*, *22*(11), 657–673. https://doi.org/10.1038/S41583-021-00507-Y

Feldman, M. E., Apsel, B., Uotila, A., Loewith, R., Knight, Z. A., Ruggero, D., & Shokat, K. M. (2009). Active-site inhibitors of mTOR target rapamycin-resistant outputs of mTORC1 and mTORC2. *PLoS Biology*, *7*(2), 0371–0383. https://doi.org/10.1371/JOURNAL.PBIO.1000038

Fenn, A. M., Henry, C. J., Huang, Y., Dugan, A., & Godbout, J. P. (2012). Lipopolysaccharide-induced interleukin (IL)-4 receptor-α expression and corresponding sensitivity to the M2 promoting effects of IL-4 are impaired in microglia of aged mice. *Brain, Behavior, and Immunity*, *26*(5), 766–777. https://doi.org/10.1016/j.bbi.2011.10.003

Flowers, A., Bell-Temin, H., Jalloh, A., Stevens, S. M., & Bickford, P. C. (2017). Proteomic anaysis of aged microglia: Shifts in transcription, bioenergetics, and nutrient response. *Journal of Neuroinflammation*, *14*(1), 1–15. https://doi.org/10.1186/s12974-017-0840-7

Franceschi, C., Garagnani, P., Morsiani, C., Conte, M., Santoro, A., Grignolio, A., Monti, D., Capri, M., & Salvioli, S. (2018). The continuum of aging and age-related diseases: Common mechanisms but different rates. *Frontiers in Medicine*, *5*(MAR), 349810. https://doi.org/10.3389/FMED.2018.00061/BIBTEX

Fukunaga, R., & Hunter, T. (1997). MNK1, a new MAP kinase-activated protein kinase, isolated by a novel expression screening method for identifying protein kinase substrates. *The EMBO Journal*, *16*(8), 1921–1933. https://doi.org/10.1093/EMBOJ/16.8.1921

Furic, L., Rong, L., Larsson, O., Koumakpayi, I. H., Yoshida, K., Brueschke, A., Petroulakis, E., Robichaud, N., Pollak, M., Gabouryd, L. A., Pandolfi, P. P., Saad, F.,

& Sonenberg, N. (2010). EIF4E phosphorylation promotes tumorigenesis and is associated with prostate cancer progression. *Proceedings of the National Academy of Sciences of the United States of America*, *107*(32), 14134–14139. https://doi.org/10.1073/PNAS.1005320107/-/DCSUPPLEMENTAL/PNAS.201005320SI.PDF

Gabandé-Rodríguez, E., Keane, L., & Capasso, M. (2020). Microglial phagocytosis in aging and Alzheimer's disease. *Journal of Neuroscience Research*, *98*(2), 284–298. https://doi.org/10.1002/JNR.24419

Ganeshan, K., & Chawla, A. (2014). Metabolic regulation of immune responses. *Annual Review of Immunology*, *32*, 609–634. https://doi.org/10.1146/annurev-immunol-032713-120236

Gebreyesus, S. T., Siyal, A. A., Kitata, R. B., Chen, E. S. W., Enkhbayar, B., Angata, T., Lin, K. I., Chen, Y. J., & Tu, H. L. (2022). Streamlined single-cell proteomics by an integrated microfluidic chip and data-independent acquisition mass spectrometry. *Nature Communications 2022 13:1*, *13*(1), 1–13. https://doi.org/10.1038/s41467-021-27778-4

Gingras, A. C., Gygi, S. P., Raught, B., Polakiewicz, R. D., Abraham, R. T., Hoekstra, M. F., Aebersold, R., & Sonenberg, N. (1999). Regulation of 4E-BP1 phosphorylation: a novel two-step mechanism. *Genes & Development*, *13*(11), 1422–1437. https://doi.org/10.1101/GAD.13.11.1422

Gingras, A. C., Raught, B., Gygi, S. P., Niedzwiecka, A., Miron, M., Burley, S. K., Polakiewicz, R. D., Wyslouch-Cieszynska, A., Aebersold, R., & Sonenberg, N. (2001). Hierarchical phosphorylation of the translation inhibitor 4E-BP1. *Genes & Development*, *15*(21), 2852–2864. https://doi.org/10.1101/GAD.912401

Ginhoux, F., Lim, S., Hoeffel, G., Low, D., & Huber, T. (2013). Origin and differentiation of microglia. *Frontiers in Cellular Neuroscience*, *7*(MAR), 46040. https://doi.org/10.3389/FNCEL.2013.00045/BIBTEX

Ginhoux, F., & Prinz, M. (2015). Origin of microglia: current concepts and past controversies. *Cold Spring Harbor Perspectives in Biology*, *7*(8). https://doi.org/10.1101/CSHPERSPECT.A020537

Godbout, J. P., Chen, J., Abraham, J., Richwine, A. F., Berg, B. M., Kelley, K. W., & Johnson, R. W. (2005). *Exaggerated neuroinflammation and sickness behavior in aged mice after activation of the peripheral innate immune system*. *24*(1), 1–24.

Godbout, J. P., Moreau, M., Lestage, J., Chen, J., Sparkman, N. L., O'Connor, J., Castanon, N., Kelley, K. W., Dantzer, R., & Johnson, R. W. (2008). Aging exacerbates depressive-like behavior in mice in response to activation of the peripheral innate immune system. *Neuropsychopharmacology*, *33*(10), 2341–2351. https://doi.org/10.1038/sj.npp.1301649

Gomes-Duarte, A., Lacerda, R., Menezes, J., & Romão, L. (2017). eIF3: a factor for human health and disease. *Https://Doi.Org/10.1080/15476286.2017.1391437*, *15*(1), 26–34. https://doi.org/10.1080/15476286.2017.1391437

Gomez Perdiguero, E., Klapproth, K., Schulz, C., Busch, K., Azzoni, E., Crozet, L., Garner, H., Trouillet, C., De Bruijn, M. F., Geissmann, F., & Rodewald, H. R. (2015). Tissue-resident macrophages originate from yolk-sac-derived erythro-myeloid progenitors. *Nature*, *518*(7540), 547–551. https://doi.org/10.1038/NATURE13989

Gong, Q., Li, W., Ali, T., Hu, Y., Mou, S., Liu, Z., Zheng, C., Gao, R., Li, A., Li, T., Li, N., Yu, Z., & Li, S. (2023). eIF4E phosphorylation mediated LPS induced depressive-like behaviors via ameliorated neuroinflammation and dendritic loss. *Translational Psychiatry 2023 13:1*, *13*(1), 1–11. https://doi.org/10.1038/s41398-023-02646-5

Gorgoulis, V., Adams, P. D., Alimonti, A., Bennett, D. C., Bischof, O., Bishop, C., Campisi, J., Collado, M., Evangelou, K., Ferbeyre, G., Gil, J., Hara, E., Krizhanovsky, V., Jurk, D., Maier, A. B., Narita, M., Niedernhofer, L., Passos, J. F., Robbins, P. D., … Demaria, M. (2019). Cellular Senescence: Defining a Path Forward. *Cell*, *179*(4), 813–827. https://doi.org/10.1016/j.cell.2019.10.005

Grabert, K., Michoel, T., Karavolos, M. H., Clohisey, S., Kenneth Baillie, J., Stevens, M. P., Freeman, T. C., Summers, K. M., & McColl, B. W. (2016). Microglial brain

region−dependent diversity and selective regional sensitivities to aging. *Nature Neuroscience 2016 19:3*, *19*(3), 504–516. https://doi.org/10.1038/nn.4222

Groh, J., Knöpper, K., Arampatzi, P., Yuan, X., Lößlein, L., Saliba, A. E., Kastenmüller, W., & Martini, R. (2021). Accumulation of cytotoxic T cells in the aged CNS leads to axon degeneration and contributes to cognitive and motor decline. *Nature Aging*, *1*(4), 357–367. https://doi.org/10.1038/S43587-021-00049-Z

Grubman, A., Choo, X. Y., Chew, G., Ouyang, J. F., Sun, G., Croft, N. P., Rossello, F. J., Simmons, R., Buckberry, S., Landin, D. V., Pflueger, J., Vandekolk, T. H., Abay, Z., Zhou, Y., Liu, X., Chen, J., Larcombe, M., Haynes, J. M., McLean, C., … Polo, J. M. (2021). Transcriptional signature in microglia associated with Aβ plaque phagocytosis. *Nature Communications 2021 12:1*, *12*(1), 1–22. https://doi.org/10.1038/s41467-021-23111-1

Guillemin, A., Kumar, A., Wencker, M., & Ricci, E. P. (2022). Shaping the Innate Immune Response Through Post-Transcriptional Regulation of Gene Expression Mediated by RNA-Binding Proteins. *Frontiers in Immunology*, *12*, 796012. https://doi.org/10.3389/FIMMU.2021.796012/BIBTEX

Gulen, M. F., Samson, N., Keller, A., Schwabenland, M., Liu, C., Glück, S., Thacker, V. V., Favre, L., Mangeat, B., Kroese, L. J., Krimpenfort, P., Prinz, M., & Ablasser, A. (2023). cGAS–STING drives ageing-related inflammation and neurodegeneration. *Nature 2023 620:7973*, *620*(7973), 374–380. https://doi.org/10.1038/s41586-023-06373-1

Hammond, T. R., Dufort, C., Dissing-Olesen, L., Giera, S., Young, A., Wysoker, A., Walker, A. J., Gergits, F., Segel, M., Nemesh, J., Marsh, S. E., Saunders, A., Macosko, E., Ginhoux, F., Chen, J., Franklin, R. J. M., Piao, X., McCarroll, S. A., & Stevens, B. (2019). Single-Cell RNA Sequencing of Microglia throughout the Mouse Lifespan and in the Injured Brain Reveals Complex Cell-State Changes. *Immunity*, *50*(1), 253-271.e6. https://doi.org/10.1016/J.IMMUNI.2018.11.004

Hannan, K. M., Brandenburger, Y., Jenkins, A., Sharkey, K., Cavanaugh, A., Rothblum, L., Moss, T., Poortinga, G., McArthur, G. A., Pearson, R. B., & Hannan, R. D. (2003).

mTOR-dependent regulation of ribosomal gene transcription requires S6K1 and is mediated by phosphorylation of the carboxy-terminal activation domain of the nucleolar transcription factor UBF. *Molecular and Cellular Biology*, *23*(23), 8862–8877. https://doi.org/10.1128/MCB.23.23.8862-8877.2003

Hao, F., Kondo, K., Itoh, T., Ikari, S., Nada, S., Okada, M., & Noda, T. (2018). Rheb localized on the Golgi membrane activates lysosomelocalized mTORC1 at the Golgi-lysosome contact site. *Journal of Cell Science*, *131*(3). https://doi.org/10.1242/JCS.208017/265484/AM/RHEB-LOCALIZED-ON-THE-GOLGI-MEMBRANE-ACTIVATES

Hart, A. D., Wyttenbach, A., Perry, V. H., & Teeling, J. L. (2012). Brain , Behavior , and Immunity Age related changes in microglial phenotype vary between CNS regions : Grey versus white matter differences. *Brain Behavior and Immunity*, *26*(5), 754–765. https://doi.org/10.1016/j.bbi.2011.11.006

Helmut, K., Hanisch, U. K., Noda, M., & Verkhratsky, A. (2011). Physiology of microglia. *Physiological Reviews*, *91*(2), 461–553. https://doi.org/10.1152/PHYSREV.00011.2010

Henry, C. J., Huang, Y., Wynne, A. M., & Godbout, J. P. (2009). *Peripheral LPS challenge promotes microglial hyperactivity in aged mice that is associated with exaggerated induction of both proinflammatory IL1β and antiinflammatory IL10 cytokines.pdf*. *23*(3), 309–317. https://doi.org/10.1016/j.bbi.2008.09.002.Peripheral

Herbert, T. P., Tee, A. R., & Proud, C. G. (2002). The extracellular signal-regulated kinase pathway regulates the phosphorylation of 4E-BP1 at multiple sites. *Journal of Biological Chemistry*, *277*(13), 11591–11596. https://doi.org/10.1074/jbc.M110367200

Herdy, B., Jaramillo, M., Svitkin, Y. V., Rosenfeld, A. B., Kobayashi, M., Walsh, D., Alain, T., Sean, P., Robichaud, N., Topisirovic, I., Furic, L., Dowling, R. J. O., Sylvestre, A., Rong, L., Colina, R., Costa-Mattioli, M., Fritz, J. H., Olivier, M., Brown, E., … Sonenberg, N. (2012). Translational control of the activation of transcription factor

NF-κB and production of type I interferon by phosphorylation of the translation factor eIF4E. *Nature Immunology*, *13*(6), 543–550. https://doi.org/10.1038/NI.2291

Hershey, J. W. B., Sonenberg, N., & Mathews, M. B. (2019). Principles of Translational Control. *Cold Spring Harbor Perspectives in Biology*, *11*(9). https://doi.org/10.1101/CSHPERSPECT.A032607

Hickman, S. E., Kingery, N. D., Ohsumi, T. K., Borowsky, M. L., Wang, L., Means, T. K., & El Khoury, J. (2013). The microglial sensome revealed by direct RNA sequencing. *Nature Publishing Group*. https://doi.org/10.1038/nn.3554

Holtman, I. R., Raj, D. D., Miller, J. A., Schaafsma, W., Yin, Z., Brouwer, N., Wes, P. D., Möller, T., Orre, M., Kamphuis, W., Hol, E. M., Boddeke, E. W. G. M., & Eggen, B. J. L. (2015). Induction of a common microglia gene expression signature by aging and neurodegenerative conditions: a co-expression meta-analysis. *Acta Neuropathologica Communications*, *3*(1), 31. https://doi.org/10.1186/S40478-015-0203-5/FIGURES/6

Hosokawa, N., Hara, T., Kaizuka, T., Kishi, C., Takamura, A., Miura, Y., Iemura, S. I., Natsume, T., Takehana, K., Yamada, N., Guan, J. L., Oshiro, N., & Mizushima, N. (2009). Nutrient-dependent mTORC1 Association with the ULK1–Atg13–FIP200 Complex Required for Autophagy. *Molecular Biology of the Cell*, *20*(7), 1981. https://doi.org/10.1091/MBC.E08-12-1248

Hou, J., Chen, Y., Grajales-Reyes, G., & Colonna, M. (2022). TREM2 dependent and independent functions of microglia in Alzheimer's disease. *Molecular Neurodegeneration 2022 17:1*, *17*(1), 1–19. https://doi.org/10.1186/S13024-022-00588-Y

Huang, B., Jin, P., Yi, K., & Duan, J. (2023). MAPK-interacting kinases inhibition by eFT508 overcomes chemoresistance in preclinical model of osteosarcoma. *Human & Experimental Toxicology*, *42*. https://doi.org/10.1177/09603271231158047

Huang, Y., Henry, C. J., Dantzer, R., Johnson, R. W., & Godbout, J. P. (2008). Exaggerated sickness behavior and brain proinflammatory cytokine expression in

aged mice in response to intracerebroventricular lipopolysaccharide. *Neurobiology of Aging*, *29*(11), 1744–1753. https://doi.org/10.1016/j.neurobiolaging.2007.04.012

Iwasaki, S., & Ingolia, N. T. (2017). The Growing Toolbox for Protein Synthesis Studies. *Trends in Biochemical Sciences*, *42*(8), 612–624. https://doi.org/10.1016/J.TIBS.2017.05.004

Jackson, R. J., Hellen, C. U. T., & Pestova, T. V. (2010). The mechanism of eukaryotic translation initiation and principles of its regulation. *Nature Reviews Molecular Cell Biology 2010 11:2*, *11*(2), 113–127. https://doi.org/10.1038/nrm2838

Jurga, A. M., Paleczna, M., & Kuter, K. Z. (2020). Overview of General and Discriminating Markers of Differential Microglia Phenotypes. *Frontiers in Cellular Neuroscience*, *14*(August), 1–18. https://doi.org/10.3389/fncel.2020.00198

Kapur, M., & Ackerman, S. L. (2018). mRNA Translation Gone Awry: Translation Fidelity and Neurological Disease. *Trends in Genetics : TIG*, *34*(3), 218. https://doi.org/10.1016/J.TIG.2017.12.007

Keane, L., Antignano, I., Riechers, S. P., Zollinger, R., Dumas, A. A., Offermann, N., Bernis, M. E., Russ, J., Graelmann, F., McCormick, P. N., Esser, J., Tejera, D., Nagano, A., Wang, J., Chelala, C., Biederbick, Y., Halle, A., Salomoni, P., Heneka, M. T., & Capasso, M. (2021). mTOR-dependent translation amplifies microglia priming in aging mice. *Journal of Clinical Investigation*, *131*(1), 1–16. https://doi.org/10.1172/JCI132727

Kierdorf, K., Erny, D., Goldmann, T., Sander, V., Schulz, C., Perdiguero, E. G., Wieghofer, P., Heinrich, A., Riemke, P., Hölscher, C., Müller, D. N., Luckow, B., Brocker, T., Debowski, K., Fritz, G., Opdenakker, G., Diefenbach, A., Biber, K., Heikenwalder, M., … Prinz, M. (2013). Microglia emerge from erythromyeloid precursors via Pu.1- and Irf8-dependent pathways. *Nature Neuroscience*, *16*(3), 273–280. https://doi.org/10.1038/NN.3318

Kim, J., Kundu, M., Viollet, B., & Guan, K. L. (2011). AMPK and mTOR regulate autophagy through direct phosphorylation of Ulk1. *Nature Cell Biology*, *13*(2), 132–141. https://doi.org/10.1038/NCB2152

Kim, Y. M., Jung, C. H., Seo, M., Kim, E. K., Park, J. M., Bae, S. S., & Kim, D. H. (2015). mTORC1 Phosphorylates UVRAG to Negatively Regulate Autophagosome and Endosome Maturation. *Molecular Cell*, *57*(2), 207–218. https://doi.org/10.1016/J.MOLCEL.2014.11.013

Kiss, T., Nyúl-Tóth, Á., DelFavero, J., Balasubramanian, P., Tarantini, S., Faakye, J., Gulej, R., Ahire, C., Ungvari, A., Yabluchanskiy, A., Wiley, G., Garman, L., Ungvari, Z., & Csiszar, A. (2022). Spatial transcriptomic analysis reveals inflammatory foci defined by senescent cells in the white matter, hippocampi and cortical grey matter in the aged mouse brain. *GeroScience*, *44*(2), 661. https://doi.org/10.1007/S11357-022-00521-7

Klionsky, D. J., Elazar, Z., Seglen, P. O., & Rubinsztein, D. C. (2008). Does bafilomycin A1 block the fusion of autophagosomes with lysosomes? *Autophagy*, *4*(7), 849–850. https://doi.org/10.4161/AUTO.6845

Krishnarajah, S., Ingelfinger, F., Friebel, E., Cansever, D., Amorim, A., Andreadou, M., Bamert, D., Litscher, G., Lutz, M., Mayoux, M., Mundt, S., Ridder, F., Sparano, C., Stifter, S. A., Ulutekin, C., Unger, S., Vermeer, M., Zwicky, P., Greter, M., … Becher, B. (2021). Single-cell profiling of immune system alterations in lymphoid, barrier and solid tissues in aged mice. *Nature Aging 2021 2:1*, *2*(1), 74–89. https://doi.org/10.1038/s43587-021-00148-x

Laplante, M., & Sabatini, D. M. (2009). mTOR signaling at a glance. *Journal of Cell Science*, *122*(20), 3589–3594. https://doi.org/10.1242/JCS.051011

Lee, A. S. Y., Kranzusch, P. J., & Cate, J. H. D. (2015). eIF3 targets cell-proliferation messenger RNAs for translational activation or repression. *Nature 2015 522:7554*, *522*(7554), 111–114. https://doi.org/10.1038/nature14267

Li, D., Wang, C., Yao, Y., Chen, L., Liu, G., Zhang, R., Liu, Q., Shi, F. D., & Hao, J. (2016). MTORC1 pathway disruption ameliorates brain inflammation following stroke via a shift in microglia phenotype from M1 type to M2 type. *FASEB Journal*, *30*(10), 3388–3399. https://doi.org/10.1096/fj.201600495R

Lin, Y., Li, F., Huang, L., Polte, C., Duan, H., Fang, J., Sun, L., Xing, X., Tian, G., Cheng, Y., Ignatova, Z., Yang, X., & Wolf, D. A. (2020). eIF3 Associates with 80S Ribosomes to Promote Translation Elongation, Mitochondrial Homeostasis, and Muscle Health. *Molecular Cell*, *79*(4), 575-587.e7. https://doi.org/10.1016/J.MOLCEL.2020.06.003

Liu, G. Y., & Sabatini, D. M. (2020). mTOR at the nexus of nutrition, growth, ageing and disease. *Nature Reviews Molecular Cell Biology*, *21*(4), 183–203. https://doi.org/10.1038/s41580-019-0199-y

Liu, H., Leak, R. K., & Hu, X. (2016). Neurotransmitter receptors on microglia. *Stroke and Vascular Neurology*, *1*(2), 52. https://doi.org/10.1136/SVN-2016-000012

Liu, T., Zhang, L., Joo, D., & Sun, S. C. (2017). NF-κB signaling in inflammation. *Signal Transduction and Targeted Therapy 2017 2:1*, *2*(1), 1–9. https://doi.org/10.1038/sigtrans.2017.23

Livak, K. J., & Schmittgen, T. D. (2001). Analysis of relative gene expression data using real-time quantitative PCR and the 2(-Delta Delta C(T)) Method. *Methods (San Diego, Calif.)*, *25*(4), 402–408. https://doi.org/10.1006/METH.2001.1262

Livingstone, M., & Bidinosti, M. (2012). Rapamycin-insensitive mTORC1 activity controls eIF4E:4E-BP1 binding. *F1000Research*, *1*. https://doi.org/10.12688/F1000RESEARCH.1-4.V1

López-Otín, C., Blasco, M. A., Partridge, L., Serrano, M., & Kroemer, G. (2013). The hallmarks of aging. *Cell*, *153*(6), 1194. https://doi.org/10.1016/j.cell.2013.05.039

López-Otín, C., Blasco, M. A., Partridge, L., Serrano, M., & Kroemer, G. (2023). Hallmarks of aging: An expanding universe. *Cell*, *186*(2), 243–278. https://doi.org/10.1016/J.CELL.2022.11.001

Lu, D. Y., Liou, H. C., Tang, C. H., & Fu, W. M. (2006). Hypoxia-induced iNOS expression in microglia is regulated by the PI3-kinase/Akt/mTOR signaling pathway and activation of hypoxia inducible factor-1α. *Biochemical Pharmacology*, *72*(8), 992–1000. https://doi.org/10.1016/j.bcp.2006.06.038

Magnuson, B., Ekim, B., & Fingar, D. C. (2012). Regulation and function of ribosomal protein S6 kinase (S6K) within mTOR signalling networks. *The Biochemical Journal*, *441*(1), 1–21. https://doi.org/10.1042/BJ20110892

Marschallinger, J., Iram, T., Zardeneta, M., Lee, S. E., Lehallier, B., Haney, M. S., Pluvinage, J. V., Mathur, V., Hahn, O., Morgens, D. W., Kim, J., Tevini, J., Felder, T. K., Wolinski, H., Bertozzi, C. R., Bassik, M. C., Aigner, L., & Wyss-Coray, T. (2020). Lipid-droplet-accumulating microglia represent a dysfunctional and proinflammatory state in the aging brain. *Nature Neuroscience*, *23*(2), 194–208. https://doi.org/10.1038/s41593-019-0566-1

Matsuo, H., Li, H., McGuire, A. M., Mark Fletcher, C., Gingras, A. C., Sonenberg, N., & Wagner, G. (1997). Structure of translation factor eIF4E bound to m7GDP and interaction with 4E-binding protein. *Nature Structural Biology 1997 4:9*, *4*(9), 717–724. https://doi.org/10.1038/nsb0997-717

Mauvezin, C., & Neufeld, T. P. (2015). Bafilomycin A1 disrupts autophagic flux by inhibiting both V-ATPase-dependent acidification and Ca-P60A/SERCA-dependent autophagosome-lysosome fusion. *Autophagy*, *11*(8), 1437. https://doi.org/10.1080/15548627.2015.1066957

Mayer, C., Zhao, J., Yuan, X., & Grummt, I. (2004). mTOR-dependent activation of the transcription factor TIF-IA links rRNA synthesis to nutrient availability. *Genes & Development*, *18*(4), 423–434. https://doi.org/10.1101/GAD.285504

Merrick, W. C., & Pavitt, G. D. (2018). Protein Synthesis Initiation in Eukaryotic Cells. *Cold Spring Harbor Perspectives in Biology*, *10*(12). https://doi.org/10.1101/CSHPERSPECT.A033092

Meyer, K. D., Patil, D. P., Zhou, J., Zinoviev, A., Skabkin, M. A., Elemento, O., Pestova, T. V., Qian, S. B., & Jaffrey, S. R. (2015). 5’ UTR m(6)A Promotes Cap-Independent Translation. *Cell*, *163*(4), 999–1010. https://doi.org/10.1016/J.CELL.2015.10.012

Meyuhas, O. (2015). Ribosomal Protein S6 Phosphorylation: Four Decades of Research. In *International Review of Cell and Molecular Biology* (Vol. 320). Elsevier Ltd. https://doi.org/10.1016/bs.ircmb.2015.07.006

Michels, A. A., Robitaille, A. M., Buczynski-Ruchonnet, D., Hodroj, W., Reina, J. H., Hall, M. N., & Hernandez, N. (2010). mTORC1 Directly Phosphorylates and Regulates Human MAF1. *Molecular and Cellular Biology*, *30*(15), 3749. https://doi.org/10.1128/MCB.00319-10

Minhas, P. S., Latif-Hernandez, A., McReynolds, M. R., Durairaj, A. S., Wang, Q., Rubin, A., Joshi, A. U., He, J. Q., Gauba, E., Liu, L., Wang, C., Linde, M., Sugiura, Y., Moon, P. K., Majeti, R., Suematsu, M., Mochly-Rosen, D., Weissman, I. L., Longo, F. M., … Andreasson, K. I. (2021). Restoring metabolism of myeloid cells reverses cognitive decline in ageing. *Nature*, *590*(7844), 122–128. https://doi.org/10.1038/s41586-020-03160-0

Morrison, J. H., & Baxter, M. G. (2012). The ageing cortical synapse: hallmarks and implications for cognitive decline. *Nature Reviews. Neuroscience*, *13*(4), 240–250. https://doi.org/10.1038/NRN3200

Mosher, K. I., & Wyss-Coray, T. (2014). Microglial dysfunction in brain aging and Alzheimer's disease. *Biochemical Pharmacology*, *88*(4), 594–604. https://doi.org/10.1016/j.bcp.2014.01.008

Mothe-Satney, I., Yang, D., Fadden, P., Haystead, T. A. J., & Jr., J. C. L. (2000). Multiple Mechanisms Control Phosphorylation of PHAS-I in Five (S/T)P Sites That Govern Translational Repression. *Molecular and Cellular Biology*, *20*(10), 3558–3567. https://doi.org/10.1128/MCB.20.10.3558-3567.2000

Mrdjen, D., Pavlovic, A., Hartmann, F. J., Schreiner, B., Utz, S. G., Leung, B. P., Lelios, I., Heppner, F. L., Kipnis, J., Merkler, D., Greter, M., & Becher, B. (2018). High-Dimensional Single-Cell Mapping of Central Nervous System Immune Cells Reveals Distinct Myeloid Subsets in Health, Aging, and Disease. *Immunity*, *48*(2), 380-395.e6. https://doi.org/10.1016/J.IMMUNI.2018.01.011

Neshat, M. S., Mellinghoff, I. K., Tran, C., Stiles, B., Thomas, G., Petersen, R., Frost, P., Gibbons, J. J., Wu, H., & Sawyers, C. L. (2001). Enhanced sensitivity of PTEN-deficient tumors to inhibition of FRAP/mTOR. *Proceedings of the National Academy*

of Sciences of the United States of America, *98*(18), 10314–10319. https://doi.org/10.1073/pnas.171076798

Nikolcheva, T., Pyronnet, S., Chou, S., Sonenberg, N., Song, A., Clayberger, C., & Krensky, A. M. (2002). A translational rheostat for RFLAT-1 regulates RANTES expression in T lymphocytes. *The Journal of Clinical Investigation*, *110*(1), 119. https://doi.org/10.1172/JCI15336

Niraula, A., Sheridan, J. F., & Godbout, J. P. (2017). Microglia Priming with Aging and Stress. *Neuropsychopharmacology*, *42*(1), 318–333. https://doi.org/10.1038/npp.2016.185

Norden, D. M., & Godbout, J. P. (2013). Review: Microglia of the aged brain: Primed to be activated and resistant to regulation. *Neuropathology and Applied Neurobiology*, *39*(1), 19–34. https://doi.org/10.1111/j.1365-2990.2012.01306.x

Norden, D. M., Muccigrosso, M. M., & Godbout, J. P. (2015). Microglial priming and enhanced reactivity to secondary insult in aging, and traumatic CNS injury, and neurodegenerative disease. *Neuropharmacology*, *96*(PA), 29–41. https://doi.org/10.1016/j.neuropharm.2014.10.028

Ogrodnik, M., Evans, S. A., Fielder, E., Victorelli, S., Kruger, P., Salmonowicz, H., Weigand, B. M., Patel, A. D., Pirtskhalava, T., Inman, C. L., Johnson, K. O., Dickinson, S. L., Rocha, A., Schafer, M. J., Zhu, Y., Allison, D. B., von Zglinicki, T., LeBrasseur, N. K., Tchkonia, T., … Jurk, D. (2021). Whole-body senescent cell clearance alleviates age-related brain inflammation and cognitive impairment in mice. *Aging Cell*, *20*(2), 1–16. https://doi.org/10.1111/acel.13296

Paolicelli, R. C., Sierra, A., Stevens, B., Tremblay, M. E., Aguzzi, A., Ajami, B., Amit, I., Audinat, E., Bechmann, I., Bennett, M., Bennett, F., Bessis, A., Biber, K., Bilbo, S., Blurton-Jones, M., Boddeke, E., Brites, D., Brône, B., Brown, G. C., … Wyss-Coray, T. (2022). Microglia states and nomenclature: A field at its crossroads. *Neuron*, *110*(21), 3458–3483. https://doi.org/10.1016/j.neuron.2022.10.020

Parkhurst, C. N., Yang, G., Ninan, I., Savas, J. N., Yates, J. R., Lafaille, J. J., Hempstead, B. L., Littman, D. R., & Gan, W. B. (2013). Microglia promote learning-dependent

synapse formation through brain-derived neurotrophic factor. *Cell*, *155*(7), 1596–1609. https://doi.org/10.1016/J.CELL.2013.11.030

Pause, A., Belsham, G. J., Gingras, A. C., Donzé, O., Lin, T. A., Lawrence, J. C., & Sonenberg, N. (1994). Insulin-dependent stimulation of protein synthesis by phosphorylation of a regulator of 5'-cap function. *Nature*, *371*(6500), 762–767. https://doi.org/10.1038/371762A0

Pedersen, S., Celis, J. E., Nielsen, J., Christiansen, J., & Nielsen, F. C. (1997). Distinct repression of translation by wortmannin and rapamycin. *European Journal of Biochemistry*, *247*(1), 449–456. https://doi.org/10.1111/j.1432-1033.1997.00449.x

Pegoraro, G., Voss, T. C., Martin, S. E., Tuzmen, P., Guha, R., & Misteli, T. (2012). Identification of mammalian protein quality control factors by high-throughput cellular imaging. *PloS One*, *7*(2). https://doi.org/10.1371/JOURNAL.PONE.0031684

Peng, H., Kasada, A., Ueno, M., Hoshii, T., Tadokoro, Y., Nomura, N., Ito, C., Takase, Y., Vu, H. T., Kobayashi, M., Xiao, B., Worley, P. F., & Hirao, A. (2018). Distinct roles of Rheb and Raptor in activating mTOR complex 1 for the self-renewal of hematopoietic stem cells. *Biochemical and Biophysical Research Communications*, *495*(1), 1129–1135. https://doi.org/10.1016/J.BBRC.2017.11.140

Perkins, N. D. (2007). Integrating cell-signalling pathways with NF-kappaB and IKK function. *Nature Reviews. Molecular Cell Biology*, *8*(1), 49–62. https://doi.org/10.1038/NRM2083

Perry, V. H., Matyszak, M. K., & Fearn, S. (1993). Altered antigen expression of microglia in the aged rodent CNS. *Glia*, *7*(1), 60–67. https://doi.org/10.1002/GLIA.440070111

Peters, A., Josephson, K., & Vincent, S. L. (1991). Effects of aging on the neuroglial cells and pericytes within area 17 of the rhesus monkey cerebral cortex. *The Anatomical Record*, *229*(3), 384–398. https://doi.org/10.1002/AR.1092290311

Piccirillo, C. A., Bjur, E., Topisirovic, I., Sonenberg, N., & Larsson, O. (2014). Translational control of immune responses: from transcripts to translatomes. *Nature Immunology 2014 15:6*, *15*(6), 503–511. https://doi.org/10.1038/ni.2891

Pluvinage, J. V., Haney, M. S., Smith, B. A. H., Sun, J., Iram, T., Bonanno, L., Li, L., Lee, D. P., Morgens, D. W., Yang, A. C., Shuken, S. R., Gate, D., Scott, M., Khatri, P., Luo, J., Bertozzi, C. R., Bassik, M. C., & Wyss-Coray, T. (2019). CD22 blockade restores homeostatic microglial phagocytosis in ageing brains. *Nature*, *568*(7751), 187–192. https://doi.org/10.1038/s41586-019-1088-4

Pluvinage, J. V, Sun, J., Claes, C., Flynn, R. A., Haney, M. S., Iram, T., Meng, X., Lindemann, R., Riley, N. M., Danhash, E., Paul Chadarevian, J., Tapp, E., Gate, D., Kondapavulur, S., Cobos, I., Chetty, S., Pașca, A. M., Pașca, S. P., Berry-Kravis, E., … Wyss-Coray, T. (2021). The CD22-IGF2R interaction is a therapeutic target for microglial lysosome dysfunction in Niemann-Pick type C. *Sci. Transl. Med*, *13*, 2919. https://www.science.org

Poulin, F., Gingras, A. C., Olsen, H., Chevalier, S., & Sonenberg, N. (1998). 4E-BP3, a new member of the eukaryotic initiation factor 4E-binding protein family. *The Journal of Biological Chemistry*, *273*(22), 14002–14007. https://doi.org/10.1074/JBC.273.22.14002

Proud, C. G. (2015). Mnks, eIF4E phosphorylation and cancer. *Biochimica et Biophysica Acta (BBA) - Gene Regulatory Mechanisms*, *1849*(7), 766–773. https://doi.org/10.1016/J.BBAGRM.2014.10.003

Pyronnet, S., Imataka, H., Gingras, A. C., Fukunaga, R., Hunter, T., & Sonenberg, N. (1999). Human eukaryotic translation initiation factor 4G (eIF4G) recruits Mnk1 to phosphorylate eIF4E. *The EMBO Journal*, *18*(1), 270–279. https://doi.org/10.1093/EMBOJ/18.1.270

Qin, X., Jiang, B., & Zhang, Y. (2016). 4E-BP1, a multifactor regulated multifunctional protein. *Cell Cycle*, *15*(6), 781. https://doi.org/10.1080/15384101.2016.1151581

Rangaraju, S., Verrier, J. D., Madorsky, I., Nicks, J., Dunn, W. A., & Notterpek, L. (2010). Rapamycin Activates Autophagy and Improves Myelination in Explant Cultures from Neuropathic Mice. *The Journal of Neuroscience*, *30*(34), 11388. https://doi.org/10.1523/JNEUROSCI.1356-10.2010

Reich, S. H., Sprengeler, P. A., Chiang, G. G., Appleman, J. R., Chen, J., Clarine, J., Eam, B., Ernst, J. T., Han, Q., Goel, V. K., Han, E. Z. R., Huang, V., Hung, I. N. J., Jemison, A., Jessen, K. A., Molter, J., Murphy, D., Neal, M., Parker, G. S., … Webster, K. R. (2018). Structure-based Design of Pyridone-Aminal eFT508 Targeting Dysregulated Translation by Selective Mitogen-activated Protein Kinase Interacting Kinases 1 and 2 (MNK1/2) Inhibition. *Journal of Medicinal Chemistry*, *61*(8), 3516–3540. https://doi.org/10.1021/ACS.JMEDCHEM.7B01795/SUPPL_FILE/JM7B01795_SI_001.CSV

Safaiyan, S., Besson-Girard, S., Kaya, T., Cantuti-Castelvetri, L., Liu, L., Ji, H., Schifferer, M., Gouna, G., Usifo, F., Kannaiyan, N., Fitzner, D., Xiang, X., Rossner, M. J., Brendel, M., Gokce, O., & Simons, M. (2021). White matter aging drives microglial diversity. *Neuron*, *109*(7), 1100-1117.e10. https://doi.org/10.1016/J.NEURON.2021.01.027

Safaiyan, S., Kannaiyan, N., Snaidero, N., Brioschi, S., Biber, K., Yona, S., Edinger, A. L., Jung, S., Rossner, M. J., & Simons, M. (2016). *Age-related myelin degradation burdens the clearance function of microglia during aging*. *19*(8), 995–998. https://www.nature.com/articles/nn.4325

Sahasrabuddhe, V., & Ghosh, H. S. (2022). Cx3Cr1-Cre induction leads to microglial activation and IFN-1 signaling caused by DNA damage in early postnatal brain. *Cell Reports*, *38*(3). https://doi.org/10.1016/J.CELREP.2021.110252

Saitoh, T., Fujita, N., Jang, M. H., Uematsu, S., Yang, B. G., Satoh, T., Omori, H., Noda, T., Yamamoto, N., Komatsu, M., Tanaka, K., Kawai, T., Tsujimura, T., Takeuchi, O., Yoshimori, T., & Akira, S. (2008). Loss of the autophagy protein Atg16L1 enhances endotoxin-induced IL-1beta production. *Nature*, *456*(7219), 264–268. https://doi.org/10.1038/NATURE07383

Sala Frigerio, C., Wolfs, L., Fattorelli, N., Thrupp, N., Voytyuk, I., Schmidt, I., Mancuso, R., Chen, W. T., Woodbury, M. E., Srivastava, G., Möller, T., Hudry, E., Das, S., Saido, T., Karran, E., Hyman, B., Perry, V. H., Fiers, M., & De Strooper, B. (2019). The Major Risk Factors for Alzheimer's Disease: Age, Sex, and Genes Modulate the

Microglia Response to Aβ Plaques. *Cell Reports*, *27*(4), 1293-1306.e6. https://doi.org/10.1016/J.CELREP.2019.03.099

Sanz, E., Bean, J. C., Carey, D. P., Quintana, A., & McKnight, G. S. (2019). RiboTag: Ribosomal Tagging Strategy to Analyze Cell-Type-Specific mRNA Expression In Vivo. *Current Protocols in Neuroscience*, *88*(1). https://doi.org/10.1002/CPNS.77

Sanz, E., Yang, L., Su, T., Morris, D. R., McKnight, G. S., & Amieux, P. S. (2009). Cell-type-specific isolation of ribosome-associated mRNA from complex tissues. *Proceedings of the National Academy of Sciences of the United States of America*, *106*(33), 13939–13944. https://doi.org/10.1073/PNAS.0907143106/SUPPL_FILE/0907143106SI.PDF

Saxton, R. A., & Sabatini, D. M. (2017). mTOR Signaling in Growth, Metabolism, and Disease. In *Cell* (Vol. 168, Issue 6, pp. 960–976). Cell Press. https://doi.org/10.1016/j.cell.2017.02.004

Saxton, R. A., & Sabatini, D. M. (2017c). mTOR Signaling in Growth, Metabolism, and Disease. *Cell*, *168*(6), 960–976. https://doi.org/10.1016/j.cell.2017.02.004

Schott, J., Reitter, S., Philipp, J., Haneke, K., Schäfer, H., & Stoecklin, G. (2014). Translational Regulation of Specific mRNAs Controls Feedback Inhibition and Survival during Macrophage Activation. *PLOS Genetics*, *10*(6), e1004368. https://doi.org/10.1371/JOURNAL.PGEN.1004368

Scott-Hewitt, N., Perrucci, F., Morini, R., Erreni, M., Mahoney, M., Witkowska, A., Carey, A., Faggiani, E., Schuetz, L. T., Mason, S., Tamborini, M., Bizzotto, M., Passoni, L., Filipello, F., Jahn, R., Stevens, B., & Matteoli, M. (2020). Local externalization of phosphatidylserine mediates developmental synaptic pruning by microglia. *The EMBO Journal*, *39*(16). https://doi.org/10.15252/EMBJ.2020105380

Sekiyama, N., Arthanari, H., Papadopoulos, E., Rodriguez-Mias, R. A., Wagner, G., & Léger-Abraham, M. (2015). Molecular mechanism of the dual activity of 4EGI-1: Dissociating eIF4G from eIF4E but stabilizing the binding of unphosphorylated 4E-BP1. *Proceedings of the National Academy of Sciences of the United States of*

America, *112*(30), E4036–E4045. https://doi.org/10.1073/PNAS.1512118112/SUPPL_FILE/PNAS.201512118SI.PDF

Shi, Q., Chang, C., Saliba, A., & Bhat, M. A. (2022). Microglial mTOR Activation Upregulates Trem2 and Enhances b-Amyloid Plaque Clearance in the 5XFAD Alzheimer's Disease Model. *Journal of Neuroscience*, *42*(27), 5294–5313. https://doi.org/10.1523/JNEUROSCI.2427-21.2022

Shor, B., Wu, J., Shakey, Q., Toral-Barza, L., Shi, C., Follettie, M., & Yu, K. (2010). Requirement of the mTOR Kinase for the Regulation of Maf1 Phosphorylation and Control of RNA Polymerase III-dependent Transcription in Cancer Cells. *The Journal of Biological Chemistry*, *285*(20), 15380. https://doi.org/10.1074/JBC.M109.071639

Shor, B., Zhang, W. G., Toral-Barza, L., Lucas, J., Abraham, R. T., Gibbons, J. J., & Yu, K. (2008). A new pharmacologic action of CCI-779 involves FKBP12-independent inhibition of mTOR kinase activity and profound repression of global protein synthesis. *Cancer Research*, *68*(8), 2934–2943. https://doi.org/10.1158/0008-5472.CAN-07-6487

Shukla, T., de la Peña, J. B., Perish, J. M., Ploski, J. E., Stumpf, C. R., Webster, K. R., Thorn, C. A., & Campbell, Z. T. (2021). A Highly Selective MNK Inhibitor Rescues Deficits Associated with Fragile X Syndrome in Mice. *Neurotherapeutics : The Journal of the American Society for Experimental NeuroTherapeutics*, *18*(1), 624–639. https://doi.org/10.1007/S13311-020-00932-4

Sierra, A., Encinas, J. M., Deudero, J. J. P., Chancey, J. H., Enikolopov, G., Overstreet-Wadiche, L. S., Tsirka, S. E., & Maletic-Savatic, M. (2010). Microglia shape adult hippocampal neurogenesis through apoptosis-coupled phagocytosis. *Cell Stem Cell*, *7*(4), 483. https://doi.org/10.1016/J.STEM.2010.08.014

Silvin, A., Uderhardt, S., Piot, C., Da Mesquita, S., Yang, K., Geirsdottir, L., Mulder, K., Eyal, D., Liu, Z., Bridlance, C., Thion, M. S., Zhang, X. M., Kong, W. T., Deloger, M., Fontes, V., Weiner, A., Ee, R., Dress, R., Hang, J. W., … Ginhoux, F. (2022). Dual ontogeny of disease-associated microglia and disease inflammatory macrophages in

aging and neurodegeneration. *Immunity*, *55*(8), 1448-1465.e6. https://doi.org/10.1016/J.IMMUNI.2022.07.004

Sonenberg, N., & Hinnebusch, A. G. (2009). Regulation of translation initiation in eukaryotes: mechanisms and biological targets. *Cell*, *136*(4), 731–745. https://doi.org/10.1016/J.CELL.2009.01.042

Talma, N., Gerrits, E., Wang, B., Eggen, B. J. L., & Demaria, M. (2021). Identification of distinct and age-dependent p16High microglia subtypes. *Aging Cell*, *20*(10). https://doi.org/10.1111/ACEL.13450

Tamai, T., Yamaguchi, O., Hikoso, S., Takeda, T., Taneike, M., Oka, T., Oyabu, J., Murakawa, T., Nakayama, H., Uno, Y., Horie, K., Nishida, K., Sonenberg, N., Shah, A. M., Takeda, J., Komuro, I., & Otsu, K. (2013). Rheb (Ras Homologue Enriched in Brain)-dependent Mammalian Target of Rapamycin Complex 1 (mTORC1) Activation Becomes Indispensable for Cardiac Hypertrophic Growth after Early Postnatal Period. *The Journal of Biological Chemistry*, *288*(14), 10176. https://doi.org/10.1074/JBC.M112.423640

Taylor, M. J., Lukowski, J. K., & Anderton, C. R. (2021). Spatially Resolved Mass Spectrometry at the Single Cell: Recent Innovations in Proteomics and Metabolomics. *Journal of the American Society for Mass Spectrometry*, *32*(4), 872–894. https://doi.org/10.1021/JASMS.0C00439/ASSET/IMAGES/LARGE/JS0C00439_0008.JPEG

Thoreen, C. C., Chantranupong, L., Keys, H. R., Wang, T., Gray, N. S., & Sabatini, D. M. (2012). A unifying model for mTORC1-mediated regulation of mRNA translation. *Nature*, *485*(7396), 109–113. https://doi.org/10.1038/nature11083

Thoreen, C. C., Kang, S. A., Chang, J. W., Liu, Q., Zhang, J., Gao, Y., Reichling, L. J., Sim, T., Sabatini, D. M., & Gray, N. S. (2009). An ATP-competitive mammalian target of rapamycin inhibitor reveals rapamycin-resistant functions of mTORC1. *Journal of Biological Chemistry*, *284*(12), 8023–8032. https://doi.org/10.1074/jbc.M900301200

Ulland, T. K., Song, W. M., Huang, S. C. C., Ulrich, J. D., Sergushichev, A., Beatty, W. L., Loboda, A. A., Zhou, Y., Cairns, N. J., Kambal, A., Loginicheva, E., Gilfillan, S., Cella,

M., Virgin, H. W., Unanue, E. R., Wang, Y., Artyomov, M. N., Holtzman, D. M., & Colonna, M. (2017). TREM2 Maintains Microglial Metabolic Fitness in Alzheimer's Disease. *Cell*, *170*(4), 649-663.e13. https://doi.org/10.1016/J.CELL.2017.07.023

Uttam, S., Wong, C., Amorim, I. S., Jafarnejad, S. M., Tansley, S. N., Yang, J., Prager-Khoutorsky, M., Mogil, J. S., Gkogkas, C. G., & Khoutorsky, A. (2018). Translational profiling of dorsal root ganglia and spinal cord in a mouse model of neuropathic pain. *Neurobiology of Pain*, *4*, 35. https://doi.org/10.1016/J.YNPAI.2018.04.001

VanInsberghe, M., van den Berg, J., Andersson-Rolf, A., Clevers, H., & van Oudenaarden, A. (2021). Single-cell Ribo-seq reveals cell cycle-dependent translational pausing. *Nature 2021 597:7877*, *597*(7877), 561–565. https://doi.org/10.1038/s41586-021-03887-4

Vaughan, D. W., & Peters, A. (1974). Neuroglial cells in the cerebral cortex of rats from young adulthood to old age: an electron microscope study. *Journal of Neurocytology*, *3*(4), 405–429. https://doi.org/10.1007/BF01098730

Wagner, S., Herrmannová, A., Hronová, V., Gunišová, S., Sen, N. D., Hannan, R. D., Hinnebusch, A. G., Shirokikh, N. E., Preiss, T., & Valášek, L. S. (2020). Selective Translation Complex Profiling Reveals Staged Initiation and Co-translational Assembly of Initiation Factor Complexes. *Molecular Cell*, *79*(4), 546-560.e7. https://doi.org/10.1016/J.MOLCEL.2020.06.004

Wang, Q., & Mao, Y. (2023). Principles, challenges, and advances in ribosome profiling: from bulk to low-input and single-cell analysis. *Advanced Biotechnology 2023 1:4*, *1*(4), 1–14. https://doi.org/10.1007/S44307-023-00006-4

Wang, R., Wang, J., Hassan, A., Lee, C. H., Xie, X. S., & Li, X. (2021). Molecular basis of V-ATPase inhibition by bafilomycin A1. *Nature Communications 2021 12:1*, *12*(1), 1–8. https://doi.org/10.1038/s41467-021-22111-5

Wang, W., Wu, J., Zhang, Z., & Tong, T. (2001). Characterization of regulatory elements on the promoter region of p16(INK4a) that contribute to overexpression of p16 in senescent fibroblasts. *The Journal of Biological Chemistry*, *276*(52), 48655–48661. https://doi.org/10.1074/JBC.M108278200

Wang, X., Li, M., Gao, Y., Gao, J., Yang, W., Liang, H., Ji, Q., Li, Y., Liu, H., Huang, J., Cheng, T., & Yuan, W. (2016). Rheb1-mTORC1 maintains macrophage differentiation and phagocytosis in mice. *Experimental Cell Research*, *344*(2), 219–228. https://doi.org/10.1016/J.YEXCR.2016.04.017

Wang, X., Zhao, B. S., Roundtree, I. A., Lu, Z., Han, D., Ma, H., Weng, X., Chen, K., Shi, H., & He, C. (2015). N(6)-methyladenosine Modulates Messenger RNA Translation Efficiency. *Cell*, *161*(6), 1388–1399. https://doi.org/10.1016/J.CELL.2015.05.014

Waskiewicz, A. J., Flynn, A., Proud, C. G., & Cooper, J. A. (1997). Mitogen-activated protein kinases activate the serine/threonine kinases Mnk1 and Mnk2. *The EMBO Journal*, *16*(8), 1909–1920. https://doi.org/10.1093/EMBOJ/16.8.1909

Weichhart, T., Costantino, G., Poglitsch, M., Rosner, M., Zeyda, M., Stuhlmeier, K. M., Kolbe, T., Stulnig, T. M., Hörl, W. H., Hengstschläger, M., Müller, M., & Säemann, M. D. (2008). The TSC-mTOR signaling pathway regulates the innate inflammatory response. *Immunity*, *29*(4), 565–577. https://doi.org/10.1016/J.IMMUNI.2008.08.012

Weichhart, T., Hengstschläger, M., & Linke, M. (2015). Regulation of innate immune cell function by mTOR. *Nature Reviews. Immunology*, *15*(10), 599–614. https://doi.org/10.1038/NRI3901

Weischenfeldt, J., & Porse, B. (2008). Bone Marrow-Derived Macrophages (BMM): Isolation and Applications. *CSH Protocols*, *2008*(12). https://doi.org/10.1101/PDB.PROT5080

Wolf, D. A., Lin, Y., Duan, H., & Cheng, Y. (2020). eIF-Three to Tango: emerging functions of translation initiation factor eIF3 in protein synthesis and disease. *Journal of Molecular Cell Biology*, *12*(6), 403–409. https://doi.org/10.1093/JMCB/MJAA018

World report on Ageing And HeAltH. (2015). www.who.int

Ximerakis, M., Lipnick, S. L., Innes, B. T., Simmons, S. K., Adiconis, X., Dionne, D., Mayweather, B. A., Nguyen, L., Niziolek, Z., Ozek, C., Butty, V. L., Isserlin, R., Buchanan, S. M., Levine, S. S., Regev, A., Bader, G. D., Levin, J. Z., & Rubin, L. L. (2019). Single-cell transcriptomic profiling of the aging mouse brain. *Nature*

Neuroscience 2019 22:10, *22*(10), 1696–1708. https://doi.org/10.1038/s41593-019-0491-3

Xu, H., Zhu, J., Smith, S., Foldi, J., Zhao, B., Chung, A. Y., Outtz, H., Kitajewski, J., Shi, C., Weber, S., Saftig, P., Li, Y., Ozato, K., Blobel, C. P., Ivashkiv, L. B., & Hu, X. (2012). Notch-RBP-J signaling regulates the transcription factor IRF8 to promote inflammatory macrophage polarization. *Nature Immunology*, *13*(7), 642–650. https://doi.org/10.1038/NI.2304

Xu, Y., Poggio, M., Jin, H. Y., Shi, Z., Forester, C. M., Wang, Y., Stumpf, C. R., Xue, L., Devericks, E., So, L., Nguyen, H. G., Griselin, A., Gordan, J. D., Umetsu, S. E., Reich, S. H., Worland, S. T., Asthana, S., Barna, M., Webster, K. R., … Ruggero, D. (2019). Translation control of the immune checkpoint in cancer and its therapeutic targeting. *Nature Medicine*, *25*(2), 301–311. https://doi.org/10.1038/S41591-018-0321-2

Yanagiya, A., Suyama, E., Adachi, H., Svitkin, Y. V., Aza-Blanc, P., Imataka, H., Mikami, S., Martineau, Y., Ronai, Z. A., & Sonenberg, N. (2012). Translational Homeostasis via the mRNA Cap-Binding Protein, eIF4E. *Molecular Cell*, *46*(6), 847–858. https://doi.org/10.1016/J.MOLCEL.2012.04.004

Yang, H., Zhang, W., Pan, H., Feldser, H. G., Lainez, E., Miller, C., Leung, S., Zhong, Z., Zhao, H., Sweitzer, S., Considine, T., Riera, T., Suri, V., White, B., Ellis, J. L., Vlasuk, G. P., & Loh, C. (2012). SIRT1 Activators Suppress Inflammatory Responses through Promotion of p65 Deacetylation and Inhibition of NF-κB Activity. *PLoS ONE*, *7*(9). https://doi.org/10.1371/JOURNAL.PONE.0046364

Yang, X., Zhong, W., & Cao, R. (2020). Phosphorylation of the mRNA cap-binding protein eIF4E and cancer. *Cellular Signalling*, *73*, 109689. https://doi.org/10.1016/J.CELLSIG.2020.109689

Yang, Y. C., Boen, C., Gerken, K., Li, T., Schorpp, K., & Harris, K. M. (2016). Social relationships and physiological determinants of longevity across the human life span. *Proceedings of the National Academy of Sciences of the United States of America*, *113*(3), 578–583. https://doi.org/10.1073/PNAS.1511085112/-/DCSUPPLEMENTAL

Yona, S., Kim, K. W., Wolf, Y., Mildner, A., Varol, D., Breker, M., Strauss-Ayali, D., Viukov, S., Guilliams, M., Misharin, A., Hume, D. A., Perlman, H., Malissen, B., Zelzer, E., & Jung, S. (2013). Fate mapping reveals origins and dynamics of monocytes and tissue macrophages under homeostasis. *Immunity*, *38*(1), 79–91. https://doi.org/10.1016/J.IMMUNI.2012.12.001

Zhang, X., Pearsall, V. M., Carver, C. M., Atkinson, E. J., Clarkson, B. D. S., Grund, E. M., Baez-Faria, M., Pavelko, K. D., Kachergus, J. M., White, T. A., Johnson, R. K., Malo, C. S., Gonzalez-Suarez, A. M., Ayasoufi, K., Johnson, K. O., Tritz, Z. P., Fain, C. E., Khadka, R. H., Ogrodnik, M., … Schafer, M. J. (2022). Rejuvenation of the aged brain immune cell landscape in mice through p16-positive senescent cell clearance. *Nature Communications*, *13*(1). https://doi.org/10.1038/S41467-022-33226-8

Zhang, Y., Hu, W., & Li, H. B. (2023). RNA modification-mediated translational control in immune cells. *RNA Biology*, *20*(1), 603–613. https://doi.org/10.1080/15476286.2023.2246256

Zou, J., Zhou, L., Du, X. X., Ji, Y., Xu, J., Tian, J., Jiang, W., Zou, Y., Yu, S., Gan, L., Luo, M., Yang, Q., Cui, Y., Yang, W., Xia, X., Chen, M., Zhao, X., Shen, Y., Chen, P. Y., … Xiao, B. (2011). Rheb1 is Required for mTORC1 and Myelination in Postnatal Brain Development. *Developmental Cell*, *20*(1), 97. https://doi.org/10.1016/J.DEVCEL.2010.11.020

9. Acknowledgment

First and foremost, I would like to thank Dr. Melania Capasso for giving me the opportunity to complete the PhD in her lab. For the last five years, you supervised me and supported me in every possible way due to incredible challenges of this project. Thanks for our endless scientific meetings and for allowing me to personally, and scientifically, grow so much in your lab.

Furthermore, I would like to thank Prof. Dr. Martin Fuhrman, Prof. Dr. Eicke Latz, Prof. Dr. Gabor Petzold and Dr. Marc Beyer for agreeing to be my supervisors of my PhD thesis, and for the fruitful scientific discussions and great feedbacks about my research project.

I would not be the person, and the scientist, I am today without the support of all the people that I had the privilege to meet here at DZNE, in the Capasso Lab and in Germany.

Many thanks to you all for making this adventure unforgettable!

Last, but not least, I want to thank my family, to whom I dedicate this work.